Title
Behavioral State Modulates Primary Visual Cortex Responsiveness in Mice

Author
Einstein, Michael

Publication Date
2017

Peer reviewed|Thesis/dissertation

UNIVERSITY OF CALIFORNIA

Los Angeles

Behavioral State Modulates Primary Visual Cortex Responsiveness in Mice

A dissertation submitted in partial satisfaction of the

Requirements for the degree of Doctor of Philosophy

In Neuroscience

by

Michael Einstein

2017

ABSTRACT OF THE DISSERTATION

Behavioral State Modulates Primary Visual Cortex Responsiveness in Mice

by

Michael Einstein

Doctor of Philosophy in Neuroscience

University of California, Los Angeles, 2017

Professor Peyman Golshani, Chair

The brain is constantly bombarded with sensory stimuli. In order to process and perceive such diverse information streams simultaneously, the brain prioritizes information relevant to an animal's current behavioral needs. In this thesis, I investigate the neural mechanisms that enable the brain to increase or decrease visual signals depending on an animal's behavioral state. In chapter 1, I illustrate a novel mechanism, 3-5 Hz membrane potential (Vm) oscillations, that decreases the responsiveness of neurons in the primary visual cortex (V1) of mice. Using 2-photon guided whole-cell recordings as mice passive viewed and actively engaged drifting sine-wave gratings, I discovered that these visually-evoked phenomena were not influenced by changes in arousal or animal movement, but their timing was influenced by an animal's behavioral state. In addition to uncovering a novel mechanism for reducing the responsiveness of neurons in the brain, this chapter substantially furthers the field's knowledge of how behavior and arousal affect the membrane potential of neurons in the cerebral cortex. In chapter 2, I develop a method to train animals how to perform a visual attention task. I describe the hardware and software tools used to

actuate the task and the method used to train the animals. Using the method outlined in this chapter, I was able to routinely train animals to perform a multimodal attention task with approximately one month of training. In chapter 3, I employed this new attention model and, using 2-photon guided whole-cell recordings in behaving animals, I discovered that attention boosts the depolarization associated with visual stimulation in layer 2/3 V1 neurons, illustrating a potential mechanism that causes neurons to be more responsive to visual cues during attention. Finally, using 128 channel silicon nanoprobes chronically implanted in V1, I verified that the attention task increased the responsiveness of V1 neurons and desynchronized the local network in mice, replicating results previously obtained in non-human primate models and setting the groundwork for future study. As a result, my thesis details novel neural mechanisms for enhancing or dampening visual signals and expands our knowledge of how the brain prioritizes information according to an animal's behavioral context.

The dissertation of Michael Einstein is approved.

James W. Bisley

Dean V. Buonomano

Dario L. Ringach

Peyman Golshani, Committee Chair

University of California, Los Angeles

2017

Dedication

To my family and friends. Thanks for your support.

TABLE OF CONTENTS

LIST OF FIGURES

ACKNOWLDEGMENTS

Chapter 1 is a version of “Visually-evoked 3-5 Hz membrane potential oscillations reduce the responsiveness of visual cortex neurons in awake behaving mice,” which has been accepted for publication in *The Journal of Neuroscience*. This work was co-authored by Peyman Golshani (principal investigator, advisor, and committee chair), Pierre-Olivier Polack (post-doctoral advisor, co-first author), and Duy Tran (undergraduate research assistant). Pierre-Olivier Polack performed the electrophysiological recordings in non-behaving animals. Michael Einstein and Pierre-Olivier Polack performed the electrophysiological recordings in behaving animals. Michael Einstein, Pierre-Olivier Polack and Peyman Golshani designed the study. Michael Einstein and Pierre-Olivier Polack designed the behavioral paradigm. Michael Einstein analyzed the data. Michael Einstein wrote the manuscript with contribution from Peyman Golshani and Pierre-Olivier Polack. All co-authors have agreed to the publication of this version of the journal article in this dissertation.

Chapter 2 and 3 contains work co-authored by Michael Einstein, Duy Tran, Elissa Ye, Pierre-Olivier Polack, and Peyman Golshani. Results from this work have not been published in a journal. Michael Einstein and Pierre-Olivier conceived the task design and Michael Einstein executed the creation of hardware and software to actuate the novel multimodal task. Michael Einstein and Pierre-Olivier Polack carried out the electrophysiological experiments. Peyman Golshani gave constructive advice and was the primary investigator. Duy Tran and Elissa Ye trained animals used for study. Michael Einstein performed the analysis, created the figures, and wrote the text.

I gratefully acknowledge the sources of financial support for this work. Studies presented in this dissertation were supported by the NIH/National Institute of Mental Health 1R01-MH101198-01 and R01-MH105427-A1 granted to Peyman Golshani. Michael Einstein

was also funded by the UCLA Neuroimaging Training Program and the NIH/National Eye Institute (NIH-NEI) National Research Service Award F31 fellowship F31EY025185-02.

VITA

Michael Chang Einstein

Education:

Bachelor of Arts in Biology, 2012

Carleton College, Minnesota, USA

Selected Publications:

2017 Einstein, M.C., Polack, P.-O., Tran, D., Golshani, P. Visually-evoked 3-5 Hz membrane potential oscillations reduce the responsiveness of visual cortex neurons in awake behaving mice. *Accepted for publication by* The Journal of Neuroscience *on 4-1-17*.

Grants Awarded

2013-2014 UCLA-Semel Institute for Neuroscience NeuroImaging Training Program sponsored by NIH RFA-DA-06-011

2014-2017 Pre-doctoral (F31) National Research Service Award from NIH-NEI, F31EY025185-02

Foreword

The brain prioritizes information so that an animal can act appropriately on immediate behavioral demands (Harris and Thiele, 2011; Posner, 1980). This fundamental process is essential for sorting out the massive amount of incoming sensory data processed on a moment-by-moment basis. As a result, some of the most debilitating neural disorders, including schizophrenia, Alzheimer's disease, and autism spectrum disorders, are marked by sensory selection and attentional deficits (Doniger et al., 2001; Javitt, 2009; Mottron et al., 2006; Perry, 1999). Efforts to treat these deficits are not adequate and largely stem from a fundamental lack of knowledge of the physiological mechanisms that facilitate the interaction of executive control and raw sensory processing (Perry, 1999). Therefore, understanding the mechanisms that enable the brain to prioritize information is not only important for understanding how the brain works, but also essential for treating mental illness.

Modulation of neuronal responsiveness is likely a key mechanism for prioritizing sensory information in the brain. Sensory neurons that carry important information relevant to immediate behavioral demands become more sensitive to cues that are important for achieving behavioral goals (Reynolds et al., 2000a). This phenomenon has been studied extensively in the context of attention in non-human primates. When non-human primates are trained to direct attention to a cue by requiring animals to make a decision based on difficult perceptual tasks, neurons throughout the visual cortex significantly increase their responsiveness to attended visual cues (Chalk et al., 2010; Luck et al., 1997; Moran and Desimone, 1985; Motter, 1993; Reynolds et al., 2000a; Roelfsema et al., 1998; Treue and Maunsell, 1996a). Even when multiple cues are coded by one neuron, attention can entrain the neuron to just one cue and increase its responsiveness to that single cue (Reynolds et al., 1999). But these effects are not limited to single neurons as entire networks cooperate and synchronize activity to improve transmission of attended information (Bosman et al., 2012; Fries et al., 2001b; Gregoriou et al., 2009a). As a result, behaviors and cognitive

processes, such as attention, influence sensory neuron and network responsiveness as a means of prioritizing behaviorally relevant information.

Several cellular and network mechanisms that modulate the responsiveness of sensory neurons in the visual system during behavior have been identified. Signals from the prefrontal cortex (Zhang et al., 2014; Gregoriou et al., 2014; Moore & Armstrong et al., 2003), thalamus (McAlonan et al., 2008; Purushothaman et al., 2012; Wimmer et al., 2015), and neuromodulatory centers (Polack et al., 2013; Pinto et al., 2013; Fu et al., 2014) have all been shown to contribute to increasing the responsiveness of visual cortical neurons in behaving animals. Yet, two central questions remain: 1) what mechanisms exist to reduce the responsiveness of a neuron's responsiveness, and 2) how do response modulating mechanisms act at a synaptic level to scale a neuron's response properties in behaving animals? This thesis is devoted to answering these two important questions.

Chapter 1 details a novel subthreshold mechanism for reducing the responsiveness of neurons in the primary visual cortex (V1) of mice. I describe stereotyped 3-5 Hz membrane potential (Vm) oscillations which are evoked by visual cues during decision making regardless of an animal's arousal state. During these oscillatory epochs, the baseline Vm hyperpolarizes and performs high amplitude fluctuations between 3 and 5 Hz which functionally places neuron's in a low-level state where only time-locked inputs to the depolarized phase of the oscillations have the potential of eliciting spike output from neurons. In addition to demonstrating a novel mechanism for reducing the responsiveness of visual cortex neurons, this research establishes new known modes of Vm activity animals and expands the role of low frequency Vm oscillations in awake behaving animals.

Chapters 2 and 3 illustrate new research on the synaptic mechanisms attention employs to increase the responsiveness of neurons in V1 of mice. One major reason why little is known about these mechanics is a lack of adequate tools. Non-human primates have been the dominant animal model for studies of attention where advanced

electrophysiological and genetic tools are technically challenging. I developed a mouse behavioral paradigm to overcome these technical challenges and applied 2-photon guided whole-cell recordings to show that neurons in V1 depolarize when animals direct their attention to visual cues. This depolarization likely serves as a mechanism to increase the responsiveness of V1 neurons. Moreover, I used 128 channel nanoprobe extracellular recordings to validate the electrophysiological profile of attention in the mouse visual cortex against prior non-human primate research, proving that this model is appropriate for studying the neural basis of attention. In the future, this robust behavioral model can be used to map and quantify the relative contribution of different brain regions to the attentional modulation of visual cortex.

In conclusion, this thesis addresses mechanisms that decrease and increase the responsiveness of visual cortex neurons in awake behaving animals during behavior. While just a decade ago, experiments using mouse vision were viewed as unfavorable (Baker, 2013). Due to the techniques now available in mice, however, mouse visual research has exploded, especially following efforts led by Chris Neill and Michael Stryker (Niell and Stryker, 2010; 2008). While mouse visual cortex differs considerably from primate visual cortex, there are enough similarities, such as the general hierarchical organization based on feedforward and feedback connections and similar response properties of V1 neurons, that combined with ease of study has moved mouse vision research into the mainstream (Laramee and Boire, 2015; Q. Wang and Burkhalter, 2007). The research presented in this thesis furthers the claims that mice are a suitable model for studying how sensory streams interact with complex behaviors and cognition such as attention. With the advent of even more advanced imaging, genetic, and electrophysiological tools built around mice, the utility of models, such as the ones presented here, is set to increase for the foreseeable future.

Chapter 1: 3-5 Hz Vm Oscillations

1.1 Abstract

Low frequency membrane potential (Vm) oscillations were once thought to only occur in sleeping and anesthetized states. Recently, low frequency Vm oscillations have been described in inactive awake animals, but it is unclear if they shape sensory processing in neurons and whether they occur during active awake behavioral states. To answer these questions, we performed two-photon guided whole-cell Vm recordings from primary visual cortex layer 2/3 excitatory and inhibitory neurons in awake mice during passive visual stimulation and performance of visual and auditory discrimination tasks. We recorded stereotyped 3-5 Hz Vm oscillations where the Vm baseline hyperpolarized as the Vm underwent high amplitude rhythmic fluctuations lasting 1-2 seconds in duration. When 3-5 Hz Vm oscillations coincided with visual cues, excitatory neuron responses to preferred cues were significantly reduced. Despite this disruption to sensory processing, visual cues were critical for evoking 3-5 Hz Vm oscillations when animals performed discrimination tasks and passively viewed drifting grating stimuli. Using pupilometry and animal locomotive speed as indicators of arousal, we found that 3-5 Hz oscillations were not restricted to unaroused states and that they occurred equally in aroused and unaroused states. Therefore, low frequency Vm oscillations play a role in shaping sensory processing in visual cortical neurons, even during active wakefulness and decision making.

1.2 Introduction

Low frequency (<15 Hz) membrane potential (Vm) oscillations were first described during slow-wave sleep and anesthetized states, but were found to be absent in the Vm of awake animals (Destexhe et al., 2003; Steriade et al., 1993; 2001; Woody and Gruen, 1978). Over time, studies have shown that strong low frequency Vm fluctuations exist in the cortical neurons of awake animals, but only when animals are immobile(Bennett et al., 2013; Crochet and Petersen, 2006; Polack et al., 2013; Poulet and Petersen, 2008; Schneider et al., 2014; Wiest and Nicolelis, 2003; Zhou et al., 2014), unaroused (as indicated by pupilometry; (McGinley et al., 2015; Reimer et al., 2014; Vinck et al., 2015), or unstimulated (Tan et al., 2014). Yet, it is still unclear if low frequency Vm oscillations play a functional role in processing sensory signals in awake animals and if they are exclusive to quiescent periods associated with low arousal.

We identified stereotyped 3-5 Hz Vm oscillations occurring in primary visual cortex (V1) layer 2/3 (L2/3) neurons of awake mice placed in a wide range of behavioral and sensory contexts. During these 3-5 Hz Vm oscillations, neurons' baseline Vm became hyperpolarized and displayed high-amplitude (10-20 mV) fluctuations that lasted only 1-2 seconds in length. Functionally, 3-5 Hz Vm oscillations significantly reduced the responsiveness of excitatory neurons, whereas inhibitory parvalbumin- and somatostatin-positive (PV+, SOM+) neurons fired rhythmically at the peak of each oscillatory cycle. Even though 3-5 Hz Vm oscillations disrupted visual processing, visual stimulation was critical for eliciting 3-5 Hz Vm oscillations when animals actively discriminated and passively viewed drifting grating visual stimuli. Moreover, we found that these low frequency Vm oscillations were not exclusive to unaroused behavioral states and occurred at equal rates in aroused and unaroused animals. As a result, our findings show a distinct role for low frequency Vm oscillations in aroused and unaroused

animals, challenging the hypothesis that low frequency Vm oscillations are restricted to unaroused behavioral states.

1.3 3-5 Hz Vm oscillations are highly stereotyped, synchronized, and transient network events that selectively reduce the responsiveness of excitatory neurons

We performed two-photon guided whole-cell Vm recordings from 40 excitatory V1 L2/3 neurons in head-fixed mice free to run or rest on a spherical treadmill (Figure 1A). For each recording, electrocorticogram (ECoG) activity was simultaneously acquired within the vicinity (300-500 μm) of the patch-clamp pipette tip. In all our recordings, we detected distinct epochs of high amplitude 3-5 Hz Vm oscillations that appeared very similar across recordings (Figure 1). During 3-5 Hz Vm oscillations, the neuron's baseline Vm substantially hyperpolarized (Figure 1B,C,F, mean change in Vm baseline = -11.6 mV, σ (standard deviation) = 4.5 mV) and displayed high amplitude (Figure 1B,C,G, mean trough to peak amplitude = 17.3 mV, σ = 4.2 mV) rhythmic depolarizations (Figure 1B,D,E,H, mean frequency = 4.2 Hz, σ = 0.4 Hz) that typically lasted for 1-2 seconds (Figure 1B,E,I, mean duration = 1.6 seconds σ = 0.38 seconds). When we calculated the Pearson correlation coefficient comparing 3-5 Hz Vm oscillation to each other and a portion of the recording of equal length 4 seconds prior to each 3-5 Hz Vm oscillation, we found that 3-5 Hz Vm oscillations were correlated to each other, but not to the periods without oscillations in single neuron examples (cell 8; WSRT, $p < 0.0001$; Figure 1J-K) and across all excitatory neurons (WSRT, $p < 0.0001$; Figure 1L). As a result, 3-5 Hz Vm oscillations are stereotyped events defined by a specific frequency, oscillation amplitude, baseline hyperpolarization, and duration.

Because excitatory neurons' Vm hyperpolarized and neared threshold only during the depolarized phase of 3-5 Hz oscillations, we hypothesized that their responsiveness to visual stimuli could decrease during 3-5 Hz oscillations. So, we investigated how excitatory neurons responded when mice were presented with full-screen drifting gratings to the monocular visual field contralateral to the hemisphere of the brain where the recording was made. In the presence of 3-5 Hz Vm oscillations, the response to preferred stimuli was nearly abolished (2.82 ± 0.71 $Sp.s^{-1}$ No Osc. & Preferred stimulus; 0.75 ± 0.18 $Sp.s^{-1}$ Osc. & Preferred stimulus; n=40 neurons; WSRT, $p = 8.1 \times 10^{-5}$; Figure 2A,B). Moreover 3-5 Hz Vm oscillations dominate Vm spectral properties when 3-5 Hz Vm oscillations coincide with visual cues (Figure 2C).

To investigate if 3-5 Hz Vm oscillations were specific to excitatory neurons, we also performed two-photon guided whole-cell Vm recordings from PV+ (n = 6) and SOM+ (n = 7) neurons in separate experiments as animals passively viewed identical drifting gratings (Figure 3). The oscillation frequency (One-Way ANOVA p = 0.81), duration (One-Way ANOVA, p = 0.69), and baseline hyperpolarization (One-Way ANOVA, p = 0.55) were similar in excitatory, PV+, and SOM+ neurons (Figure 3E-F). However, PV+ interneurons exhibited larger amplitude depolarizing events (One-Way ANOVA, p= 0.01) than excitatory (WRST, Bonferroni adjusted p=0.04) and SOM+ (WRST, Bonferroni adjusted p = 0.01) neurons did during oscillatory periods. As a result, 3-5 Hz Vm oscillations are present and nearly identical in excitatory, PV+, and SOM+ V1 L2/3 neurons.

In contrast to excitatory neurons, PV+ and SOM+ neurons tended to fire strongly at the peak of 3-5 Hz Vm oscillations (Figure 3B). The percent of peaks where at least one action potential was elicited was significantly lower (One-Way ANOVA, $p < 0.0001$) in excitatory neurons than in PV+ (WRST, Bonferroni adjusted p = 0.0001) and SOM+ neurons (WRST, p = 0.0008). On average, the firing rate per cycle of the oscillation was also significantly lower (One-Way ANOVA, $p < 0.0001$) in excitatory neurons than in PV+ (WRST, Bonferroni adjusted p = 0.0001) and SOM+ (WRST, Bonferroni adjusted p = 0.0006). Correspondingly, the visually-

evoked firing rate in the presence and absence of 3-5 Hz Vm oscillations was not different in PV+ (two-way repeated-measures ANOVA, $p = 0.83$) and in SOM+ neurons (two-way repeated-measures ANOVA, $p = 0.86$) (Figure 3C). The spontaneous firing rate was slightly reduced in excitatory neurons (Figure 3D, WSRT, $p = 0.034$), but not in PV+ (Figure 3D, WSRT, $p = 0.13$) and SOM+ (Figure 3D, WSRT, $p = 0.25$) neurons, during 3-5 Hz Vm oscillations

To identify whether 3-5 Hz Vm oscillations were isolated to individual neurons or if other neurons in the local network oscillated synchronously with each other, we compared the timing of the average cycle in the Vm to the local V1 ECoG trace (Figure 4A-C). The mean phase offset between the ECoG and Vm was not different (One-Way ANOVA, $p = 0.28$) between all three cell types (mean phase offset, excitatory neurons: -7.5° ± 2.2°, PV+ neurons: -12.3° ± 3.8°, SOM+ neurons: -14.6° ± 3.1°; Figure 4C). Additionally, the Vm and ECoG were significantly more correlated during 3-5 Hz Vm oscillations than in the second following oscillation offset in excitatory (WSRT, $p = 3.2e\text{-}8$), PV+ (WSRT, $p = 0.004$), and SOM+ (WSRT, $p = 5.8e\text{-}4$) neurons (Figure 4D). There was no difference in peak Vm-ECoG correlation coefficient during oscillations in excitatory, PV+, and SOM+ neurons (One-Way ANOVA, $p = 0.64$; Figure 4D). These data suggest that 3-5 Hz Vm oscillations occurred synchronously in L2/3 V1 neurons. Yet, only excitatory neurons showed a reduction in responsiveness to visual cues.

To understand if 3-5 Hz Vm oscillations altered the local network state, we analyzed how low and high frequency ECoG power varied before, during, and after 3-5 Hz Vm oscillations (Figure 4E). During 3-5 Hz Vm oscillations in all neurons, 30-50 Hz ECoG power was decreased (One-Way ANOVA, $p < 0.0001$) during the oscillation as compared to the two seconds before (WSRT, Bonferroni adjusted $p < 0.0001$) and after (WSRT, Bonferroni adjusted $p = 0.0001$) the oscillatory epoch. Likewise, 3-5 Hz ECoG power increased (One-Way ANOVA, $p = 0.0012$) during the oscillation as compared to before (WSRT, Bonferroni adjusted $p <$

0.0001) and after (WSRT, Bonferroni adjusted $p < 0.0001$) the oscillatory epoch. In tandem, 3-5 Hz Vm power was significantly raised (One-Way ANOVA, $p < 0.0001$) during the oscillation as compared to directly before (WSRT, Bonferroni adjusted $p < 0.0001$) and after (WSRT, Bonferroni adjusted $p < 0.0001$) the oscillatory epoch (Figure 4F). Therefore, 3-5 Hz Vm oscillations occur during distinct periods of increased low and decreased high frequency ECoG power and constitute a brief interruption of ongoing network dynamics.

1.4 3-5 Hz Vm oscillations are recruited by visual stimuli

Visual stimulation, activity, arousal, and behavior have all been shown to affect the presence of low frequency Vm fluctuations in visual cortical neurons of awake animals (Bennett et al., 2013; McGinley et al., 2015; Polack et al., 2013; Reimer et al., 2014; Tan et al., 2014). To test these variables in relation to 3-5 Hz Vm oscillations, we decided to investigate the Vm dynamics in animals performing visual and auditory discrimination tasks. Mice were trained to perform a visually ($n = 17$) or auditory ($n = 7$) guided go/no-go discrimination task prior to whole-cell recordings (Figure 5A,B). During the task, animals had to decide whether to lick for a water drop (go) or withhold licking (no-go) based on visual cues (go stimulus: 45° drifting gratings or 5 kHz pure tone; no-go stimulus: 135° drifting gratings or 10 kHz pure tone; Figure 5B). Visual or auditory stimuli were displayed for 3 seconds, and animals had to make their decision in the final second of the visual stimulus presentation (the response period). Animals reliably learned how to perform the visual task in 5 to 10 training sessions and the auditory task in 1-3 sessions (Figure 5C). All task behavioral parameters were identical in the visual and auditory tasks, except for the modality of the stimuli. During the auditory task, the monitor remained in the recording apparatus in the same location as the visual task and displayed an isoluminant grey screen which was identical to the grey screen displayed during inter-trial intervals during the visual task.

When whole-cell recordings from V1 L2/3 were obtained in the trained animals, oscillations were recruited much more frequently during behavior when animals were exposed to drifting grating stimuli (Figure 6A-C). The probability of a 3-5 Hz Vm oscillation occurring during a trial was approximately four-fold higher during the visual task than during the auditory task (auditory n = 7, visual n= 21, p = 0.003 WRST). During the visual task, oscillations were initiated on average 1.71 ± 0.12 seconds (n = 21 neurons) after visual stimulus onset and were twice as likely to occur during visual stimulation than during inter-trial intervals (Figure 6D, right). As found previously, 3-5 Hz Vm oscillations coinciding with visual stimulation reduced the responsiveness of neurons to optimal visual stimuli (WSRT, p = 0.001) but not orthogonal stimuli where response magnitude was already low (WSRT, p = 0.68; Figure 6E). No difference was detected in oscillation duration (WRST, p = 0.27) and oscillation onset latency from stimulus onset (WRST, p = 0.64) between animals performing the visual and auditory tasks. The difference between oscillation probability during visual and auditory discrimination tasks was unlikely to be explained by differences in locomotion given that the probability of locomotion (WRST, p = 0.76, Figure 6F) was not different during visual and auditory discrimination tasks. Similarly, the animal's performance was similar for visual and auditory tasks (WRST, p = 0.37, Figure 6F); the mean D' for both tasks exceeded 2, and the median hit and false alarm rates were 96% and 33%, respectively, during visual discrimination.

To test whether non-salient visual cues could elicit 3-5 Hz Vm oscillations during behavior, a subset of animals (n = 5) performed trials of the auditory task where non-salient visual cues (the visual cues did not predict reward) were displayed simultaneously with salient auditory cues (Figure 6G). Displaying visual cues rescued oscillation recruitment during the auditory task as there was no difference in the probability of evoking an oscillation during the auditory task + visual cues (A+V Task) and the traditional visual discrimination task (Figure 6G-H). However, oscillations probability was not significantly different between when the stimulus was on or off in the A+V task (WSRT, p = 0.17, Figure 6H). This finding suggests that

visual stimulation itself, not its behavioral salience, plays a critical role in provoking 3-5 Hz oscillations.

1.5 Behavioral context does not change the overall probability of oscillations, but does affect their timing

Visual cues reliably recruited 3-5 Hz Vm oscillations in untrained animals not performing a behavior (Figure 7). The number of 3-5 Hz Vm oscillations elicited per minute of recording during passive viewing of drifting gratings was significantly higher than during periods when no visual cues were shown for at least 5 minutes (WSRT, p = 1e-7) in untrained animals naïve to the visual stimuli (Figure 7A). Similarly, the number of 3-5 Hz Vm oscillations per minute was significantly different when animals performed the visual task in comparison to the auditory discrimination task (WRST, p = 0.008; Figure 7B). Finally, the probability of evoking an oscillation during a trial (stimulus and inter-trial interval) of the visual task and passive viewing was not different (WRST, p = 0.26, Figure 7C). Note that visual cues during passive viewing and visual discrimination were identical except in their duration (1.5 seconds during passive viewing, 3 seconds during visual discrimination). Therefore, 3-5 Hz Vm oscillations were elicited by visual cues to a similar degree in trained animals performing a visual discrimination task and untrained animals passively viewing drifting gratings.

However, the timing of 3-5 Hz Vm oscillations in relation to visual stimuli was markedly different in these two behavioral contexts. During passive viewing of either 1.5 or 3 second visual stimuli, the mean probability of oscillations occurring at the offset of the stimulus was 2.2 (n = 53, WSRT, p = 7.2e-9) and 2.5 (n = 9, WSRT, p = 0.004) fold greater than the probability of occurrence during visual stimuli, respectively (Figure 7D-E). As a result, 3-5 Hz Vm oscillation probability was higher during the visual stimulus (WRST, p = 0.001; Figure 7E, left) and lower after the visual stimulus (WRST, p = 0.007; Figure 7E, right) in active behavior as compared to passive viewing. Though, when 3-5 Hz Vm oscillations coincided with visual

cues, the responsiveness of excitatory neurons to cues that evoked a strong response was reduced during passive viewing (Figure 2A-B). The probability that a neuron was recruited in a 3-5 Hz Vm oscillation did not depend its orientation tuning in passive viewing (One-Way ANOVA, $p = 0.76$) and visual discrimination (WSRT, $p = 0.34$, Figure 7F-G).

3-5 Hz Vm oscillation prevalence and timing were also investigated in the context of animals' responses during visually-guided behavior (Figure 8). 3-5 Hz Vm oscillation prevalence was significantly higher during trials when animals correctly withheld licking (correct rejection, CR; see Figure 4B for schematic of behavior) than during trials when animals initiated a licking response either correctly (hit) or incorrectly (false-alarm, FA; n=21, WSRT Bonferroni Corrected $p = 0.046$, $p = 0.04$, respectively; Figure 8A). Importantly, the visual stimulus was identical in FA and CR trials. Yet, there was no difference in 3-5 Hz Vm oscillation prevalence between incorrect and correct behavioral response (Hit vs FA, WSRT Bonferroni Corrected, $p = 0.9$; CR vs Miss, WSRT Bonferroni Corrected, $p = .86$; Figure 8A). Additionally, 3-5 Hz Vm oscillation duration was slightly longer during CR trials than during hit trials (WSRT Bonferroni Corrected, $p = 0.035$), but not FA trials (WSRT Bonferroni Corrected, $p = 0.3$; Figure 8B). The high prevalence of 3-5 Hz Vm oscillations during CR trials disproves the hypothesis that the motor action associated with licking response triggers oscillations because licking is typically absent during CR trials. Moreover, animals did not receive rewards during CR trials, indicating that reward expectation was not the primary factor in evoking 3-5 Hz oscillations in V1.

Additionally, 3-5 Hz oscillation onset typically occurred after licking onset for correct (Hit, WSRT, $p = 0.01$) and incorrect (FA, WSRT, $p = 0.001$) go responses (Figure 8C). On a trial by trial basis, oscillation onset followed licking in 86 ± 0.6% (n=21) of Hit and FA trials on average by 0.47 ± 0.05 seconds. For trials where licking preceded the response period in correct no-go trials (CR), licking offset occurred prior to 3-5 Hz oscillation onset (WSRT, $p = 0.031$). There was no difference in oscillation onset time across behavioral responses

(Repeated Measures One-Way ANOVA, p = 0.35). Therefore, 3-5 Hz oscillations tended to follow the animal's behavioral response to the go/no-go visual cue.

1.6 3-5 Hz Vm oscillations occur during high and low arousal states during visual discrimination

Locomotion and dilated pupils, both indicators of a high arousal state and increased noradrenergic tone, have been linked to suppression of 1-10 Hz Vm fluctuations in V1 neurons of awake mice (Bennett et al., 2013; McGinley et al., 2015; Polack et al., 2013; Reimer et al., 2014; Vinck et al., 2015). To investigate how arousal contributes to 3-5 Hz oscillation generation, we analyzed how locomotion and pupil size correlated with oscillation probability during the visual discrimination task (Figure 9A). Locomotion was measured in all animals who completed the visual discrimination task (n = 21). Four animals who completed visual discrimination also had pupil size measured concurrently to whole-cell recording. Presence of locomotion (sustained treadmill motion greater than 2 cm/s for at least 1 second, see methods) during trials of the visual discrimination task did not change oscillation probability during a trial of task (WSRT, p = 0.76; Figure 9B,D). Moreover, the oscillation incidence was not different during the locomotion and stationary periods (Figure 9F). Similarly, there was no difference in oscillation probability between trials when the mean pupil size was dilated (pupil size greater than 50%) or constricted (pupil size less than 50%; WSRT, p = 0.63; Figure 9C,E). In addition, the oscillation incidence was similar across a wide range of pupil sizes (One-Way ANOVA, p = 0.96; Figure 9G), showing that 3-5 Hz Vm oscillations occur during both low and high arousal states.

3-5 Hz Vm oscillations were correlated with small reductions in speed and pupil size during oscillations (Figure 10B). Locomotion speed was slightly lower (One-Way repeated measures ANOVA, p < 0.0001) during the oscillations compared to before (WSRT, Bonferroni

corrected p = 0.0001) and after (WSRT, Bonferroni corrected p = 0.0176) the oscillation (Figure 10B). Locomotion speed was also slightly lower after 3-5 Hz Vm oscillations than before oscillations occurred (p = 0.0011; Figure 10B). While animals on average slowed during the oscillation, they did not terminate locomotion. Pupil size was more constricted during the oscillation as compared to before the oscillation (WSRT, Bonferroni corrected p = 0.028), but was no different as compared to after the oscillation (WSRT, Bonferroni corrected p = 0.34; Figure 10C). Moreover, there was no difference in pupil size before and after the oscillation (WSRT, Bonferroni corrected p = 0.79; Figure 10C, right).

In other studies of Vm in awake mice, locomotion onset and offset has been explicitly linked to the reduction and generation of 1-10 Hz fluctuations in the Vm of cortical neurons, respectively (Poulet and Petersen, 2008; Reimer et al., 2014; Vinck et al., 2015). To investigate whether locomotion onset or offset affects 3-5 hz Vm oscillation probability, we calculated the probability of an oscillation occurring in 3 seconds before or after locomotion onset and offset (Figure 9D-E). We found that the probability of evoking a 3-5 Hz Vm oscillation just after locomotion onset was slightly lower than prior to locomotion onset (WSRT, p = 0.012; Figure 9D). However, the probability of an oscillation occurring following locomotion offset was no different than the probability of an oscillation occurring just prior to locomotion offset (WSRT, p = 0.36; Figure 9E). Therefore, locomotion onset may have a slightly suppressive effect on 3-5 Hz Vm generation, however locomotion offset has no discernable effect on evoking 3-5 Hz Vm oscillations.

Pupil constriction has recently been shown to closely correspond with increased 2-10 Hz Vm amplitude (Reimer et al., 2014). We identified when the pupil was dilating or constricting (Figure 10A) in our recordings and then analyzed 3-5 Hz Vm oscillation probability at pupil dilation and constriction onset (Figure 10F,G). The probability of evoking a 3-5 Hz Vm oscillation was no greater after pupil dilation (WSRT, p = 0.91) or pupil constriction (WSRT, p = 0.25) onset than immediately preceding the dilation or constriction. These data do not

contradict prior findings 1-10 Hz Vm power can be tracked by following pupil size, especially since pupil size tends to decrease during 3-5 Hz Vm oscillations (Figure 10C). Instead, our data suggest that 3-5 Hz Vm oscillations are distinct events that exist within the 2-10 Hz power band, but do not represent all periods when 2-10 Hz power is increased in awake animals. This hypothesis is corroborated by the finding that the Vm power spectra differ significantly during 3-5 Hz Vm oscillations and at constriction onset (Figure 10H). Finally, the pupil size did not increase during visual stimulus presentations, and pupil x and y movements were limited during visual stimulation (Figure 10I,J).

1.7 Discussion

We describe stereotyped 3-5 Hz Vm oscillations in V1 L2/3 neurons that significantly reduce the responsiveness of excitatory neurons. During these oscillations, individual neuron's Vm fluctuated in phase with the local network, creating a transient synchronous brain state marked by rhythmic firing of inhibitory PV+ and SOM+ neurons. Despite this disruption in coding of visual information, 3-5 Hz Vm oscillations were evoked by visual stimulation and occurred frequently in animals passively viewing drifting gratings or performing an active discrimination task. The probability of an oscillation occurring during a stimulus was unchanged by locomotion or pupil size, suggesting that these transient oscillations occur in both high and low arousal states.

Similar low frequency Vm oscillations have been observed in passing in visual (Bennett et al., 2013; Polack et al., 2013), barrel (Crochet and Petersen, 2006; Poulet and Petersen, 2008), auditory (McGinley et al., 2015; Schneider et al., 2014; Zhou et al., 2014), and motor (Zagha et al., 2015) cortex neurons in awake mice. While the 3-5 Hz Vm oscillations described in this study seem to be present in example traces in these prior studies, they were not isolated as specific events and clumped together with other factors that contributed to increased 1-10

Hz Vm power during long periods where animals were inactive or lowly aroused. We show that these 3-5 Hz Vm oscillations are distinct low frequency events that occur when animals are active or inactive, challenging the hypothesis that significant low frequency fluctuations in Vm are exclusive to idle animals. Moreover, 3-5 Hz Vm oscillations are not canonical UP and DOWN states as these Vm oscillations are faster with significantly shorter depolarized time than the UP and DOWN oscillations that are typically square shaped (Haider et al., 2012; Petersen et al., 2003). In the future, it will be important to examine when 3-5 Hz Vm oscillations occur in other sensory areas and whether they have similar effects on sensory processing.

We hypothesize that 3-5 Hz Vm oscillations are local phenomena. Precedent exists for transient low frequency microsleep LFP events that reduce the firing of the network occurring in an isolated cortical network (Vyazovskiy et al., 2011). While the Vm of neurons becomes significantly more correlated to the ECoG (which was collected ~0.5 mm away from the whole-cell recording), the correlation coefficient magnitude tends to be low (~-0.2; Figure 3C) and variable between oscillatory epochs (Figure 2A). In similar Vm oscillations (1-10 Hz) observed in anesthetized cat preparations, weak correlations between Vm and EEG have been described as local to the cortical area (Lampl et al., 1999). Vm oscillations that extend across cortical areas, and even hemispheres, have been found in anesthetized animals, but tend to be at very low frequencies (<1Hz) and present with strong correlations between the Vm and EEG (Amzica and Steriade, 1995; Contreras and Steriade, 1995). As a result, 3-5 Hz Vm oscillations may be local and not global cortical events.

3-5 Hz Vm oscillations may decrease the responsiveness of excitatory neurons to sensory cues in at least one of the following ways: (a) the hyperpolarized Vm baseline during oscillatory sequences likely reduces the response magnitude to incoming signals (Carandini and Ferster, 1997; Cardin et al., 2008; Nowak et al., 2005); (b) during the depolarizing phases of the oscillations where excitatory neurons' Vm is closest to reaching spike threshold, excitatory neurons received strong perisomatic and dendritic inhibition from GABAergic PV+

and SOM+ neurons, respectively (Taniguchi, 2014) (Figure 2); (c) sensory signals out of phase with 3-5 Hz Vm oscillations could filter inbound sensory signals of a different time structure (i.e. incoming EPSPs at the trough of the oscillation would be less likely to drive the Vm to threshold) (Engel et al., 2001; Lakatos et al., 2008; Schroeder and Lakatos, 2009). The exact contribution of each of these three components to the suppression of visual responsiveness is still unclear. However, considering the combination of these three mechanisms, 3-5 Hz Vm oscillations represent a potent combination of inhibitory strategies to reduce the responsiveness of excitatory sensory neurons.

One role 3-5 Hz Vm oscillations could play is to reduce processing of irrelevant visual information. In our behavioral experiments, we found that 3-5 Hz Vm oscillations were most prevalent after animals had expressed their decision during visual discrimination, a point in the task when additional visual inputs were irrelevant to completing the task. Such a mechanism could be particularly useful during behaviors such as attention and working memory. When non-human primates ignore visual cues during attention tasks, neurons in V4 increase their correlated firing at frequencies between 3 and 5 Hz, spiking synchronizes within low frequency bands (<10 Hz) of the LFP (Fries et al., 2001b; Mitchell et al., 2009), and LFP power between 3-5 Hz increases (Fries et al., 2008). During visually-guided working memory tasks in non-human primates, prominent high-amplitude 4-8 Hz LFP oscillations appear in visual cortex and synchronize single-unit firing to the peaks of the oscillations during the delay period (Lee et al., 2005; Liebe et al., 2012). If coordinated subthreshold oscillations are responsible for producing these LFP and spiking patterns, their role may be to exclude processing of unattended cues during attention and task irrelevant visual information during working memory.

However, this hypothesis is challenged by our finding that 3-5 Hz Vm oscillations are provoked following visual stimulation during passive viewing. This phenomenon was independent of visual stimulus duration, disproving the hypothesis that oscillations are recruited at a fixed time following visual stimulus onset. While 3-5 Hz Vm oscillations remotely

resemble microsleep events, 3-5 Hz Vm oscillations did not disrupt task performance as microsleep events do in rats (Vyazovskiy et al., 2011). Visually evoked 3-5 Hz Vm oscillation recruitment did not significantly vary with motor activities, including licking and locomotion. So, it is very unlikely that grooming, which occurred rarely in our well-trained animals, or other unmeasured motor actions played a significant role in evoking 3-5 Hz Vm oscillations. Alternatively, 3-5 Hz Vm oscillations could be a transient analog of alpha LFP/EEG oscillations (8-12 Hz), a brain state in humans characterized by inhibition and thought to represent idling in cortical circuits (Klimesch, 2012; Moosmann et al., 2003; Pfurtscheller et al., 1996). But if this were the case, one would hypothesize 3-5 Hz Vm oscillations to be most frequent during times when the visual cortex is not engaged, such as during the auditory task or extended periods where visual cues were not shown to untrained animals. We observe the opposite of this in our study.

While the differences in the timing of oscillations during active behavior and passive viewing raises several questions, it does suggest that 3-5 Hz Vm oscillations are pertinent to behavior. This is reinforced by the finding that behavioral response in the visual discrimination task influences oscillation timing and recruitment. To better understand the role of 3-5 Hz Vm oscillations in behavior, it will be important to understand how 3-5 Hz Vm oscillations affect visual perception during behavior. Specifically, if short visual stimuli (<500 ms) coincide completely with 3-5 Hz Vm oscillations, animals may not be able perceive the stimulus to make a cued decision. If this were the case, 3-5 Hz Vm oscillations coinciding with a distracting visual cue could help an animal make the correct decision. This could be accomplished with a system that triggers short visual cues when oscillations occur. In addition, our study only examined interneuron activity during oscillations observed during passive viewing. Given the effects of pupil dilation and activity on SOM+ neurons, it will be important to confirm that interneurons behave similarly during 3-5 Hz Vm oscillations in active behaviors (Reimer et al., 2014). As a

result, many more studies will need to be completed to fully understand the role of 3-5 Hz Vm oscillations in behaving animals.

3-5 Hz Vm oscillation generation could be the result of resonant activity in the thalamocortical network. The thalamocortical loop is responsible for generating several natural and pathological oscillations, including oscillations in the 3-5 Hz range (Buzsáki and Draguhn, 2004; Desthexhe and Sejnowski, 2003; Steriade et al., 1993). Thalamocortical neurons switch between tonic spiking and oscillatory burst firing depending on their resting membrane potential, a phenomenon largely due to low-voltage activated T-type Ca^{2+} channels (Contreras, 2006; Halassa, 2011; Jahnsen and Llinás, 1984). Neuromodulatory inputs, including cholinergic and monoaminergic sources, regulate the resting membrane potential of thalamic neurons to allow or block the generation of oscillations (McCormick, 1989; Saper et al., 2005; Steriade et al., 1993). Given that neuromodulatory tone can play a key role in modulating visual processing (Chubykin et al., 2013; Disney et al., 2007a; McCormick et al., 1993; Pinto et al., 2013; Polack et al., 2013), it is conceivable that 3-5 Hz oscillations could be caused by a change in thalamic neuromodulation, allowing thalamocortical neurons to hyperpolarize and enter a burst state capable of generating 3-5 Hz oscillations. In support of this hypothesis, we find that 3-5 Hz Vm oscillations are correlated with a small decline in pupil size, which could be indicative of reduced locus coeruleus activity and norepinephrine signaling (Aston-Jones et al., 1999; Gilzenrat et al., 2010).

In conclusion, future studies will be needed to fully understand the cellular and network properties and behavioral significance of subthreshold 3-5 Hz oscillations. Further studies should focus on understanding how and where these oscillations are generated. In addition, it will be important to record these subthreshold oscillations in other brain areas during different behavioral tasks to understand whether they exert a similar role in sensory processing as in visual cortex and to clarify their role in during behavior.

1.8 Materials and Methods

All experimental procedures were approved by the University of California, Los Angeles Office for Animal Research Oversight and by the Chancellor's Animal Research Committees. Adult (2–12 months old) male and female C57Bl6/J, SOM-Cre (JAX number 013044) × Ai9 (JAX number 007909), and PV-Cre (JAX number 008069) × Ai9 mice were anesthetized with isoflurane (3–5% induction, 1.5% maintenance) ten minutes after injection of a systemic analgesic (carprofen, 5 mg per kg of body weight) and placed in a stereotaxic frame. Mice were kept at 37°C at all times using a feedback-controlled heating pad. Pressure points and incision sites were injected with lidocaine (2%), and eyes were protected from desiccation using artificial tear ointment. The skin above the skull was incised, a custom-made lightweight metal head holder was implanted on the skull using Vetbond (3M) and a recording chamber was built using dental cement (Ortho-Jet, Lang). Mice had a recovery period from surgery of five days, during which they were administered amoxicillin (0.25 mg per ml in drinking water through the water supply). After the recovery period, mice were habituated to head fixation on the spherical treadmill. On the day of the recording, mice were anesthetized with isoflurane. To fix the ground wire, a small craniotomy (0.5 mm diameter) was made above the right cerebellum and a silver wire was implanted at the surface of the craniotomy and fixed with dental cement. A circular craniotomy (diameter = 3 mm) was performed above V1 and a 3-mm diameter coverslip drilled with a 500-μm diameter hole was placed over the dura, such that the coverslip fit entirely in the craniotomy and was flush with the skull surface. The coverslip was kept in place using Vetbond and dental cement, and the recording chamber was filled with cortex buffer containing 135 mM NaCl, 5 mM KCl, 5 mM HEPES, 1.8 mM $CaCl_2$ and 1 mM $MgCl_2$. The head-bar was fixed to a post and the mouse was placed on the spherical treadmill to recover from anesthesia. The spherical treadmill was a ball floating on small cushion of air allowing for full 2D movement. Ball motions were tracked with a custom-made tracker that reported x and y speeds at 100 Hz.

All recordings were performed at least two hours after the end of anesthesia, when the mouse was alert and could actively participate in the behavioral task.

Long-tapered micropipettes made of borosilicate glass (1.5-mm outer diameter, 0.86-mm inner diameter, Sutter Instrument) were pulled on Sutter Instruments P-1000 pipette puller to a resistance of 3–7 MΩ, and filled with an internal solution containing 115 mM potassium gluconate, 20 mM KCl, 10 mM HEPES, 10 mM phosphocreatine, 14 mM ATP-Mg, 0.3 mM GTP, and 0.01–0.05 mM Alexa-594 (for experiments with C57Bl/6 mice) or Alexa-488 (for interneuron recordings). Pipettes were lowered into the brain under two-photon imaging guidance performed with a Sutter MOM microscope using a Ti-Sapphire Ultra-2 laser (Coherent) at 800 nm and a 40× 0.8 NA Olympus water-immersion objective. Images were acquired using Scanimage 3.2 software (Pologruto et al., 2003). Whole-cell current-clamp recordings were performed using the bridge mode of an Axoclamp 2A amplifier (Molecular Devices), then further amplified and low-pass filtered at 5 kHz using a Warner Instruments amplifier (LPF 202A). Recordings typically lasted 30 min (range 5 to 60 min). Recordings or parts of recordings with unstable membrane potential and/or action potentials < 35 mV were excluded from analysis. ECoG recordings were performed with an alternating/direct current differential amplifier (Model 3000, A-M system) and band-pass filtered at 0.1–3,000 Hz. Analog signals were digitized at 12415 Hz with WinEDR (Strathclyde University) using a NIDAQ card (National Instruments). To ensure synchrony between physiological signals and behavioral epochs, signals relevant to the behavioral task (licking, water delivery, visual/auditory cue characteristics and timing, locomotion, and pupil size) were recorded in tandem with electrophysiological signals by the same NIDAQ card. We recorded 40 excitatory, 6 PV+, and 7 SOM+ neurons from 29, 5, and 6 untrained mice, respectively, in separate experiments to ascertain 3-5 Hz oscillation activity during spontaneous behavior and passive viewing. Excitatory neurons were identified *post hoc* by using half-height spike widths (>0.6 ms) and

mean evoked firing rate (< 4 sp/s) to cluster units. We recorded 21 neurons from 17 trained mice in separate experiments to ascertain 3-5 Hz oscillation activity during visual and auditory discrimination.

A 40-cm diagonal LCD monitor was placed in the monocular visual field of the mouse at a distance of 30 cm, contralateral to the craniotomy. Custom-made software developed with Psychtoolbox in MATLAB was used to display drifting sine wave gratings (series of 12 orientations spaced by 30 degrees randomly permuted, temporal frequency = 2 Hz, spatial frequency = 0.04 cycle per degree, contrast = 100%). For passive viewing, the presentation of each orientation lasted 1.5 or 3 s and was followed by the presentation of a gray isoluminant screen for an additional 1.5 or 3 s, respectively. The electrophysiological signal was digitized simultaneously with two analog signals coding for the spatial and temporal properties of the grating. The treadmill motion was measured every 25 ms (40 Hz) by an optical mouse whose signal was converted into two servo pulse analog signals (front-back and left-right) using an external PIC microcontroller, and acquired simultaneously with the electrophysiological data. Importantly, the monitor was placed in the exactly the same way during the auditory discrimination task as it was placed during the visual discrimination task, and a grey screen, which was identical to that during the inter-trial interval of the visual discrimination task and isoluminant to the drifting visual cues, was displayed throughout auditory discrimination trials. As a result, the luminance conditions were identical during visual and auditory discrimination trials.

C57Bl/6J mice (Jackson Labs) with head-bar implants were water-deprived to 90% of their body weight and acclimated to head-fixation on a spherical treadmill in custom-built, sound-proof training rigs. Each rig was equipped with a monitor (Dell), water dispenser with a built-in lickometer (to monitor licking, infrared beam break) (Island-Motion), an infrared camera

(Microsoft), and stereo speakers (Logitech). In addition, data acquisition boards (National Instruments) were used to actuate water delivery and vacuum reward retrieval as well as monitor animal licking. Data acquisition boards and the monitor were connected to a laptop (Dell), which ran the custom-made training program (MATLAB). Once animals reached the target weight, animals were acclimated to the spherical treadmill over 3 days before being trained to discriminate visual stimuli or auditory. In the visual discrimination task, drifting sine-wave gratings at one orientation were paired with a water reward, and the animal was expected to lick (go). Orthogonal drifting gratings signaled the absence of reward, and the animal was expected to withhold licking (no-go) during these trials. In the auditory discrimination task, a 100 dB 5 kHz pure tone indicated Go trials and a 100 dB 10 kHz pure tone indicated No-Go trials.

Each trial lasted three seconds. The visual or auditory stimulus was present for the duration of the trial. When the stimulus instructed the animal to lick, water was dispensed two seconds after stimulus onset. No water was dispensed in the no-lick condition. Licking was only assessed during the final second of the trial. If the animal responded correctly, the inter-trial interval (ITI) was 3 seconds. If the animal responded incorrectly, the ITI was increased to 9.5 seconds as negative reinforcement. If the animal missed a reward, the reward was removed by vacuum at the end of the trial. Animals performed 300-500 trials daily. During the auditory task with visual cues task, visual cues identical to those used in the visual discrimination task were displayed at the same times that auditory cues were played. Visual cues did not correlate with reward in this condition.

Performance was measured using the D' statistic (D'=norminv(fraction trials with correct licking) – norminv(fraction trials with incorrect licking), norminv = inverse of the normal cumulative distribution function), which compares the standard deviation from chance performance during lick and no-lick trials (chance D'=0). Animals were considered experts if

their sessions average D' > 1.7 (probability of chance behavior < 0.1%, Monte Carlo Simulation).

To record pupil size, the infrared filter and lens was removed from a webcam (Microsoft LifeCam HD-3000, ~30 Hz frame rate) and was fitted with a 50 mm fixed focal length lens (Thorlabs MVL50M23). The camera was placed approximately 0.5 meters ipsilateral to the monitor displaying visual cues, and a generic infrared lamp was used to provide strong illumination of the eye. To read the pupil size and movements, the camera was operated by custom scripts (MATLAB) that used thresholding to isolate the pupil from the eye and measure pupil properties. The software then created scaled analog signals relaying the pupil area and position to the electrophysiology recording apparatus such that pupil measurements were acquired in sync with the electrophysiological and behavioral data. Videos were also saved for *post-hoc* analysis as necessary. Pupil size was normalized to the maximum pupil size in pixels. To isolate pupil dilation and constricting episodes, we computed the first derivative of the filtered (1 Hz low pass filter) pupil area trace in time. Periods when the first derivative was greater than or less than 0 were recorded as dilation or constriction events, respectively. To remove events where constriction or dilation was negligible, events where total pupil size change was less than 5% were eliminated.

Data analysis was performed using custom routines in MATLAB. The 3-5 Hz oscillations were defined as stereotyped low frequency and high-amplitude oscillations of the Vm superimposed on a steady hyperpolarizing envelope (see examples in Figs. 1A-C, 2A, 3A, 4A, 6A-B, 9A, 10A). We were able to isolate the oscillations in all recorded neurons using a semi-automated method that detected candidate oscillation locations using these metrics and then gathered human input to finalize oscillation start and stop times. The beginning and end of 3-5 Hz Vm oscillations were defined as the start of the hyperpolarization and the time when

the neuron had repolarized, respectively (See Figure 1B for 10 detailed examples). Our MATLAB code to detect 3-5 Hz Vm oscillations is hosted at https://github.com/michaeleinstein/3-5-Hz/blob/master/get4hzOsc.m. After semi-automated detection, the whole trace was then scanned manually to ensure that all oscillations were detected. The Vm baseline was defined as the mean of the bottom 20^{th} percentile of the Vm distribution, and the change in Vm baseline during oscillations was defined as the baseline during the oscillation epoch minus the baseline one second prior to the oscillation epoch. Phase offset was obtained by calculating the difference in time between positive and negative peaks in low pass filtered (-3 dB @ 10 Hz) ECoG and Vm signals measured in degrees during oscillatory epochs. To compare firing rates evoked by visual stimuli during passive viewing and behavior with and without oscillations, trials with the presence of an oscillatory epoch at any point of visual stimuli were compared to visual stimuli without any oscillations. Plots showing oscillation probability over time were created by computing the mean oscillation probability in specific time bins. During the behavioral task, the optimal visual stimulus was defined as the stimulus that had a greater mean evoked firing rate. Locomotion on/off criteria were identical to Polack et al., 2013: locomotion onset and offset were defined when sustained treadmill was greater than and less than 2 cm/s for at least 1 second, respectively.

Unless stated otherwise, statistical significance was calculated by Wilcoxon Signed Rank Test (WSRT), Wilcoxon Rank-Sum Test (WRST), One Way Analysis of Variance (ANOVA), and Repeated Measures One-Way ANOVA. Scale bars and shading around means represent SEM unless indicated. Wilcoxon and non-repeated measures ANOVA tests were performed in MATLAB. Repeated measure ANOVA tests were performed in SPSS Statistics version 21 (IBM).

1.9 Figures

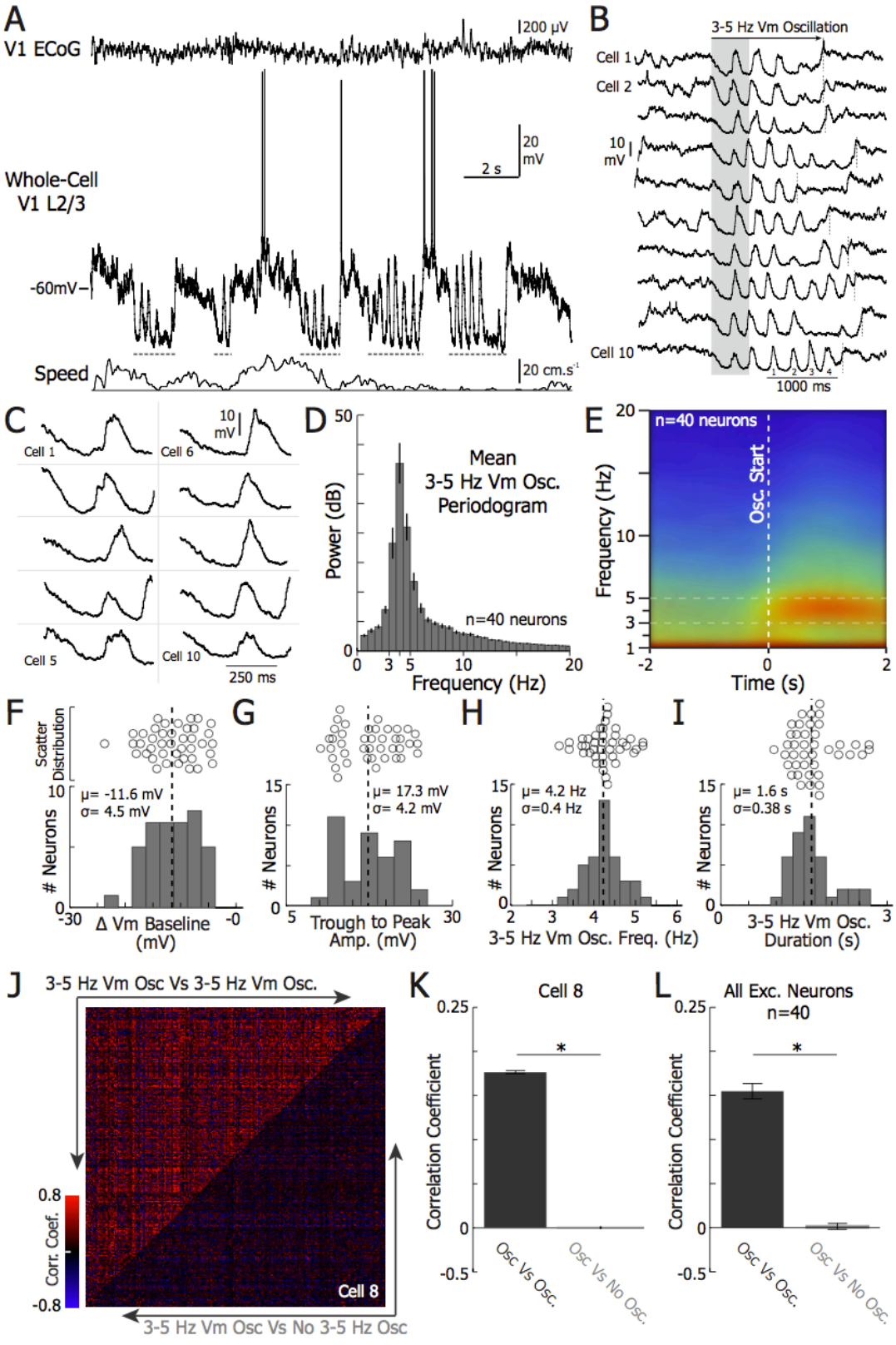
A
V1 ECoG
200 µV
Whole-Cell
V1 L2/3
2 s
20 mV
-60mV
Speed
20 cm.s-1
B
3-5 Hz Vm Oscillation
Cell 1
Cell 2
Cell 10
10 mV
1000 ms
C
Cell 1
Cell 6
Cell 5
Cell 10
10 mV
250 ms
D
Mean
3-5 Hz Vm Osc.
Periodogram
Power (dB)
n=40 neurons
Frequency (Hz)
E
n=40 neurons
Osc. Start
Frequency (Hz)
Time (s)
F
Scatter Distribution
µ= -11.6 mV
σ= 4.5 mV
Neurons
Δ Vm Baseline (mV)
G
µ= 17.3 mV
σ= 4.2 mV
Neurons
Trough to Peak Amp. (mV)
H
µ= 4.2 Hz
σ=0.4 Hz
Neurons
3-5 Hz Vm Osc. Freq. (Hz)
I
µ= 1.6 s
σ=0.38 s
Neurons
3-5 Hz Vm Osc. Duration (s)
J
3-5 Hz Vm Osc Vs 3-5 Hz Vm Osc.
Corr. Coef.
0.8
-0.8
Cell 8
3-5 Hz Vm Osc Vs No 3-5 Hz Osc
K
Cell 8
Correlation Coefficient
Osc Vs Osc.
Osc Vs No Osc.
L
All Exc. Neurons
n=40
Correlation Coefficient
Osc Vs Osc.
Osc Vs No Osc.

Figure 1-1. 3-5 Hz Vm oscillations are brief stereotyped events characterized by high amplitude 3-5 Hz fluctuations riding on a hyperpolarized baseline Vm.

(A) Example whole cell recording from a V1 layer 2/3 excitatory neuron during wakefulness, simultaneously recorded with the local electroencephalogram (ECoG, top) placed over V1 and the treadmill motion (locomotion, bottom). Grey dotted lines indicate times when 3-5 Hz oscillations were observed in the neuron's Vm. (B) Example 3-5 Hz Vm oscillations from 10 neurons. The beginning and end of the 3-5 Hz Vm oscillations are indicated by the left edge of the shaded box and the dotted vertical line, respectively. The cycles are numbered on cell 10 to demonstrate the frequency of the oscillations. (C) Zoom up of the shaded region in Figure 1B. Note the hyperpolarization and the similar amplitude of the oscillation across all 10 neurons. (D) The mean periodogram and (E) spectrogram during 3-5 Hz Vm oscillations collected from 40 neurons. (F) Histogram of the mean change in Vm baseline and (G) histogram of the mean trough to peak amplitude during 3-5 Hz Vm oscillations (n=40 neurons). (H) Histogram of the mean oscillation frequency and (I) histogram of the mean oscillation duration (n=40 neurons). Mean (μ) and standard deviation (σ) are shown on each histogram Scatter plots above each histogram further illustrate each distribution. (J) The Pearson correlation coefficient between each 3-5 Hz Vm oscillation (top left, 3-5 Hz Vm Osc Vs 3-5 Hz Vm Osc) and each 3-5 Hz Vm oscillation and a period of equal length 4 seconds preceding each 3-5 Hz Vm oscillation (bottom right, 3-5 Hz Vm Osc Vs No 3-5 Hz Vm Osc) for every oscillation in one neuron (cell 8, n = 289 3-5 Hz Vm oscillations). (K) The mean correlation coefficient between each 3-5 Hz Vm oscillation and each 3-5 Hz Vm oscillation compared to the two seconds prior to a 3-5 Hz Vm oscillation (cell 8, n = 289 3-5 Hz Vm oscillations; WSRT, $p < 0.0001$). (L) The mean correlation coefficient between each 3-5 Hz Vm oscillation and each 3-5 Hz Vm oscillation compared to the two seconds prior to a 3-5 Hz Vm oscillation averaged across all excitatory neurons (n = 40 neurons; WSRT, $p < 0.0001$). Error bars represent ±SEM.

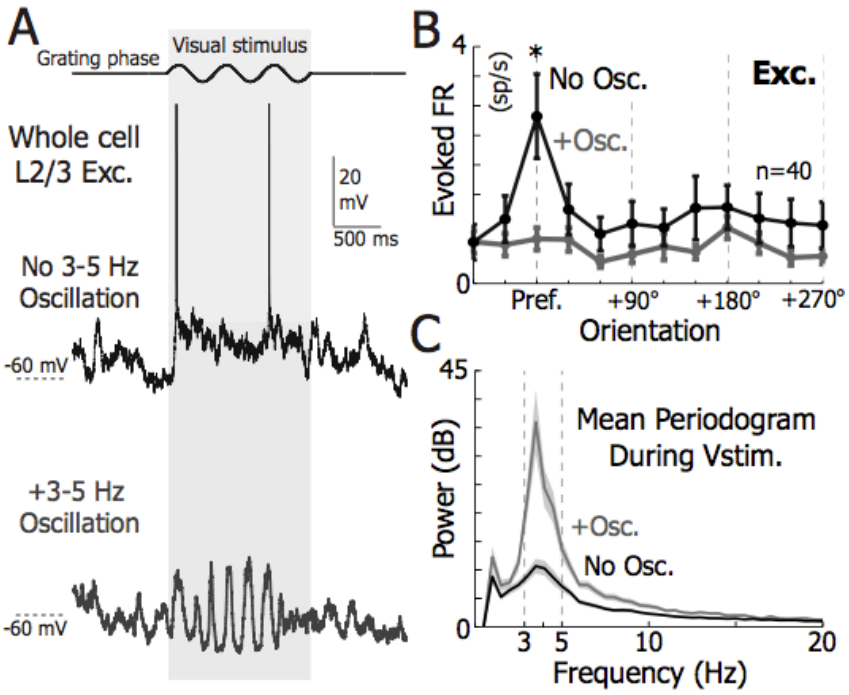

Figure 1-2. 3-5 Hz Vm oscillations reduce the responsiveness of V1 L2/3 neurons.

(A) Example response of an V1 L2/3 excitatory neuron to a 1.5 second full-screen drifting grating with (bottom) and without (top) a 3-5 Hz oscillation while stimulated at the preferred orientation. (B) The mean orientation tuning of excitatory neurons (n=40) in the presence (grey) and absence (black) of 3-5 Hz Vm oscillations. The firing rate at the preferred angle was significantly larger in the absence of oscillations for excitatory neurons (WRST, p = 8.1e-5). (C) The mean periodgram of the Vm during visual stimulation when a 3-5 Hz Vm oscillation is present (grey) and absent (black). Shading represent ±SEM.

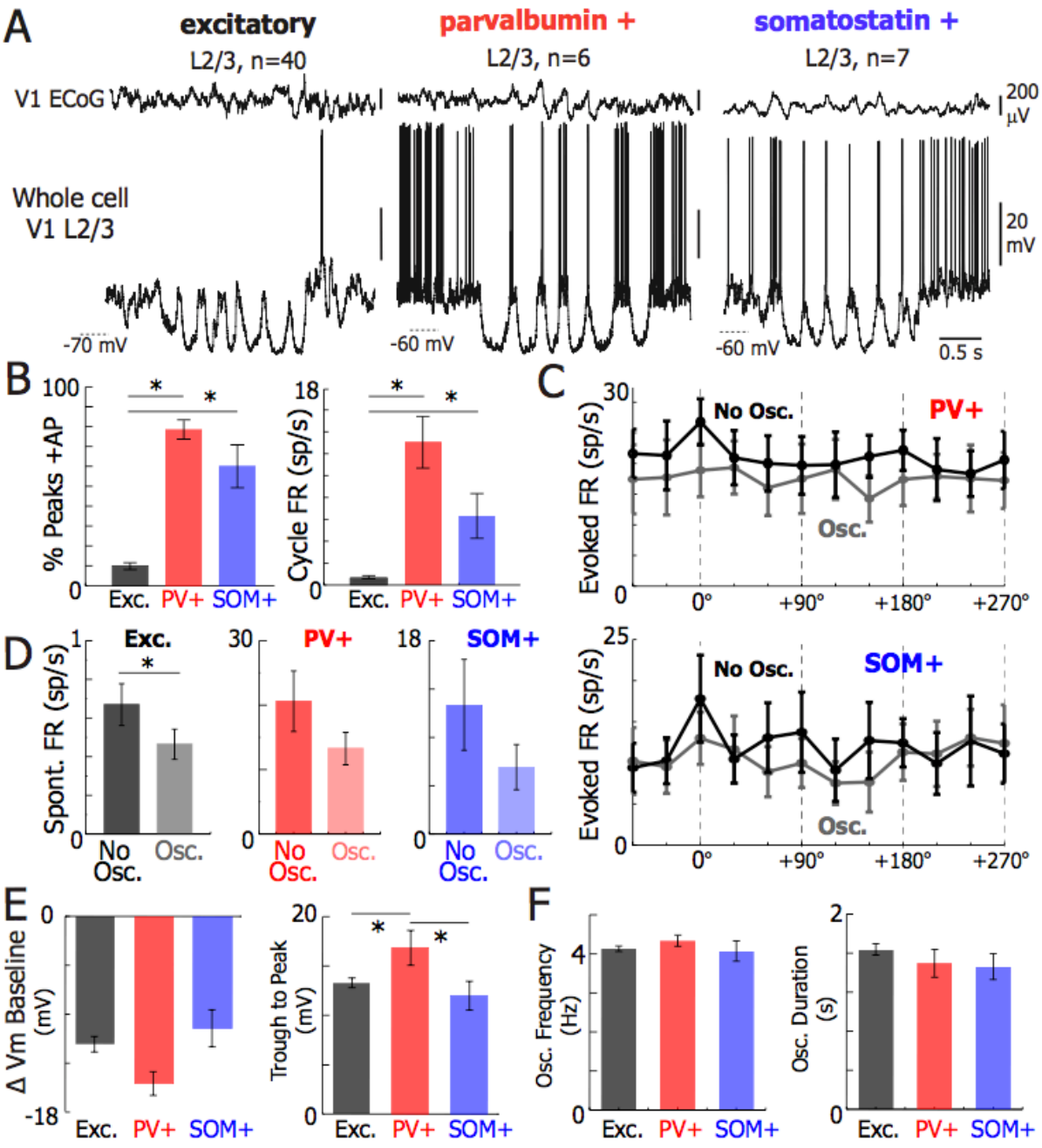

Figure 1-3. PV+ and SOM+ neurons fire at the peaks of 3-5 Hz Vm oscillatory cycles when excitatory neurons rarely fire.

(A) Simultaneous V1 ECoG (top) and whole-cell recordings (bottom) from V1 L2/3 excitatory (left), PV+ (center), and SOM+ (right) neurons during Vm 3-5 Hz oscillations. (B) The percent of peaks with at least one action potential (AP, left; One-Way ANOVA p = 2.71e-14) and the firing rate (FR) at the peaks of oscillations (One-Way ANOVA p = 2.71e-14) was significantly

lower in excitatory neurons than in PV+ (% AP, WRST, p = 0.0001; FR, WRST, p = 0.0001) and SOM+ (% AP, WRST, p = 0.0008; FR, WRST, p = 0.0006). (C) Mean tuning curve of PV+ and SOM+ neurons. (D) The baseline firing rates of excitatory (left), PV+ (middle), and SOM+ (right) neurons in the presence and absence of 3-5 Hz Vm oscillations. (E) Plots of the mean change in Vm baseline during 3-5 Hz oscillations (left) and mean oscillation trough to peak amplitude (right) for excitatory (black, n=40), PV+ (red, n=6), and SOM+ (blue, n=7) neurons. PV neurons experienced greater changes in trough to peak amplitude (One-Way ANOVA, p = 0.01) than excitatory neurons (Tukey-HSD, p = 0.01) and SOM+ neurons (Tukey-HSD, p = 0.04) during Vm 3-5 Hz oscillations. Change in Vm baseline was similar between neuronal types (One-Way ANOVA, p = 0.1). (F) Plots of mean frequency (left) and duration (right) of 3-5 Hz oscillatory periods in excitatory (black, n=40), PV+ (red, n = 6), and SOM+ (blue, n = 7). Oscillation frequency and duration were unchanged between neuronal types (One-Way ANOVA, p = 0.55 & p = 0.43, respectively). Error bars represent ±SEM.

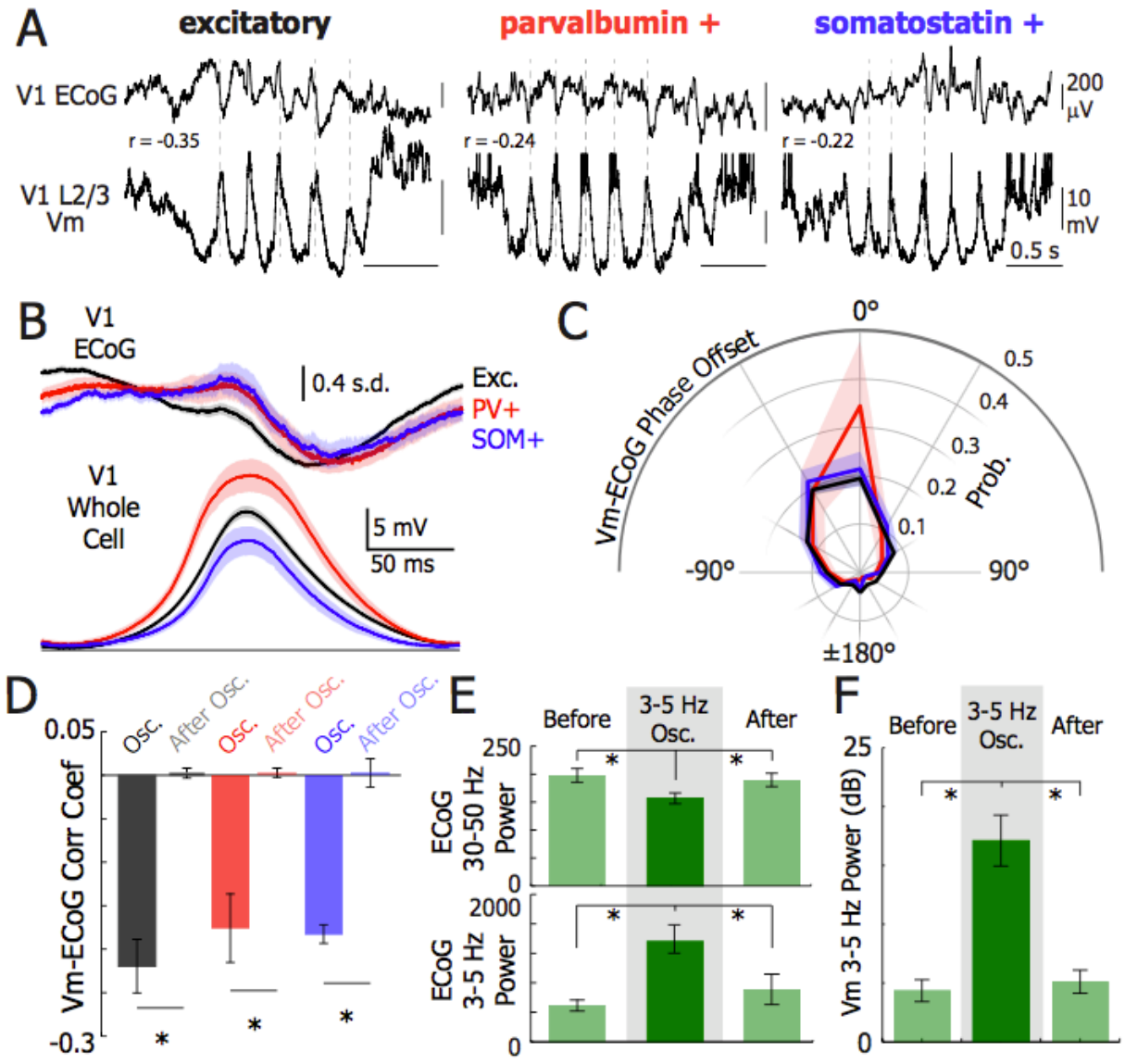

Figure 1-4. 3-5 Hz Vm oscillations represent a transient synchronized network state

(A) Example V1 ECoG (top) and V1 L2/3 Vm recordings from excitatory (left, black), PV+ (middle, red), and SOM+ (right, blue) neurons. Dotted grey lines were added to illustrate the phase relationship between the ECoG and Vm. (B) Mean V1 z-score normalized ECoG (top) and mean Vm for Exc. (black, n = 40), PV+ (red, n = 6), SOM+ (blue, n = 7) during an oscillation cycle. Traces were synchronized to the peak of the oscillation detected in the Vm. ECoG scale bar is standard-deviation (s.d.). (C) Mean Vm-ECoG phase offset for excitatory (black), PV+ (red), and SOM+ (blue) neurons. (D) Vm-ECoG correlation coefficient is higher

magnitude during oscillations than directly after an oscillation in all cell types (Exc., WSRT, p = 3.2e-8; PV+, WSRT, p = 0.004; SOM+, WSRT, p = 5.8e-4). (E) V1 ECoG 30-50 Hz power (top) is higher (One-Way ANOVA, $p < 0.0001$) before (WSRT, $p < 0.0001$) and after (WSRT, $p = 0.0001$) an oscillation. 3-5 Hz power is lower (One-Way ANOVA, $p = 0.0012$) before (WSRT, $p < 0.0001$) and after (WSRT, $p < 0.0001$) 3-5 Hz Vm oscillations. (F) 3-5 Hz power is higher (One-Way ANOVA, $p < 0.0001$) before (WSRT, $p < 0.0001$) and after (WSRT, $p < 0.0001$) 3-5 Hz Vm oscillations. Error bars and shading represent ±SEM.

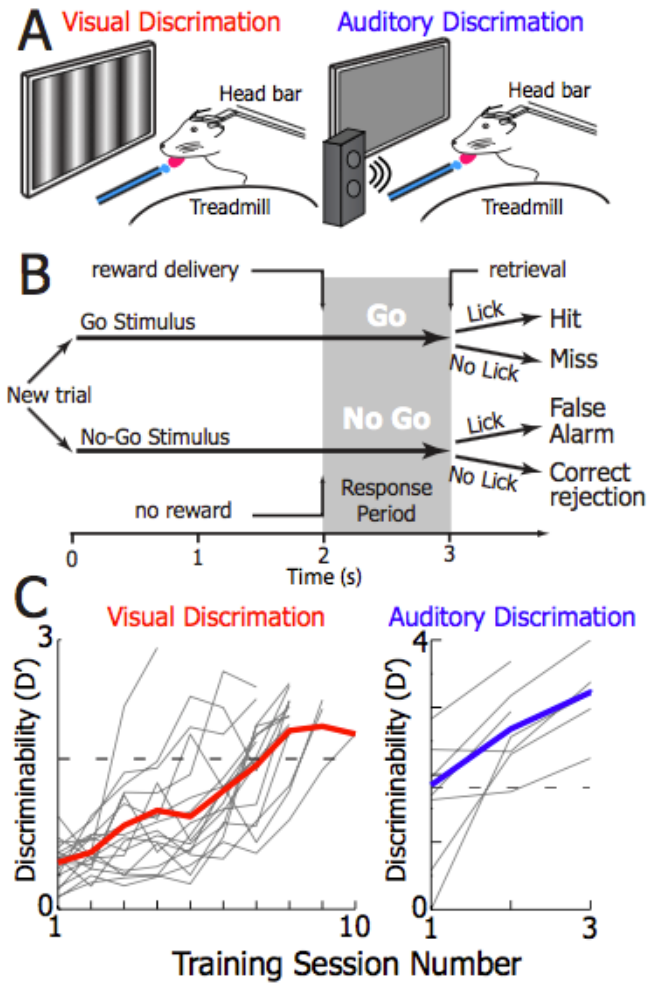

Figure 1-5. Go/No-go discrimination task schematics and learning curves.

(A) Schematic of the animal performing the visual (left) and auditory (right) discrimination tasks. During both tasks, animals were head-fixed atop a friction-less spherical treadmill, a monitor was placed in the monocular visual field, and a water dispenser with reward retrieval vacuum and lick monitoring was used to deliver rewards. Illumination levels were identical during auditory and visual discrimination tasks. See Materials and Methods for more details. (B) Task schematic. Visual and auditory stimuli were presented for three seconds. In go trials, 45° gratings or a 5 kHz tone were played and a water reward was issued two seconds after stimulus onset. During no-go trials, 135°

gratings or a 10 kHz tone were played and no reward was issued. Animal response (licking) was recorded during the response period to assess correct behavior. For more details, see Materials and Methods. (C) The mean discriminability, a measure of animal performance, of animals during learning of the visual (left, red, n=17 animals) and auditory (right, blue) discrimination tasks (n = 7 mice). Bold colored line: the mean performance of all animals on a given session date. Light grey lines: the mean performance of a single animal on a given session date. Animals were recorded once their mean discriminability surpassed D' = 1.7 (Monte Carlo Simulation, p = 0.01 random behavior) indicated by the grey dotted line.

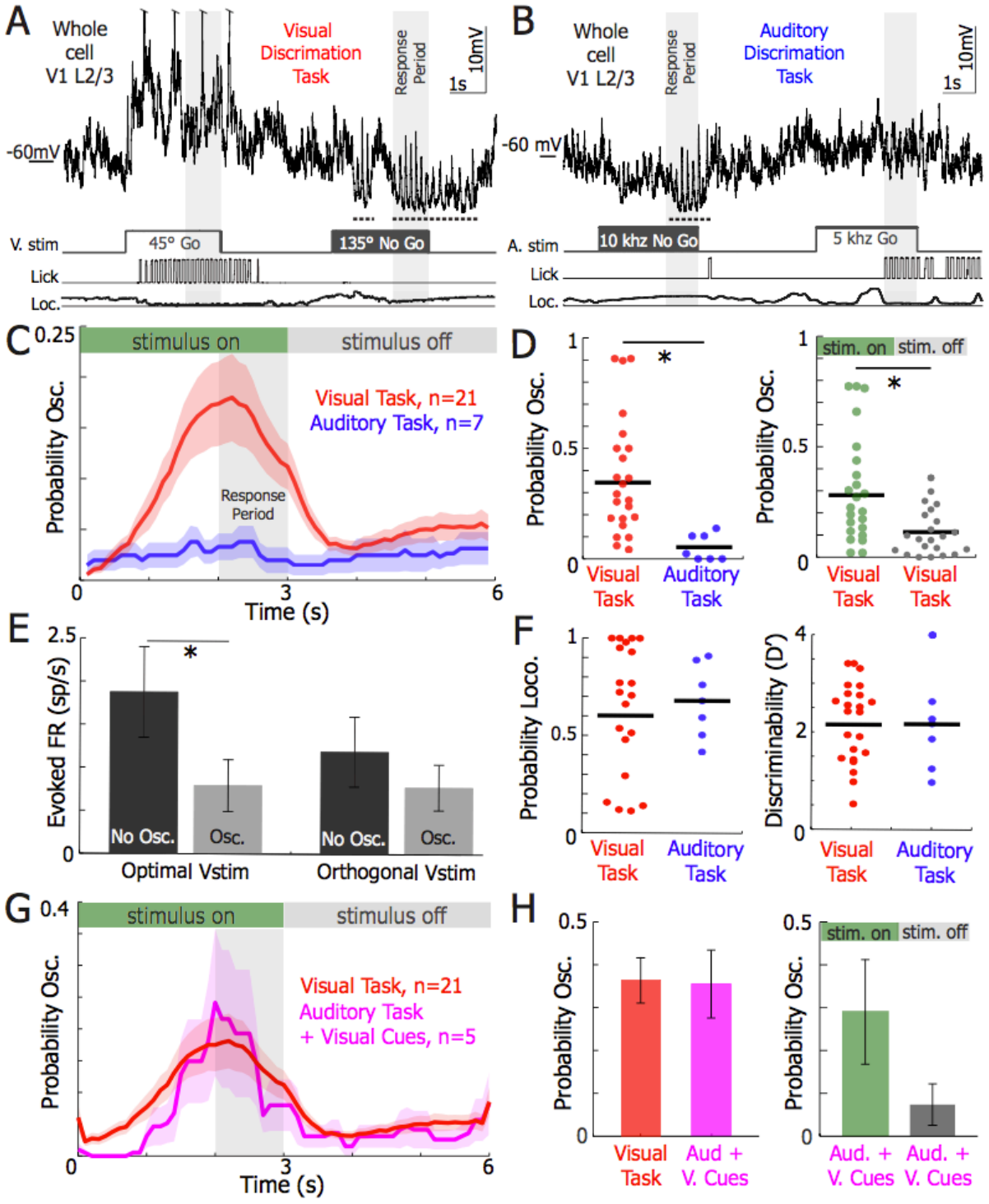

Figure 1-6. 3-5 Hz Vm oscillations are recruited during visual stimulation in behaving animals.

Example sub-threshold activity from single neurons as animals perform the (A) visual discrimination and (B) auditory discrimination tasks. Stimuli timing, licking, and locomotion were recorded simultaneously. Dotted underline shows 3-5 Hz Vm oscillation occurrences. (C) The mean probability of 3-5 Hz Vm oscillations occurring during a trial of the visual (red, n = 21 neurons) and auditory (blue, n = 7 neurons) go/no-go tasks. Periods where stimuli were on and off are marked at the top. The response period, when the animal must report its decision, is denoted in the grey region. (D) The probability of an oscillation occurring during a trial in the visual task was significantly greater than in the auditory task (left, WRST, p = 0.001). The probability of an oscillation occurring during the visual task was significantly higher than when the stimulus was off (right, WSRT, p = 0.0037). (E) The mean firing rate evoked by optimal visual stimuli (left, WSRT, p = 0.001) and orthogonal visual stimuli (right, WSRT, p = 0.68) when 3-5 Hz oscillations were present (osc.) or absent (no osc.) in neurons recorded from animals during visual discrimination (n=21 neurons). (F) There was no difference in the probability of locomotion during a trial (WRST, p=0.92) and the mean discriminability (D') during a behavioral session (WRST, p=0.72) during the visual (red) and auditory task (blue). (G) The mean probability of 3-5 Hz oscillations occurring during a trial of the visual (red, n = 21 neurons) and auditory task + visual cues (Aud. + V. Cues, pink, n=5 neurons) task. Visual cues in the auditory task + visual cues trials were not salient and were displayed simultaneously with auditory cues identical in the auditory task. (H) The probability of an oscillation occurring during a trial in the auditory task + visual cues was not different from the visual task (WRST, p = 0.82). The probability of an oscillation occurring while stimuli were on (green) versus off (grey) was statistically not different during the auditor task + visual cues (WSRT, p = 0.17). Error bars and shaded regions represent ±SEM.

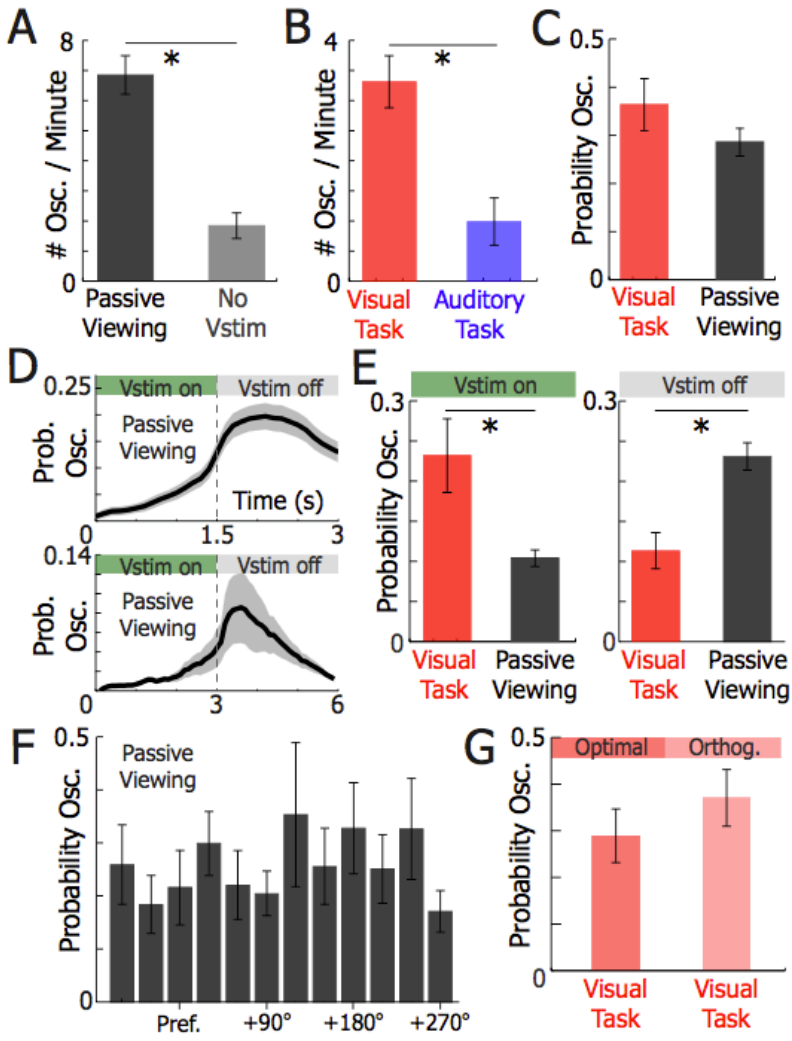

Figure 1-7. Visual stimulation recruits 3-5 Hz Vm oscillations during passive viewing, but oscillations tend to occur after the visual stimulus during passive viewing.

(A) The number of oscillations per minute was higher during passive viewing (black) of 1.5 second drifting gratings than 5-10 minute periods where no visual stimuli were shown (No vstim, grey; WSRT, p = 1.7e-5). (B) The number of oscillations per minute was higher during the visual task (red) than the auditory (blue) discrimination task (WRST, p = 0.008). (C) The probability of 3-5 Hz Vm oscillations during a trial was not different during the visual task and passive viewing (WRST, p = 0.26). (D) The probability of evoking an oscillation during passive viewing when the visual stimulus is 1.5 seconds (top, n=40) or 3 seconds (bottom, n=9). (E) Comparison of the mean probability of 3-5 Hz

Vm oscillations occurring in neurons recorded from animals during the visual task (red, n=21) and passive viewing (grey, n=53) while a visual stimulus is on (left, WRST, p = 0.001) and off (right, WRST, p = 0.007). (F) The probability of a 3-5Hz Vm oscillation occurring during passive viewing of visual cues in relation to excitatory neuron (n=40, One-Way ANOVA, p = 0.76) tuning. The pref. visual stimulus is the preferred visual stimulus. (G) The probability of a 3-5 Hz Vm oscillation occurring during visual discrimination of the optimal or orthogonal visual stimulus (n = 21 neurons, WSRT, p = 0.34). Error bars represent ±SEM.

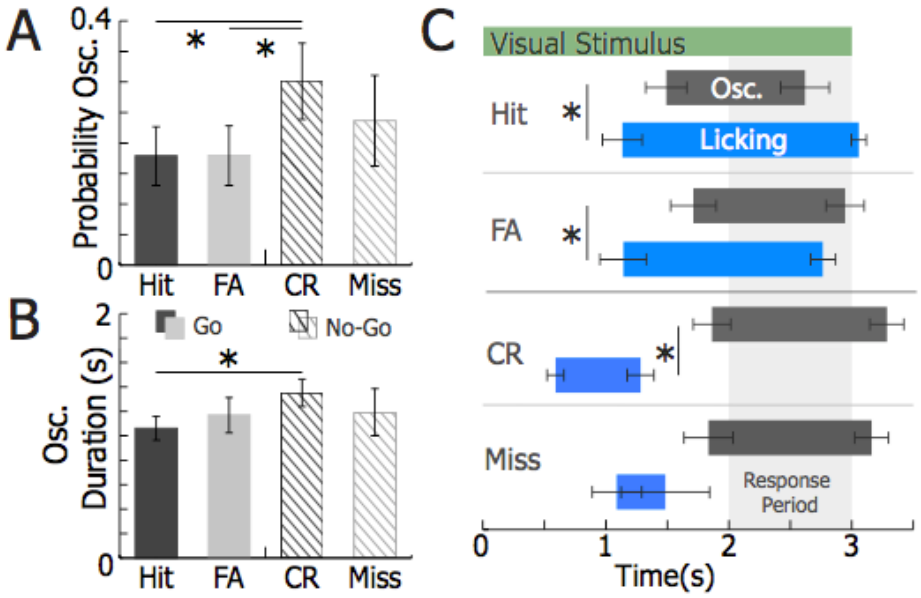

Figure 1-8. Oscillations prevalence and timing varied by trial type and oscillations typically occurred after initiation of licking.

(A) The mean probability of 3-5 Hz oscillations occurring during go trials (hits, black; false alarms (FA)) and no-go trials (correct rejections (CR), dark lines; misses, light lines) (n=21 neurons). Compared to CR trials, oscillations were less likely to occur during hit trials (WSRT Bonferroni corrected, p = 0.046) and FA trials (WSRT Bonferroni Corrected, p = 0.04). (B) The mean duration of 3-5 Hz oscillations during go trials (hits, black; false alarms (FA)) and no-go trials (correct rejections (CR), dark lines; misses, light; n=21 neurons). Oscillations were shorter during hit trials than during CR trials (WRST Bonferroni Corrected, p = 0.035). Error bars represent ±SEM.

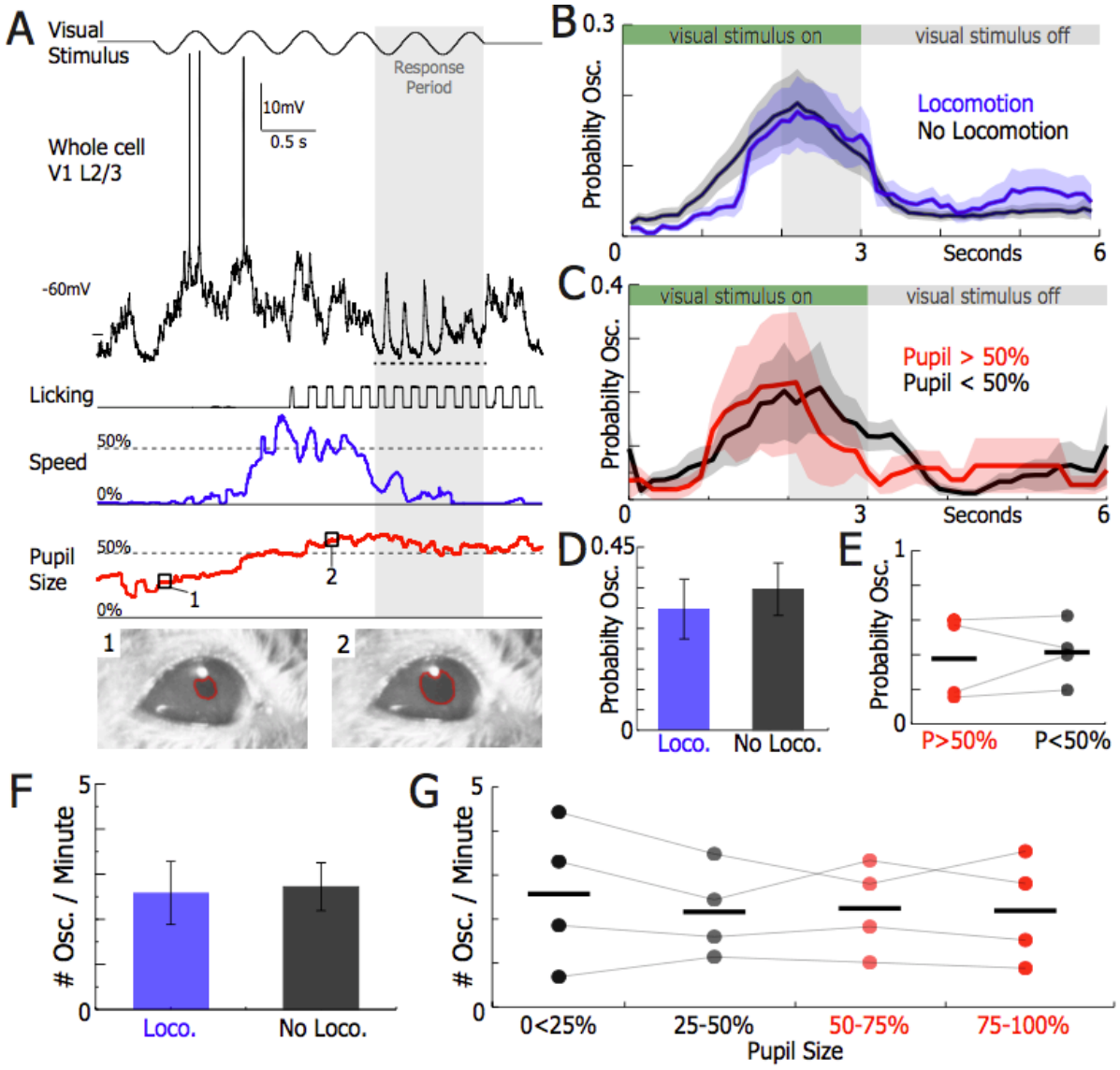

Figure 1-9. Oscillations occurred in high and low arousal states.

(A) Example of a whole-cell recording from a V1 L2/3 neuron during the visual discrimination task where speed (blue) and pupil size (red) were simultaneously recorded. The 3-5 Hz Vm oscillation is underlined by the dotted line. (B) The mean probability of 3-5 Hz oscillations occurring during trials of the visual discrimination task with locomotion (blue) and without locomotion (grey) (n=21 neurons). (C) The mean probability of 3-5 Hz oscillations occurring during trials of the visual discrimination task when the pupil is greater than (red) and less than 50% (grey) of full size (n=4 neurons). (D and E) The probability of an oscillation occurring during a trial of the visual task was no different when animals

were running or not running (n = 21, WSRT, p = 0.76) and when the pupil was greater than or less than 50% of full size (n = 4, WSRT, p = 0.63). (F) The average number of 3-5 Hz Vm oscillations per minute occurring during locomotion (blue) and when locomotion was absent (grey) was not significantly different (n=21 neurons, WSRT, p = 0.46). (G) The number of oscillations occurring when the pupil was 0-25%, 25%-50%, 50-75%, and 75-100% of its full size was unchanged across pupil sizes (n = 4 neurons, One-Way ANOVA, p = 0.96). Error bars and shading represent ±SEM.

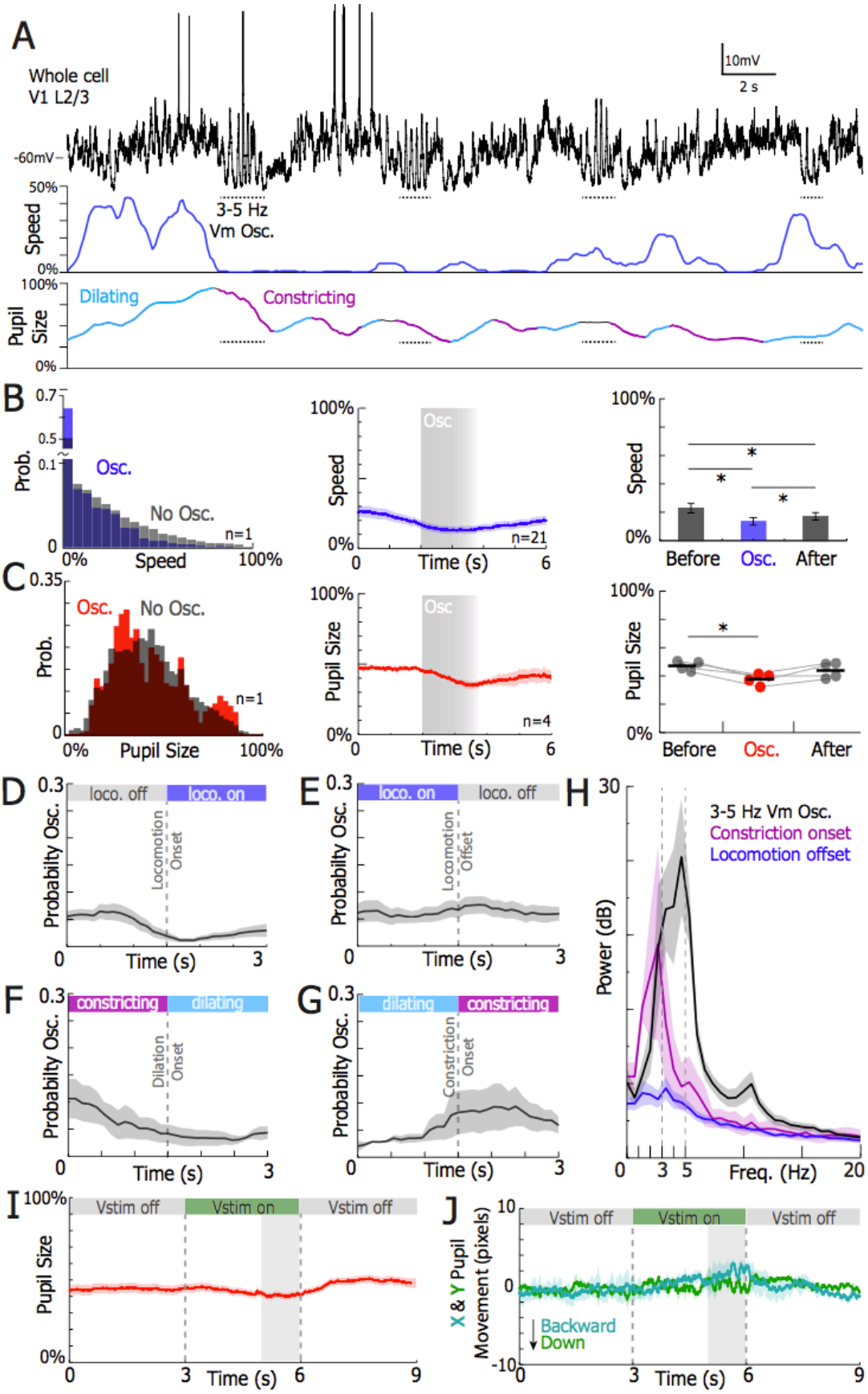
A
Whole cell
V1 L2/3
10mV
2 s
-60mV
50%
Speed
0%
3-5 Hz
Vm Osc.
100%
Pupil Size
0%
Dilating
Constricting
B
Prob.
0.7
0.5
0.1
0
Osc.
No Osc.
n=1
0%
Speed
100%
100%
Speed
0%
Osc
n=21
0
Time (s)
6
100%
Speed
0%
*
*
*
Before
Osc.
After
C
0.35
Prob.
0
Osc.
No Osc.
n=1
0%
Pupil Size
100%
100%
Pupil Size
0%
Osc
n=4
0
Time (s)
6
100%
Pupil Size
0%
*
Before
Osc.
After
D
0.3
Probabilty Osc.
0
loco. off
loco. on
Locomotion Onset
Time (s)
3
E
0.3
Probabilty Osc.
0
loco. on
loco. off
Locomotion Offset
Time (s)
3
H
30
Power (dB)
3-5 Hz Vm Osc.
Constriction onset
Locomotion offset
0
3
5
Freq. (Hz)
20
F
0.3
Probabilty Osc.
0
constricting
dilating
Dilation Onset
Time (s)
3
G
0.3
Probabilty Osc.
0
dilating
constricting
Constriction Onset
Time (s)
3
I
100%
Pupil Size
0%
Vstim off
Vstim on
Vstim off
0
3
Time (s)
6
9
J
10
X & Y Pupil Movement (pixels)
0
-10
Vstim off
Vstim on
Vstim off
Backward
Down
0
3
Time (s)
6
9

Figure 1-10. Oscillations are correlated with small reductions in speed and pupil size. (A) Example V1 L2/3 Vm, animals speed, and pupil size traces. 3-5 Hz Vm oscillations are marked by the dotted horizontal lines. Periods where the pupil was detected to be dilating and constricting are marked in teal and purple, respectively. (B and C) *left:* example histogram of speed and pupil size during (colored) and in the absence (grey) of 3-5 Hz Vm oscillations; *middle:* the oscillation triggered mean speed and pupil size. Oscillation onset and average duration are indicated by the grey box; *right:* the mean speed and pupil size before, during, and after an 3-5 Hz Vm oscillation. Speed was greater before and after oscillations (B, bottom, WSRT, B-O, p=0.0001, B-A, p=0.0011, O-A, p=0.0176). Pupil size was greater before oscillations (C, bottom, WSRT, B-O, p=0.028, B-A, p=0.79, O-A, p=0.34). (D) The mean probability of evoking a 3-5 Hz Vm oscillation at locomotion onset and (E) offset. The probability of evoking an oscillation was slightly dampened after oscillation onset (WSRT, p = 0.012). (F) The mean probability of evoking an oscillation at dilation onset and (G) constriction onset. The probability of evoking an oscillation was no different before and after dilation onset (n = 4, WSRT, p = 0.91) and constriction onset (n = 4, WSRT, p = 0.25). (H) The mean periodogram of the Vm during 3-5 Hz Vm oscillation and the 1.5 seconds following constriction onset, and locomotion offset. (I) Mean pupil size during visual cues while animals performed visual discrimination. (J) The mean x and y movement of the pupil during visual cues while animals performed visual discrimination. Error bars and shading represent ±SEM.

Chapter 2: Development of a Multimodal Attention Task for Mice

2.1 Abstract

A major limitation to understanding the neurophysiology of complex behaviors lies in the lack of strong animal models. Primates are the primary animal model for attention studies, however, technical challenges impede our ability to probe the neural mechanisms of attention. To overcome these challenges, we developed a multi-modal visual attention task for head-fixed mice amenable to advanced neurophysiological techniques. In this chapter, I describe the custom hardware and software tools that were developed, including detailed parts lists. Using these tools, we were able to consistently train animals to master the task in 2-3 weeks of training. These results in tandem with basic psychometrics and behavioral analyses indicate that animals do learn to attend to visual cues during the task, establishing a firm bedrock for future studies into the neurophysiology of attention.

2.2 Background

The ability to direct, sustain, and shift attention is impaired in a number of neuropsychiatric disorders. Children and adults with attention deficit disorder and autism have pronounced measurable deficits in sustained attention, as well as problems with shifting attention (Gadow et al., 2006; Goldstein and Schwebach, 2004; Holst and Thorell, 2017). These deficits can lead to impaired learning and poor performance at school and later at work (Adamou et al., 2013; Holwerda et al., 2013.; Hume and Odom, 2006). Cognitive deficits in schizophrenia, in particular deficits in selective attention and attention shifting do not respond to antipsychotic medications, and contribute to the inability of these patients to maintain employment (Heinrichs and Zakzanis, 1998; Palmer et al., 2009). Moreover, current pharmacological therapies have many side-effects and are not always effective (Vaughan and Kratochvil, 2012). Our inability to effectively treat these diseases stems from a fundamental lack of knowledge on the neurobiological mechanisms of attention. To devise targeted treatments for diseases with attention deficits, we must strive to understand the cellular and

network mechanisms of attention and investigate how they are disrupted in disease states.

To date, the vast majority of studies on the neurophysiology of attention have been performed in primate models (Bisley, 2011). In non-human primates, extracellular electrophysiology has been an essential tool for discovering the basic tenets of how attention shapes visual processing. For instance, attention when directed to specific visual cues increases the responsiveness of neurons throughout visual cortex (Chalk et al., 2010; McAdams, 2005; Moran and Desimone, 1985; Motter, 1993; Roelfsema et al., 1998; Treue and Maunsell, 1996b). Despite the discovery of this central phenomenon over 30 years ago, the mechanisms governing the increase in neuronal responsiveness in visual cortex during attention is still uncertain. Current theories include top-down input from executive cortical areas directly to visual cortex (Buschman and Miller, 2007; Gregoriou et al., 2009b; 2014; Moore and Armstrong, 2003; Noudoost and Moore, 2011), whereas others advocate for bottom-up modulation via thalamic centers (Krauzlis et al., 2013; McAlonan et al., 2008; Purushothaman et al., 2012a; Saalmann et al., 2012; Wimmer et al., 2015). Dopaminergic, norepinephrine, and cholinergic neuromodulation have all been implicated as well (Disney et al., 2007b; Herrero et al., 2008; Noudoost and Moore, 2011; Sarter et al., 2005). Yet, the synaptic mechanisms remain even more controversial, with little direct evidence explaining how input from these diverse sources could alter the responsiveness of visual cortical neurons.

A major reason for the uncertainty in neural attention mechanisms is the lack of adequate tools in primate models. Extracellular electrophysiology can establish correlation between outputs of neurons and behavior, but it is not sensitive enough to detect neuronal level synaptic mechanisms. While efforts have been made to adopt tools to accomplish these tasks in non-human primates (Inoue et al., 2015; Tan et al., 2014), the most advanced imaging, optical, intracellular electrophysiological, and large-scale extracellular electrophysiological tools available to probe neural circuits were developed for and are already feasible in mice. Development of a mouse behavioral model of visual attention would enable researchers to

apply these advanced techniques to settle many of the controversies concerning the mechanics of visual attention.

Therefore, I created a Go/No-Go task where mice first attend and then ignore identical visual stimuli to gain water rewards. First, mice attend to visual cues to decide whether to lick for a water reward (go) or withhold licking (no-go). Simultaneously, salient auditory stimuli are played to distract the animal and must be ignored to make the correct decision. Then, the contingencies are switched: auditory cues tell the animal to lick or not lick, and the visual stimuli distract the animal and must be ignored to make the correct decision. In order to execute the task, I created custom hardware and software. Using these tools, animals were able to reliably learn this attention task within 3 weeks of training time. Finally, we performed several control analyses to show that animals direct their attention to visual cues in order to perform the task.

2.4 Development of animal training hardware and software

In order to train mice to accomplish a multi-modal attention task, sound-proof training boxes needed to be built which would replicate conditions during recording. From scratch, I developed training boxes outfitted with the correct hardware to execute the attention task. See table 1 for a detailed parts list.

Part	Supplier	Purpose
Custom-cut expanded ¾" black PVC boards	Interstate plastics	Foamed PVC is easy to assemble and provides strong sound insulation at a low cost
Water delivery valve (LHDA1233215H)	Lee Company	These 12V solenoid valves are silent, which eliminates sound of water delivery as a factor influencing animal behavior
Sub-Miniature Lickometer with reward recovery for Headfix applications	Island-motion	A water dispensing system that includes an infrared beam-break system for detecting licking and a vacuum port for removing ignored water rewards
DAQ – NI-USB-6341	National instruments	This board was used to actuate the task. Specifically, this board allows for analog inputs to be pre-loaded to the board, enabling parallel processes to be executed during the behavioral task

DAQ – NI-USB-6008 OEM	National Instruments	This less powerful DAQ was used to monitor outputs during the behavioral task (licking, visual stimuli, auditory stimuli, water delivery).
Filter flask	Cole-Parmer	The filter flask was used to collect water residue that was vacuumed up
12V DC solenoid valve	RioRand (Amazon)	This valve was used to actuate the vacuum at the end of each trial to ensure that ignored rewards did not remain on the water dispenser
24” Monitor	Dell	To display visual cues
12”X12”/1” acoustic foam	Foam Factory	To increase the sound proofing of the foamed PVC
Super 77 spray glue	3m	To attach foam to the PVC
Christy’s Red Hot Blue Glue	Christy’s	PVC bonder to construct the outer box
Optical breadboard, posts, and connectors	Thorlabs	Used to mount the spherical treadmill, lickometer, and headpost
80 mm case fans X 2	Amazon	To provide circulation and cooling within the behavioral box
Logitech X-140 speakers	Amazon	To deliver auditory cues
HD-5000 Webcam	Microsoft	To monitor animal behavior in the box. Note: the infrared filter was removed to enable imaging using infrared light
12V infrared LED lamp	Amazon	To provide lighting for the webcam
Laptop – Windows	Dell	To actuate the task and monitor animal behavior
Headbar holder	Custom	We custom manufactured the headbar holder using the Astronomy and Physics machine shop from a Thorlabs optical post

A constructed behavioral box is shown in Figure 2-1 with key parts labeled. The expanded PVC pieces were custom ordered individually and bonded together using PVC bonder, except the front and top panels, which were attached using hinges to allow for easy entrance into the enclosure. Once the enclosure was built, fans, air holes, and routing for cables were manually drilled into the enclosure. All other equipment was placed into the enclosure, except the laptop and vacuum solenoid, which creates a loud click upon actuation. Fans are an essential addition, cooling the box from an ambient temperature of greater than 30 degrees C to room temperature (~25 degrees C).

The software was custom written in MATLAB. Gratinggui.m enables the experimenter to actuate the task and manipulate various experimental parameters (Figure 2-2). The defaults shown in Figure 2-2 illustrate the typical visual cue, auditory cue, water dispenser, and experiment parameters. Water dispenser parameters were calibrated daily to ensure that the water droplet reward was of the correct size. To complete calibration, the water system was flushed for 10 seconds by entering 10 into the box next to the button entitled “Flush” and then depressing the “Flush” button. Then, the task was started in all preferred mode (completed by checking the “always preferred” radio button, which caused a water reward to be released every trial), and the water drop was assessed for at least 10 trials to ensure consistency and quality. The drop button can be used to expel a single drop. The pump toggle button actuates the vacuum solenoid, which can be toggled on or off. Of note, the water dispensation signal is not a single digital pulse to the water dispensing solenoid. It is, in fact, four brief pulses sent via analog output from the NI-USB-6341 (pulse length is determined by the H2O time entry box). The entry in the V2 delay box sets the time between pulses. To modify the size of the water drop, just the H2O time box should be modified (default value is 0.0145 seconds).

During training, animals learned visual discrimination, auditory discrimination, and then the attention task. To actuate visual discrimination or auditory discrimination, a single radio button was selected in experimental settings. To run the attention task, both radio buttons would need to be selected. When both radio buttons are selected, the distractor toggle button appears, enabling the experimenter to execute the attend visual (auditory distractor) or ignore visual (visual distractor) tasks. The buffer entry box enables the experimenter to determine how many unimodal trials precede the start of the attention task trials (the default value is 30). Once the start button is hit, main.m is called, which pseudo-randomly selects the order of the trials, actuates the trials, collects the data, and saves all the data. The task can be quit any time by holding any keyboard button. Data is saved at the end of each trial to ensure even in

the event of a crash that data is not lost. If the task is quit accidentally or if a bug occurs, dialog at task initiation will grant the option of merging the new session with a prior session.

2.5 Training protocol

Preparing and training the animals for recording takes several weeks (Figure 2-3A). Prior to any training, a head-bar was implanted over the frontal bones to leave room for a craniotomy over visual cortex after training. Following surgery, animals recovered over 5 days and received 2 minutes of handling (held in hand) per day, habituating the animals to human interaction. After the five-day recovery period, water deprivation began where animals would receive approximately 1 mL of water per day. During this time, animals were placed on the spherical treadmill in the behavioral rig for at least 3 days to habituate to head-fixation for 15 minutes per day. Animals were habituated and trained on the same behavioral rig throughout training. Typically, animals reached their water deprivation target (90% of original body weight) by 5 days after initiating deprivation, and head-fixation habituation occurred on every other day. We found that it was most efficient to start animal training when animals essentially licked all the time, as then animals only had to learn how to stop licking when no reward was dispensed. To assess this, animals participated in 50 trials where a water reward was paired with a visual stimulus, and animals had to lick for the reward in >80% of trials.

In order to learn the multi-modal attention task, animals were first trained to perform unimodal visual and auditory lick/no-lick (go/no-go) discrimination tasks. In the visual discrimination task, drifting sine gratings at one orientation were paired with a water reward (lick; Figure 2-3B). Orthogonal drifting gratings did not signal a reward, and the animal was trained not to lick in response to the stimulus (no-lick; Fig 2B). Correct lick (go) and no-lick (no-go) trials are called hits and correct rejections (CRs), respectively; incorrect lick and no-lick trials were called misses and false-alarms (FAs), respectively. Once animals reached expert performance ($D'>1.7$, $p<.01$ as compared to chance performance, Monte-Carlo Simulation),

animals were advanced to learning the analogous auditory discrimination task where a low pure tone (5 kHz, 90 dB) indicated a lick trial and a high tone (10 kHz, 90 dB) indicated a no-lick trial. Finally, animals were trained to perform the multimodal attention task: first, they performed the visual discrimination task with auditory distractors (attend visual task, Fig. 2-3C left), then, after a two-minute break, they performed the auditory discrimination task with visual distractors (ignore visual task, Fig. 2-3C right). To cue animals to attend to the correct sensory modality, each trial set started with 30 trials without distractors.

In all task variants, each trial lasted 3 seconds (Fig. 2-3B). When the cue stimulus instructed the animal to lick, water was dispensed two seconds after stimuli onset. No water was dispensed in the no-lick condition. Licking was only assessed in the final second of the trial (Figure 2-3B, response period). If the animal responded correctly, the inter-trial interval (ITI) was 3 seconds. If the animal responded incorrectly, the ITI was increased to 9.5 seconds as a time out. If the animal missed a reward, the reward was removed by vacuum at the end of the trial. Animals performed 300-450 trials daily. Only one training session was conducted per day with the aim to give the animal all their daily water allotment during training. If animals did not receive their full allotment of water for the day during training, animals were given supplemental water one hour following training.

2.6 Training results

Animals were able to learn the attention task within 3-4 weeks. Figure 2-4A shows an example learning progression from one animal. The animal became an expert in the visual discrimination task (green) in 7 sessions. Auditory discrimination was learned much faster and required only 2 training sessions to reach criterion. On day 1, the animal was able to perform above criterion during the multimodal attention task. Over the course of learning, the animal's licking behavior changed drastically (Figure 2-4B). During the first day of learning the visual discrimination task, licking was random in both lick and no-lick trials. By session 6, where

animal performance peaked above criterion, licking became more stereotyped, especially in lick trials, where the animal initiated licking 0.5 seconds after cue onset and licked throughout the duration of the visual stimulus. These data show that animals learned to preempt water delivery and relied on the sensory cue in order to make their decision. Licking during no-lick trials became sparser as the CR rate increased. By the final day of training, licking onset occurred just before water delivery during hit trials and animals rarely licked incorrectly during no-lick trials, translating into an average D' of around 3. These data demonstrate the animals are able to reach a high degree of proficiency on this task in a relatively short amount of time.

We were able to reliably replicate these results over many animals. Figure 2-5A shows an average training curve for several mice where each dot represents the average session performance of an animal while learning visual discrimination, auditory discrimination, and the multimodal attention task. Animals learned visual discrimination and auditory discrimination tasks in 5-8 and 2-3 sessions, respectively (Figure 2-5A). Again, the majority of animals performed the multimodal attention task at or above criterion on the first day of training. During the first 3-4 sessions of the attention task, some animals had trouble switching between the attend visual and attend auditory task, indicated by the dots falling below the expert criterion line. With increased training, animals became more consistent on average and performed above criterion on sequential days.

Consistent with the single example shown in Figure 2-4, animals' licking changed dramatically over the course of training (Figure 2-5B-C). Over the course of learning the visual discrimination task, animals initiated licking prior to when the water reward was dispensed during lick trials. In no-lick trials, animals first increased the amount of licking in no-lick trials during early sessions, but decreased average licking by the final session of the task. This is reflective of our training methodology where we teach the animals to lick during 100% of trials and then have them learn how to withhold licking during no-lick trials.

To confirm that the animals could detect the high-contrast (100%) visual cues employed in our study, we performed psychophysical tests where the contrast of visual cues was systematically varied as animals performed the visual discrimination task (Figure 2-6). To run these tests, animals performed 30 trials of the task at several different contrasts ranging from 0% to 100% contrast. We found that animals could reliably detect stimuli as low as 4% contrast stimuli, showing that the 100% contrast stimuli used were easily detected by the mice (Figure 2-6B). Yet, animals were able to ignore visual cues in the ignore visual cue portion of the multimodal attention task. When we scored attend and ignore visual cue portions of the multimodal attention task with reversed contingencies (ie scored “attend” visual cue trials as if they were “ignore” visual cue trials and vice versa), we found that scores fell fall short of the expert performance criterion and were significantly lower than when the tasks were scored properly (Figure 2-7). These results further demonstrate that visual cues are used by the animal during decision making in these tasks and that animals actively ignore visual cues during the ignore visual portion of the multimodal task.

2.7 Discussion

We developed a multimodal attention task for mice to expand the tool kit of attention researchers. Using our paradigm, we can reliably and quickly train animals to attend and then ignore identical visual cues in a single training session after 2-4 weeks of training. We provide controls showing that animals attend or ignore the visual cues during task performance. Coupled with whole-cell recordings and other advanced physiological recording techniques, this behavioral model could yield several important findings concerning the neural mechanisms of attention.

We built custom behavioral training boxes to facilitate training of animals on the attention task. While these boxes contained the essentials for training, more tools should be

incorporated into the boxes in the future to monitor training. For one, a ball tracker should be incorporated to monitor speed of the animal over time. This would eliminate the need for some of the visual monitoring done via webcam and could yield interesting changes over learning. Pupil size should also be measured, which could be used as a proxy for task involvement and arousal. Moreover, extensive pupil data could serve as an important data point in showing that attention is recruiting during the multimodal task. One way to reduce the costs of each behavioral box would be to reprogram the task to utilize the microphone jack on the control laptops as a two-channel analog output device. This would make the two analog outputs on the large NI USB-6341 DAQ unnecessary, and a smaller and cheaper DAQ could be substituted in its place. The software could also be significantly streamlined by trimming code used to generate the new task and potentially switching DAQ interfacing code from legacy 32-bit to newer 64-bit functions.

Few attention task for primates have been designed as multimodal tasks. Instead, primate tasks most frequently have employed spatial attention tasks where animals were trained to direct their attention to a specific area in visual space (Harris and Thiele, 2011). While this approach has proved useful and produced the bulk of what we know on attention in non-human primates, it faces a distinct disadvantage in that it is difficult to compare the results to what is known in humans. Human studies utilize spatial attention tasks, but often use much larger spatial fields of view (Mehta, 2000a). However, multimodal visual-auditory attention tasks have a long history in the human literature and have shown significant effects in visual cortex EEG electrophysiology (Alho et al., 1992; Hackley et al., 1990; Woods et al., 1992). For this reason, multimodal visual-auditory task were developed in primates to enable a closer bridge between the primate and human literature (Bollimunta et al., 2011; Lakatos et al., 2008; Mehta, 2000a; 2000b). These studies have successfully replicated findings in humans of enhanced event-related potential (ERP) responses as well as reductions in cortical alpha in

striate and extrastriate regions during visual attention and made important contributions to the mechanisms of attention in visual cortex.

While mice may be evolutionarily more distant than non-human primates from humans, mouse behavioral research is experiencing a renaissance due to the introduction of advanced techniques for probing neural activity in behaving mice. Light activated ion channels (optogenetics)(Boyden et al., 2005; Deisseroth et al., 2006), genetically-encoded calcium indicators (Chen et al., 2013), large-scale extracellular recording techniques(Du et al., 2011), and miniaturized imaging tools (Cai et al., 2016; Ghosh et al., 2011) in mouse models have enabled new findings into memory encoding (Cai et al., 2016), working memory(Liu et al., 2014; Riga et al., 2014), learning (Komiyama et al., 2010; Makino and Komiyama, 2015), social behavior (Yizhar, 2012; Yizhar et al., 2011) and many other complex behaviors. Concurrent to our studies, mice have been used to probe the neural basis of attention (Wimmer et al., 2015). Using a similar multimodal visual and auditory task, Wimmer and colleagues used optogenetics and extracelluar electrophysiology to show that the visual thalamus, specifically the reticular nucleus, plays an important and causal role in modulating visual gain during attention. Therefore, the advent of these new tools and techniques have made mice a feasible and indispensable behavioral model for understanding the neural underpinnings of complex behaviors such as attention.

To supplement the findings shown here, more data should be collected on how presence of a salient distractor affects animal behavior. Our data show that the animals use either visual or auditory information to successfully complete the multimodal attention task (Figure 2-8). We believe that the task utilizes the animal's attentional resources because it is very difficult for the animals to master and express consistently over several days, but further evidence is needed. To show this more conclusively, psychometric data should be collected showing how behavior changes across varying contrast stimuli while animals discriminate visual cues with or without salient auditory distractors present(Wimmer et al., 2015). Showing

that the presence of salient auditory distractor cues increases detection threshold and lowers peak performance would firmly demonstrate that our task taxes the visual system and align it with prior multimodal attention studies in rodents. While these behavioral controls are helpful, electrophysiological confirmation that the task replicates increased firing rates found in visual cortex during attention.

2.8 Figures

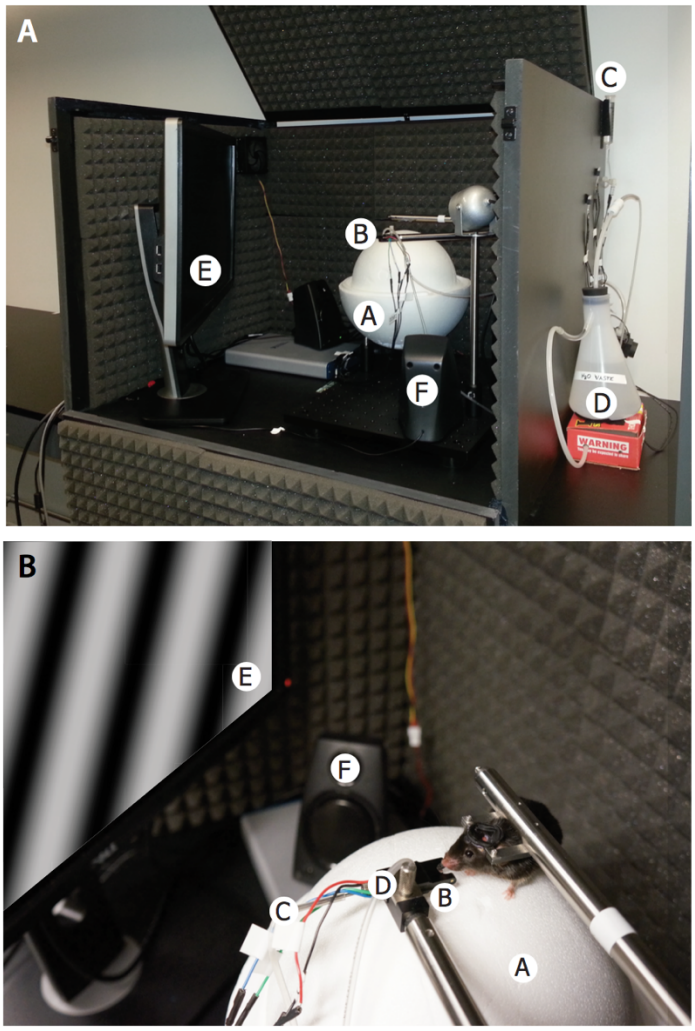

Figure 2-1. Behavioral Training Apparatus.

(A) The following parts are labeled: A) Spherical treadmill powered by air, (B) water dispenser and lickometer, (C) water reservoir, (D) vacuum flask for collecting excess water,

(E) computer monitor, (F) speakers. (B) The following parts are labeled: A) Spherical treadmill powered by air, B) lickometer casing, C) water input, D) vacuum output, E) monitor with drifting grating stimulus, F) speaker.

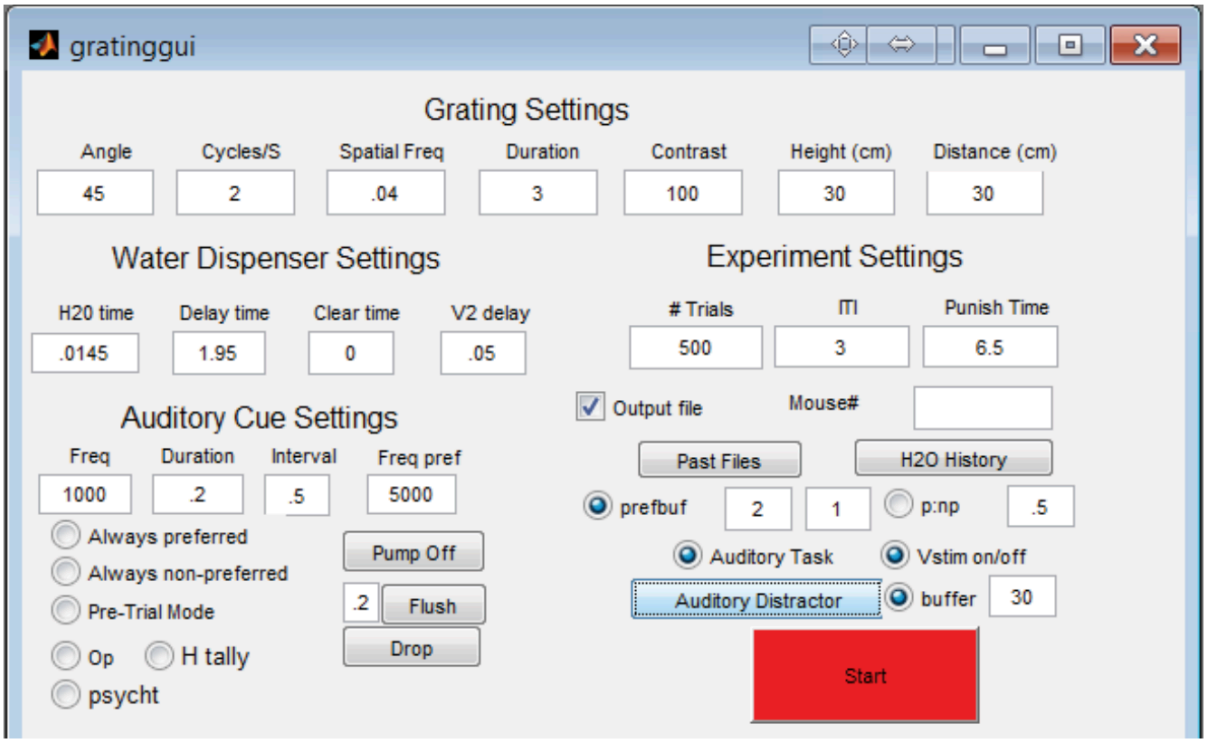

Figure 2-2. Graphic user interface for actuating the multimodal attention task.

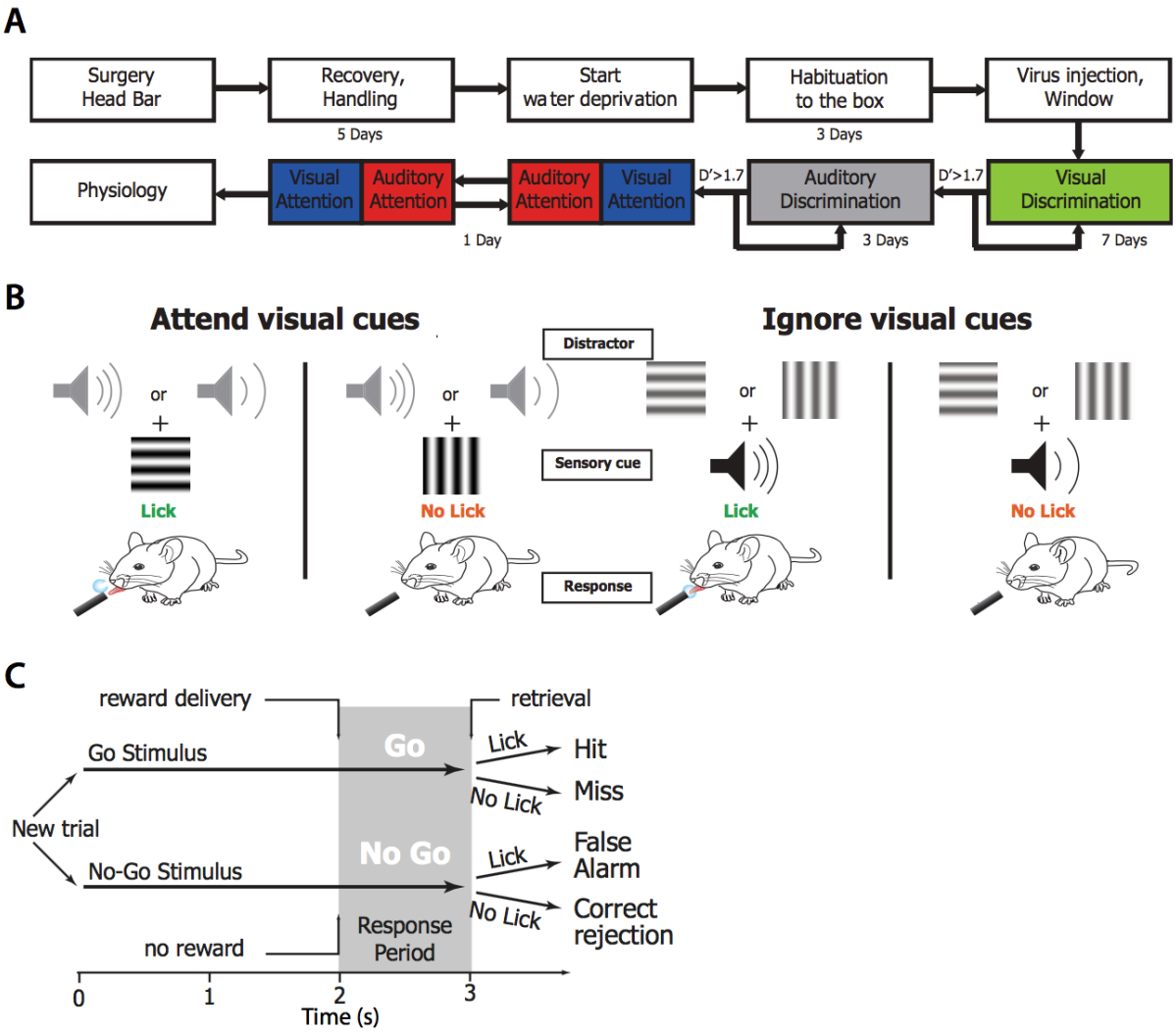

Figure 2-3. Training and attention task schematics.

(A) Training schematic. Animals progress from one task to the next after achieving a D'>1.7. Visual and auditory discrimination take approximately 7 and 3 days, respectively, of training to reach criterion. (B) Schematic for the multimodal attention task. In the attend and ignore visual cue conditions, animals see and hear the same stimuli, but the reward contingencies are switched between stimuli. (C) Trial schematic for the multimodal attention task.

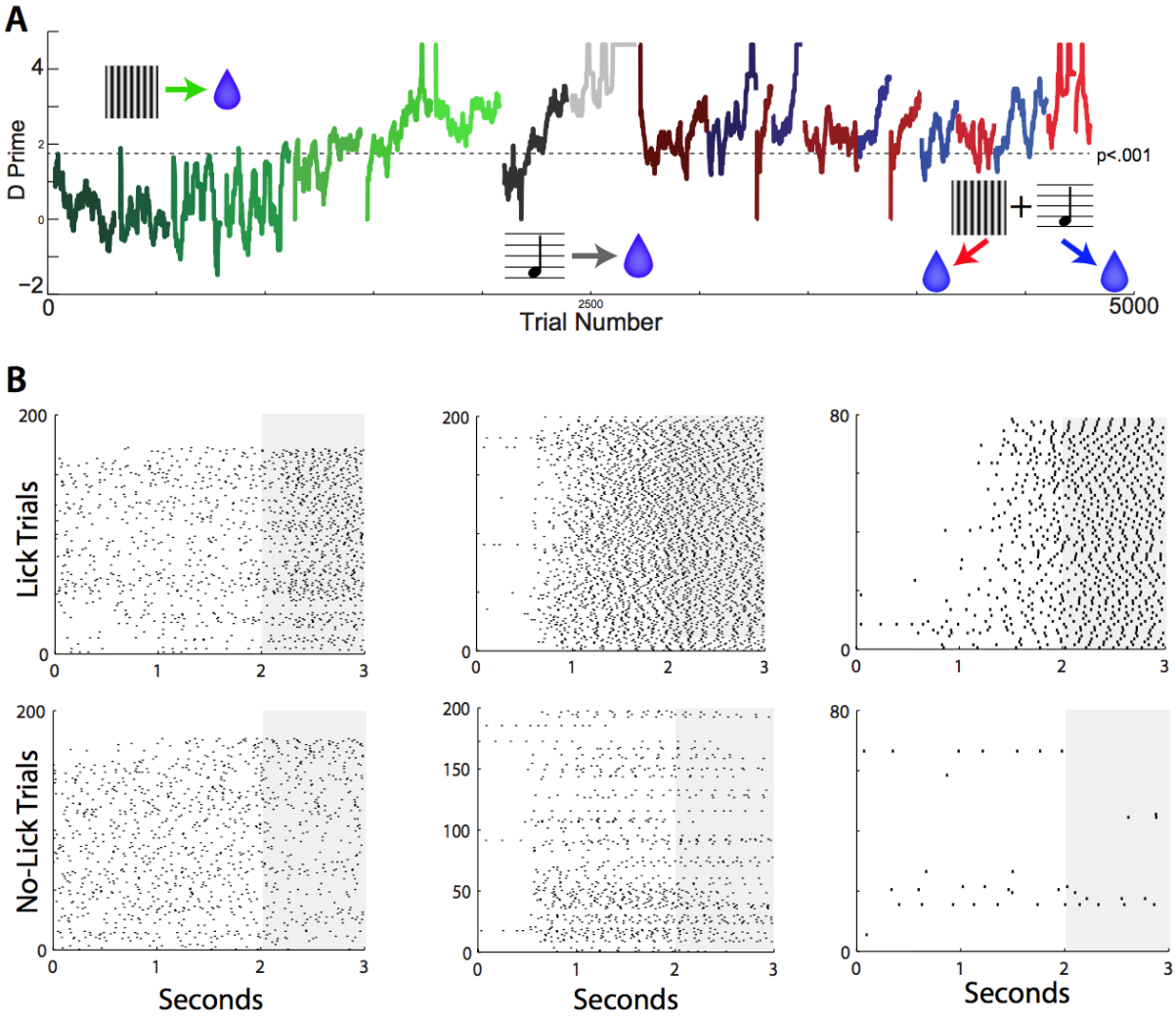

Figure 2-4. Training progression of one animal.

(A) D-prime of a single animal as it learns the visual discrimination (green), auditory discrimination (grey), attend visual (red), and attend auditory (blue) task. Changes in color brightness indicate subsequent training sessions. (B) Raster plots displaying licking over the course of training. *Left:* Licking on day 1 of visual discrimination training; *Center:* licking on day 6 of visual discrimination training; *Right:* licking on the final day of attend visual training.

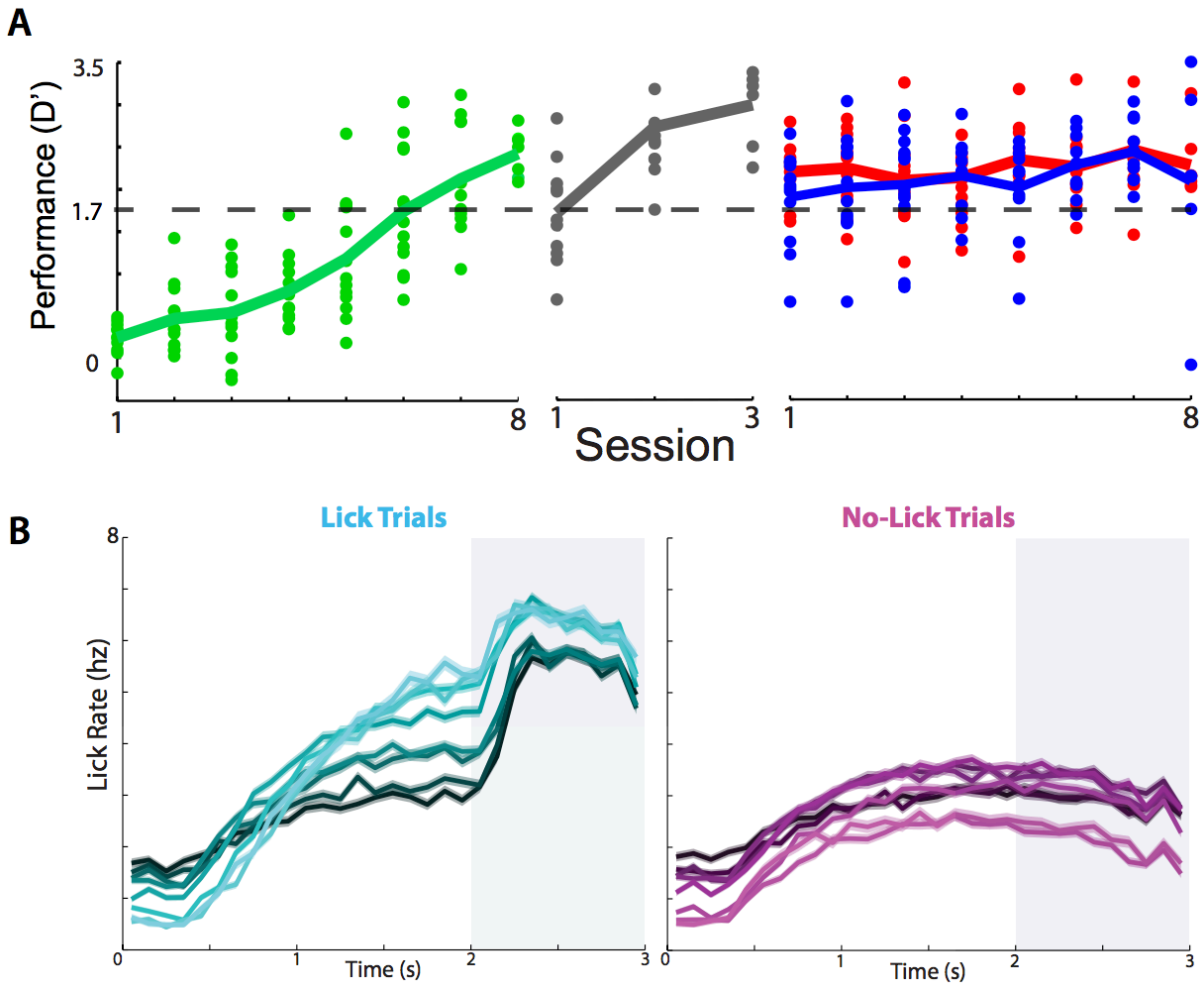

Figure 2-5. Training progression of multiple animals.

(A) The D-prime of 11 animals as they learn the visual discrimination (green), auditory discrimination (grey), attend visual (red), and attend auditory (blue) task. (B) The mean lick rate of animals as they learn the visual discrimination task during lick and no-lick trials. Changes in color brightness indicate subsequent training sessions.

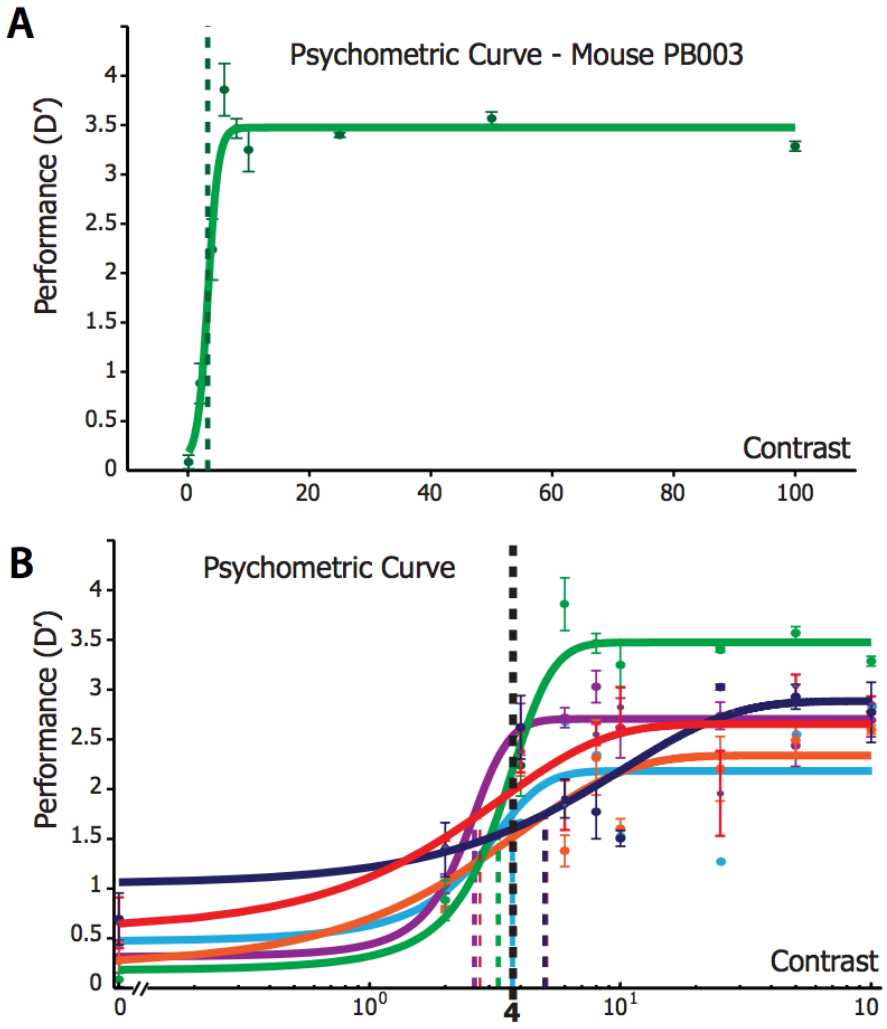

Figure 2-6. Contrast psychometrics for visual discrimination.

The psychometric curves for (A) a single mouse and (B) 6 mice. Psychometric curves were generated by decreasing the contrast of the visual cues steadily over the course of animal performance. The contrast was only decreased if the animal was performing at criterion. The contrast was increased if the behavior dipped below criterion. The mean contrast where animals could still perform above criterion was 4%.

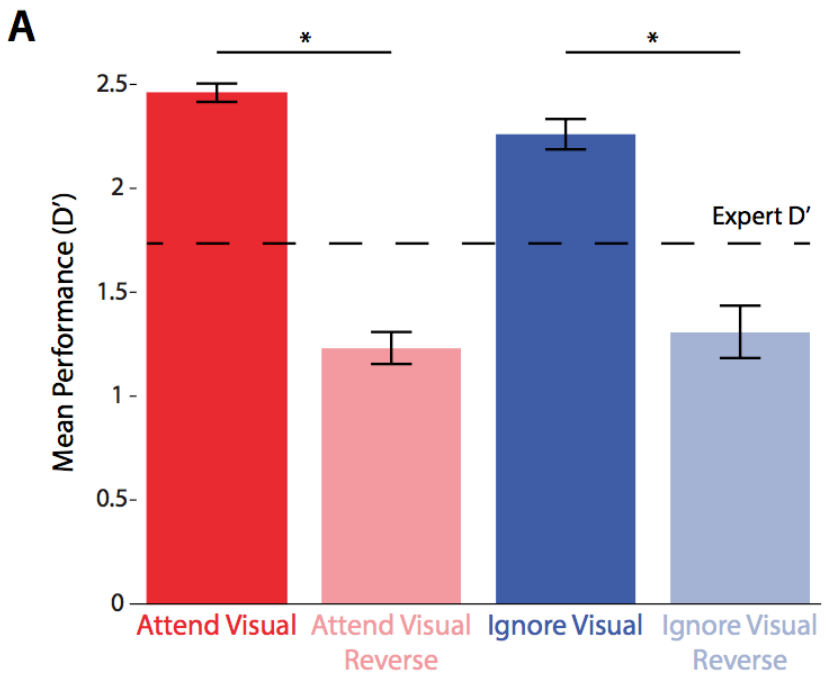

Figure 2-7. Animals employ different decision making strategies during attend and ignore visual tasks.

The opaque bars show the mean d' of 11 animals as they perform the attend and ignore visual tasks. The transparent bars show the mean d' of the same animals as they perfrom the attend and ignore visual tasks, but scored as if the opposite task (reverse; attend visual v. attend visual reverse, WSRT, $p = 0.004$; ignore visual v. ignore visual reverse, WSRT, $p = 0.008$).

Chapter 3: Electrophysiology of V1 during a Multimodal Attention Task

3.1 Abstract

Understanding the cellular and network mechanisms of attention is critical for the development of rational therapies for diseases with attention deficits. Extracellular recordings from non-human primates show that attention increases the responsiveness of visual cortical neurons encoding an attended visual stimulus, yet there is little direct evidence to explain this phenomenon due to technical shortcomings in non-human primates. Using a novel multimodal attention task for mice, we performed 2-photon guided whole-cell recordings from layer 2/3 (L2/3) primary visual cortex (V1) neurons as animals attended or ignored visual cues. These data show that L2/3 V1 neurons depolarize while animals attend visual cues relative to when they ignore visual cues. To validate the relevance of this model, we also performed 128 channel extracellular electrophysiology from animals performing the same task and found that the responsiveness of V1 neurons increased, replicating a core finding from primate models. As a result, we show the first direct evidence that a slight depolarization could account for the increased responsiveness of neurons during attention and provide a new behavioral model that lays the foundation for several future lines of investigation.

3.2 Introduction

Because of its clinical relevance, the neurophysiological correlates of attention have been intensively studied in non-human primates. Numerous studies have found that attention increases the responsiveness of neurons that encode a visual stimulus in many areas of the visual cortex, including the primary visual cortex (V1)(Chalk et al., 2010; Fries et al., 2001b; McAdams, 2005; McAdams and Maunsell, 1999; Mehta, 2000a; Motter, 1993; Reynolds et al., 2000b; Treue and Maunsell, 1996b). Yet, the precise mechanisms by which attention increases the responsiveness of visual cortical neurons are unclear.

It has been hypothesized that prefrontal, parietal, and subcortical regions play a role in modulating the gain of visual cortical neurons during attention. Subthreshold electrical stimulation of the frontal eye fields (FEF), a part of the primate prefrontal cortex, can enhance the visual responses of V4 neurons putatively via a direct connection and potentiates the behavioral effects of attention (Gregoriou et al., 2014; 2009a; Moore, 2003; Moore and Armstrong, 2003; Squire et al., 2013). Others argue that attentional modulation of the visual cortex stems from the lateral intraparietal (LIP) region, which represents visual stimuli by their behavioral priority (Bisley and Goldberg, 2010). Subcortical regions also play a role. Acetylcholine has been shown to enhance attentional modulation when applied to V1, dopamine in prefrontal cortex modulates attention effects in visual cortex, and attention increases the efficacy of thalamocortical input on to V1 (Briggs et al., 2013; Herrero et al., 2008; McAlonan et al., 2008; Noudoost and Moore, 2011; Wimmer et al., 2015). Although many brain regions and neural systems have been identified to play a role in attention, their exact roles have yet to be clarified (Squire et al., 2013). The synaptic mechanisms remain even more controversial, with little direct evidence explaining how input from these diverse sources could alter the gain of visual cortical neurons.

Attention may increase the responsiveness of visual cortical neurons by a depolarizing mechanism. By depolarizing the membrane potential (Vm) of neurons in the visual cortex, attention would set neurons closer to their action potential threshold, increasing the responsiveness of neurons to excitatory inputs (Polack et al., 2013). Recent indirect findings argue that a subthreshold depolarization could be the source of attention modulation in the visual cortex: V4 neurons reduce their propensity to fire in bursts and latency to initiate firing in response an attended stimulus, phenomena which could be explained by a subthreshold depolarization(Anderson et al., 2013; Sundberg et al., 2012). However, these findings remain controversial because the authors do not directly measure neurons' membrane potential (Briggs et al., 2013). Because it is an extreme technical challenge to measure the Vm of

neurons in primates, direct evidence for attention-dependent Vm modulation has been very difficult to capture.

Therefore, we created a mouse model of attention amenable to Vm recordings. Using 2-photon guided whole-cell recordings to record the Vm from L2/3 V1 neurons in mice attending and ignoring identical visual cues, we found that attention to visual cues correlated with a significant depolarization during visual stimulation as compared to when animals ignored visual cues. To ensure the validity of this behavioral model, we then performed 128 channel extracellular recordings which revealed that V1 neurons significantly increased their responsiveness to visual cues and V1 enters a relatively desynchronized brain state during attention, replicating core findings from experiments in non-human primates. As a result, these data provide the first direct evidence that V1 neurons are more depolarized during attention and demonstrate the feasibility of this novel animal model for future study.

3.3 Attention to visual cues depolarizes L2/3 V1 neurons during the visual stimulus

We trained 5 mice to perform the multimodal attention task (see Figure 2-3 for schematic) and recorded the Vm from V1 L2/3 neurons using a 2-photon guided whole-cell technique as animals attended or ignored visual cues. Once a neuron was successfully patched, the attention task was initiated. In 4 out of the 5 animals, attend visual trials preceded ignore visual trials. Recordings lasted 41.51 ± 5.06 minutes, which left enough time for animals to perform both the attend visual and the ignore visual tasks (Figure 3-1). We tracked the quality of the recording over time by measuring the change in Vm baseline and the height of action potentials, a proxy for access resistance, across the recording (Figure 3A-C). In 2 out of the 5 neurons, the baseline Vm changed by less than 5 mV (Figure 3-1A-B), representing recordings of exceptional quality. In the other 3 recordings, however, the baseline changed by

over 10 mV. Averaged across all 5 recordings, the baseline Vm change was trending towards significance (mean baseline at start = -71.56 ± 3.56 mV, mean baseline at end = -59.16 ± 3.14 mV; WSRT, p = 0.0625). Spike amplitude also slowly declined over the duration of each recording, however, the aggregate mean change only trended towards significance (mean spike amplitude at start = 49.32 ± 1.84 mV, mean spike amplitude at end = 29.31 ± 3.66 mV; WSRT, p = 0.0625). Therefore, we were able to obtain recordings of sufficient length for animals to perform the behavior, but recording quality changed over the duration of the recording.

To pool responses across neurons in order to compare the Vm while animals were attending or ignoring visual cues, we first determined the optimal visual stimulus (i.e. the stimulus which evoked the greatest response, see figure 3-1D-E for an example). The mean response for the optimal and non-optimal visual stimuli were 7.35 ± 2.3 sp/s and 5.1 ± 2.7 sp/s, respectively (Figure 3-1D). To confirm which stimulus was optimal, we also compared the mean Fourier spectra of the Vm for each stimulus. Because the visual stimulus was a 2 Hz drifting grating, we observed an increase in 2 Hz power in the Vm when the optimal stimulus was shown versus the non-optimal stimulus (Figure 3-1G). The optimal visual stimulus aligned with the go visual stimulus in 2 neurons and the no-go visual stimulus in 3 neurons. Then, we averaged the subthreshold responses when animals were attending or ignoring the optimal or non-optimal visual cue when the animals initiated the correct behavior. To maintain stimulus parity, the auditory cue was also identical in both the attend and ignore condition. In 3 neurons, responses were normalized to 3 seconds prior to the trial because the baseline Vm shifted more than 5 mV over the course of the recording. As a result, the animals saw and heard the same cues with the only difference being whether the animal was instructed to attend or ignore the visual cue.

When animals attended the optimal visual cue, V1 L2/3 neurons depolarized relative to when animals ignored the identical visual cue (Figure 3-2A). Over the entire duration of

when the visual stimulus was shown, the Vm was depolarized by 2.40 ± 0.7 mV when animals attended the optimal visual stimulus as compared to when they ignored it (WSRT, p = 0.0313; Figure 3-2B). The firing rate also increased in 4 out of the 5 neurons and the average firing rate trended towards significance (WSRT, p = 0.065; Figure 3-2C). These effects cannot be explained by changes in locomotion as animal locomotion was similar when animals attended or ignored the visual stimulus (WSRT, p = 0.78; Figure 3-2D).

When animals attended the non-optimal visual cue, V1 L2/3 neurons were no more depolarized as compared to when animals ignored the identical visual cue (Figure 3-3A). Over the entire duration of when the visual stimulus was shown, the Vm was not significantly different when animals attended the optimal visual stimulus as compared to when they ignored it (WSRT, p = 0.89; Figure 3-3B). Similarly, the firing rate was unchanged between attend and ignore conditions (WSRT, p = 0.55; Figure 3-3C). Moreover, animal locomotion was not different when animals attended and ignored visual cues (WSRT, p = 0.82; Figure 3-3D).

3.4 Attention to visual cues modulates the spike rates of V1 broad and narrow spiking units during the multimodal attention task

In non-human primates, attention is correlated to increased responsiveness of visual cortical neurons and a desynchronized brain state (Chalk et al., 2010; Fries et al., 2001b; McAdams, 2005; Reynolds et al., 2000b). We performed 128 channel extracellular electrophysiology throughout the depth of V1 to determine if single units and population activity in mice performing our novel attention task act similarly circuits in non-human primates performing established spatial attention tasks. Five animals were trained to perform the multimodal task as outlined in chapter 2 and were recorded from using custom-fabricated two shank silicon microprobes (Shobe et al., 2015). Each shank of the probe, spaced 0.4 mm apart, carried 64 channels spread across 1.05 mm starting from the tip of the probe (Figure 3-4A).

To isolate single units, semi-automated spike-sorting and clustering was performed (PyClust, see methods). We identified 226 high-quality units, which expressed at maximum 0.03% refractory spikes and an average unit isolation distance of 22.65 ± 1.93 (Schmitzer-Torbert et al., 2005) (Figure 3-4D,E).

To classify neurons by different subtypes, we first identified broad spiking from narrow spiking neurons, which are putative excitatory neurons and interneurons, respectively (Niell and Stryker, 2008). For each unit, the average wave form was calculated from every spike and the time between trough and peak and the trough to peak amplitude ratio (trough/peak) was calculated (Figure 3-4D). Units with a short trough to peak time and greater trough to peak amplitude ratio were clustered as narrow spiking units. Units with a long trough to peak time and low trough to peak amplitude ratio were considered broad spiking neurons. In total, we found 159 broad and 67 narrow spiking units. To verify the quality of the clustering analysis, we superimposed the z-score normalized waveforms of each unit color coded according to the clustering analysis (Figure 3-4E). We found that the waveforms of narrow and broad spiking neurons overlapped significantly and conformed to stereotyped waveforms consistent with those previously described (Niell and Stryker, 2010; 2008). We also identified whether units responded or did not respond to the visual stimuli (45º and 135º drifting gratings) employed in the multimodal attention task (Figure 3-4F). To accomplish this, we averaged the response to the visual cues in both attend and ignore conditions and compared it to the baseline firing rate. If the firing rate increased by at least 20% for either stimulus, the unit was classified as a responding unit. Broad spiking units tended to respond preferentially for one of the stimuli whereas narrow spiking units tended to respond similarly for both units. In all, 61 broad and 38 narrow spiking units exhibited a response to either of the visual cues (Figure 3-4F). To identify the relative topographic position of units in the cortex, we employed current-source density (CSD) analysis (Figure 3-4G). We calculated the second spatial derivative of the LFP signals in response to over 150 presentations of 12 different visual cues to ascertain the CSD, a map

of local current sinks and sources along the probe shown over time (Mitzdorf, 1985; Nandy et al., 2017). The input layer, layer IV, was estimated as the region with the earliest current sink followed by a reversal to current source cross-referenced with the relative depth of the probe in the brain. The superficial layers (layers I-III) and deep layers (layers V-VI) were those layers above and below the input layer, respectively. To map where units originated from, the channel which measured the greatest amplitude waveform for the neuron was found and the unit's location was assigned based on the channel's position on the probe relative to the CSD map. Out of the neurons that displayed a response to the visual cues, the majority were located in deep layers (32 and 20 broad and narrow spiking units, respectively) and the number in the input (18 and 7 broad and narrow spiking units, respectively) and superficial (11 and 11 broad and narrow spiking units, respectively) layers were relatively equal. We hypothesize that the difference in number between unit type is a result of the relative size of cortex of each region across the probe given that the deep layers comprise about half the probe channels (Figure 3-4G).

To analyze whether responding units become more responsive when animals attend visual cues, the response of each unit was averaged in attend trials and ignore trials where the visual cue that evoked a response was shown, the auditory tone was identical, and the behavior executed was the correct behavior. This ensured that animals experienced the identical sensory context with the only difference being whether the animal was directing its attention towards or away from the visual cue.

Visual cues elicited a greater response from broad spiking and narrow spiking units when animals attended them (Figure 3-5A,B). Broad spiking units fired at 3.08 ± 0.4 Sp/s and 2.58 ± 0.3 Sp/s when animals attended and ignored the visual cue, respectively ($n = 61$, WSRT, $p = 0.0134$). Narrow spiking units fired at 7.99 ± 1.3 Sp/s and 6.79 ± 1.1 Sp/s when animals attend and ignored the visual cue, respectively ($n = 38$, WSRT, $p = 0.03$). This effect was largely driven by deep layer units, which fired significantly greater when animals attended the

visual cues (broad spiking attend = 3.59 ± 0.5 Sp/s, ignore = 2.72 ± 0.4 Sp/s, n = 32, WSRT, p = 0.004; narrow spiking attend = 12.58 ± 1.7 Sp/s, ignore = 9.85 ± 1.4 Sp/s, n = 20, WSRT, p = 0.005; Figure 3-5C). The change in firing between attend and ignore visual conditions only differed in one other population of neurons: narrow spiking input layer neurons (attend = 2.55 ± 0.6 Sp/s, ignore = 2.17 ± 0.7 Sp/s, n = 7, WSRT, p = 0.047). No effect was seen in superficial layers where whole-cell recordings were made (broad spiking attend = 1.42 ± 0.6 Sp/s, ignore = 2.76 ± 0.9 Sp/s, n = 11, WSRT, p = 0.17; narrow spiking attend = 3.11 ± 1.5 Sp/s, ignore = 4.16 ± 2.2 Sp/s, n = 11, WSRT, p = 0.15). This could be due simply to a lack of neurons in the sample pool, especially given the trending finding of spike rate modulating from the whole-cell data (Figure 3-2A,C).

We also analyzed if responses during correct go (hit) and no-go (CR) response modulated firing rates differently across attend and ignore conditions. In broad spiking neurons, 30 units responded preferentially to the go stimulus and 31 units responded preferentially to the no-go stimulus. We found that the firing rate was significantly different in broad spiking neurons during CR trials across attention conditions, but no effect was seen in broad spiking neurons during hit trials across attention conditions (CR, WSRT, p = 0.0378; Hit WSRT, p = 0.18; Figure 3-5C). In narrow spiking units, 20 units showed a response to the go stimulus and 18 neurons responded to the no-go stimulus. Just as in broad spiking neurons, we found that the firing rate was significantly different during CR trials across condigions, but no effect was seen in broad spiking neurons during CR trials across attention conditions (CR, WSRT, p = 0.0378; Hit, WSRT, p = 0.18; Figure 3-5D-E). As a result, we found that the firing rate was significantly modulated during CR responses but was not significantly changed during hit responses in broad and narrow spiking units.

In primates, spatial attention has been shown to decrease the trial-by-trial variability in spiking (Cohen and Maunsell, 2009; Herrero et al., 2013; Mitchell et al., 2007; Nandy et al., 2017). In order to investigate whether attention changed the variability of unit responses in

mice, we computed the trial-by-trial Fano factor by calculating the ratio of the variance and mean of each trial's spike counts when animals attended or ignored visual cues. For broad spiking units, the Fano factor was trending to be less when animals attended visual cues, but the change was insignificant (n = 61, WSRT, p = 0.16; Figure 3-5F). For narrow spiking units, the Fano factor was no different between attend and ignore visual stimulus trials (n = 38, WSRT, p = 0.56). In addition, the Fano factor was insignificantly different when broad and narrow units from each layer were isolated and compared to each other across attend and ignore visual trials (Two-way ANOVA, p = 0.23).

3.5 Attention causes mouse visual cortex to enter a desynchronized state consistent with findings from prior studies

In addition to increasing the responsiveness of visual cortex neurons, attention alters the local cortical state as measured by LFP recordings (Harris and Thiele, 2011). Typically, the local network enters a desynchronized state where low frequency fluctuations (<20 Hz) are diminished and higher frequencies are emphasized (>25 Hz)(Bosman et al., 2012; Chalk et al., 2010; Fries et al., 2001a; Lakatos et al., 2008). To test how the cortical state varied in our mouse model of attention, we compared the mean LFP during trials where animals were attending and ignoring visual cues. We found that the mean LFP signature varied significantly between attend and ignore trials (Figure 3-6A). During the visual stimulus, select low frequency bands (0.5-2 Hz, WSRT, p<0.0001; 10-25 Hz, WSRT, p = 0.0084) experienced a reduction in power and low gamma frequencies (25-50 Hz, WSRT, p < 0.0001) were more pronounced during attend visual trials than ignore visual trials. When the visual stimulus was off, power was reduced in all frequency bands (0.5-2 Hz, WSRT, p < 0.0001; 2-10 Hz, WSRT, p < 0.0001; 10-25 Hz, WSRT p < 0.0001; 25-50 Hz, WSRT, p < 0.0001; 50-100 Hz, WSRT, p < 0.0001) during attend visual trials as compared to ignore visual trials (Figure 3-6B,C). While these

results are compelling, only one animal's data was available for full LFP analysis because of noise present in other recordings.

Attention also has been shown to modulate visually-evoked spiking synchrony in V1 illustrated by reduced power in the spike-triggered average (STA) LFP across all frequencies (Chalk et al., 2010). We computed the STA by averaging the LFP ±150 ms around each spike for each unit during visual stimulation and averaged STAs across units based on their depth and spike properties. When animals attended the visual cues, the STA for broad and narrow spiking units in deep and input layers had reduced power across all frequencies, particularly high frequencies in input layer units (deep broad spiking, WSRT, $p = 0.0055$; deep narrow spiking, WSRT, $p = 0.043$; input broad spiking, WSRT, $p < 0.0001$; input narrow spiking, WSRT, $p = 0.0007$; Figure 3-6D). However, superficial units showed no change in STA LFP power (superficial broad spiking, WSRT, $p = 0.27$; superficial narrow spiking, WSRT, $p = 0.63$; Figure 3-6). As a result, our findings are consistent with previous working showing that attention reduces spike synchronization to the LFP across all frequencies in V1.

3.6 Discussion

Using 2-photon guided whole-cell recordings to record the Vm from L2/3 V1 neurons in mice attending and ignoring identical visual cues, we found that attention to visual cues correlated with a significant depolarization as compared to when animals ignored visual cues. We also performed 128 channel extracellular recordings which confirmed that V1 neurons significantly increase their responsiveness to visual cues, however only deep and input layer narrow and broad spiking units showed an effect. Moreover, V1 entered a desynchronized brain state during attention as deep and input layer units desynchronized their spiking from the LFP across all frequencies. As a result, these data provide the first direct evidence that V1 neurons are more depolarized during attention and demonstrate the feasibility of this novel animal model for future study.

By depolarizing the Vm of neurons in the visual cortex, attention biases the Vm closer to action potential threshold, increasing the responsiveness of neurons to excitatory inputs (Polack et al., 2013). Recent indirect findings from the Reynolds lab support that a subthreshold depolarization could be the source of attention modulation in primate visual cortex. In one study, the authors show that V4 neurons reduce their propensity to fire in bursts when animals employ spatial attention (Anderson et al., 2013). Because deep layer cortical neurons leave burst mode as they become more depolarized (Z. Wang and McCormick, 1993), these results suggest that a depolarization does occur in primates. In another study, Reynolds' lab showed that the latency to initiate firing in response to an attended stimulus was reduced as compared to when the animal did not shift attention towards the stimulus, which could occur due to a slightly depolarized Vm enabling neurons to reach threshold quicker (Sundberg et al., 2012). However, these findings were highly controversial because the authors did not directly measure neurons' membrane potential. Our findings provide definitive evidence showing that a depolarization mechanism could underlie the increased responsiveness of neurons in the visual cortex.

Our novel multi-modal mouse model of attention replicates many of the findings from attention studies in primates. Similar to primate studies, we show that attention to visual cues increases the responsiveness of neurons to visual cues, induces a desynchronized state in the visual cortex marked by increased gamma power (25-50 Hz), and reduces synchronization of single-unit firing to the LFP from 0.5-100 Hz. Yet, our findings do deviate in some small ways. For one, other studies have shown that an increase in firing rate occurs across all layers, including the superficial layers (Nandy et al., 2017). Our null result for superficial layer neurons, however, is most likely an artifact of our small sample size (superficial narrow, n = 11; superficial broad, n = 11) given that other studies included results from 150+ neurons. Another surprising finding was that attention caused a reduction in slow delta oscillations (0.5-2 Hz), but did not cause a reduction in 2-10 Hz power as has been shown in V1 of primates (Chalk

et al., 2010). This finding, again, could be an artifact of low sampling (n = 1 animal). Even more interesting was the high gamma when no visual cue was present during the attend auditory condition. No other study has shown such a dramatic shift between no stimulus and stimulus on conditions, which could be attributed to the unique multimodal nature of the task and full field stimuli. Regardless, our task replicates many of the core findings of the primate literature, which legitimizes the findings collected here and future studies using this behavioral model of attention.

The increased responsiveness and corresponding depolarization of V1 neurons could be the result of sub-cortical bottom-up forces such as thalamic drive and neuromodulation. Recent studies have shown that attention has profound effects on neuronal firing in the visual thalamus in both primates and mice (Bollimunta et al., 2011; Briggs et al., 2013; McAlonan et al., 2008; Purushothaman et al., 2012b; Wimmer et al., 2015). The thalamic reticular nucleus, under control of mPFC, may play an important role in reducing feedforward inhibition which increases drive to V1 in mice. This increased glutamatergic drive could increase the signal to noise ratio of neurons in the visual cortex (Briggs et al., 2013; Herrero et al., 2013). In addition, neuromodulation likely plays a role during attention, but the specific mechanisms are still unclear. For instance, acetylcholine enhanced attention effects to firing in V1 of primates and nicotinic receptors localize to excitatory (but not inhibitory) neuron presynaptic boutons in V1 (Disney et al., 2007a; Herrero et al., 2008), but how and where endogenous acetylcholine is released in visual cortex during attention is still unknown(Pinto et al., 2013). Norepinephrine creates a subtle Vm depolarization that enhances neuronal responsiveness when mice run (Polack et al., 2013), but there is no evidence that this same mechanism subserves attention. In the future, this mouse model can be used to confirm and dissect out the influences of each of these sources on V1 modulation during attention.

In addition to these subcortical influences, other cortical areas likely play a role in controlling the responsiveness of visual cortex neurons. In primates, prefrontal regions such

as the FEF, have been implicated in attentional gain modulation in visual cortex (Squire et al., 2013). Microstimulation and dopamine injection into FEF enhances attention modulation of V4 and complete lesions of FEF nearly abolishes the attention modulation of V4 during spatial attention tasks in primates (Gregoriou et al., 2014; Moore and Armstrong, 2003; Noudoost and Moore, 2011). In mice, circuits from prefrontal areas are capable of influencing the responsiveness of visual cortex neurons to stimulation. In particular, optogenetic activation of the anterior cingulate alone is sufficient to increase the gain of V1 neurons in behaving mice (Zhang et al., 2014). Other areas including the mPFC have also been thought to exert direct effects on V1 during behavior (Kim et al., 2016; Zhang et al., 2016). Moreover, interactions within visual cortical regions has been cited as a very important influence. In primates, V1 and V4 areas selectively synchronize in the gamma band during spatial attention, which could optimize information transfer between regions and increase drive to upstream areas (Bosman et al., 2012). Using our mouse model, optogenetics paired with extracellular recordings can be used to probe the relative contribution of each of these potential sources of attentional modulation.

Therefore, we provide the first direct evidence that attention depolarizes neurons in the visual cortex and show that mice performing a multimodal attention task are suitable to study the neural basis of attention. Given the technical advantages that mice hold over primate models, precise circuit dissection techniques can be used to finally disentangle how various brain regions contribute to attention modulation of the visual cortex. Once these influences are understood, a great effort will be made to understand the synaptic mechanisms of how these diverse influences manifest in visual cortex to exact their modulatory effects. These future studies will be critical in illustrating how complex behaviors influence perception and the neural code.

3.7 Methods

All experimental procedures were approved by the University of California, Los Angeles Office for Animal Research Oversight and by the Chancellor's Animal Research Committees. Adult (2–12 months old) male and female C57Bl6/J, SOM-Cre (JAX number 013044) × Ai9 (JAX number 007909), and PV-Cre (JAX number 008069) × Ai9 mice were anesthetized with isoflurane (3–5% induction, 1.5% maintenance) ten minutes after injection of a systemic analgesic (carprofen, 5 mg per kg of body weight) and placed in a stereotaxic frame. Mice were kept at 37°C at all times using a feedback-controlled heating pad. Pressure points and incision sites were injected with lidocaine (2%), and eyes were protected from desiccation using artificial tear ointment. The skin above the skull was incised, a custom-made lightweight metal head holder was implanted on the skull using Vetbond (3M) and a recording chamber was built using dental cement (Ortho-Jet, Lang). Mice had a recovery period from surgery of five days, during which they were administered amoxicillin (0.25 mg per ml in drinking water through the water supply). After the recovery period, mice were habituated to head fixation on the spherical treadmill. On the day of the recording, mice were anesthetized with isoflurane. To fix the ground wire, a small craniotomy (0.5 mm diameter) was made above the right cerebellum and a silver wire was implanted at the surface of the craniotomy and fixed with dental cement. A circular craniotomy (diameter = 3 mm) was performed above V1 and a 3-mm diameter coverslip drilled with a 500-μm diameter hole was placed over the dura, such that the coverslip fit entirely in the craniotomy and was flush with the skull surface. The coverslip was kept in place using Vetbond and dental cement, and the recording chamber was filled with cortex buffer containing 135 mM NaCl, 5 mM KCl, 5 mM HEPES, 1.8 mM $CaCl_2$ and 1 mM $MgCl_2$. The head-bar was fixed to a post and the mouse was placed on the spherical treadmill to recover from anesthesia. The spherical treadmill was a ball floating on small cushion of air allowing for full 2D movement. Ball motions were tracked with a custom-made tracker that reported x and y speeds at 100 Hz.

All recordings were performed at least two hours after the end of anesthesia, when the mouse was alert and could actively participate in the behavioral task.

Long-tapered micropipettes made of borosilicate glass (1.5-mm outer diameter, 0.86-mm inner diameter, Sutter Instrument) were pulled on Sutter Instruments P-1000 pipette puller to a resistance of 3–7 MΩ, and filled with an internal solution containing 115 mM potassium gluconate, 20 mM KCl, 10 mM HEPES, 10 mM phosphocreatine, 14 mM ATP-Mg, 0.3 mM GTP, and 0.01–0.05 mM Alexa-594 (for experiments with C57Bl/6 mice) or Alexa-488 (for interneuron recordings). Pipettes were lowered into the brain under two-photon imaging guidance performed with a Sutter MOM microscope using a Ti-Sapphire Ultra-2 laser (Coherent) at 800 nm and a 40× 0.8 NA Olympus water-immersion objective. Images were acquired using Scanimage 3.2 software (Pologruto et al., 2003). Whole-cell current-clamp recordings were performed using the bridge mode of an Axoclamp 2A amplifier (Molecular Devices), then further amplified and low-pass filtered at 5 kHz using a Warner Instruments amplifier (LPF 202A). ECoG recordings were performed with an alternating/direct current differential amplifier (Model 3000, A-M system) and band-pass filtered at 0.1–3,000 Hz. Analog signals were digitized at 12415 Hz with WinEDR (Strathclyde University) using a NIDAQ card (National Instruments). To ensure synchrony between physiological signals and behavioral epochs, signals relevant to the behavioral task (licking, water delivery, visual/auditory cue characteristics and timing, locomotion, and pupil size) were recorded in tandem with electrophysiological signals by the same NIDAQ card. To see details on the behavior and the software and hardware used to actuate the behavior, see chapter 2.

Extracellular nanoprobes were manufactured using the same process described previously(Shobe et al., 2015). Each nanoprobe had 2 shanks with 64 electrodes on each shank. Each shank was 1.05 mm long and 86 μm at its widest point and tapered to a tip. Each prong was separated by 400 μm. A multiplexed analog output signal was sent from the head-stage (Intan Technologies, RHA-2164B) of each probe via thin flexible cables to a 16-bit analog

to digital conversion cards (USB-6356, National Instruments), which sampled each signal at a rate of 25 kHz per channel. Surgical procedures were very similar as during whole-cell recording, with the major exception that no coverslip was implanted and the craniotomy was approximately 1 mm in diameter. Signals were then filtered offline and a background signal subtraction was performed (Shobe et al., 2015). Unit clustering was performed using PyClust, a semi-automated method for clustering units based on unit spike properties across multiple channels. All analysis of spiking and LFP was performed using MATLAB. To perform CSD analysis, the second spatial derivative was taken across channels during presentations of randomly oriented 2 Hz 0.04 degree/revolution drifting gratings. Typically, over 160 stimuli were shown at 12 different angles. The Fano factor was defined as the ratio between the variance of the spike counts and the mean spike counts of each.

3.8 Figures

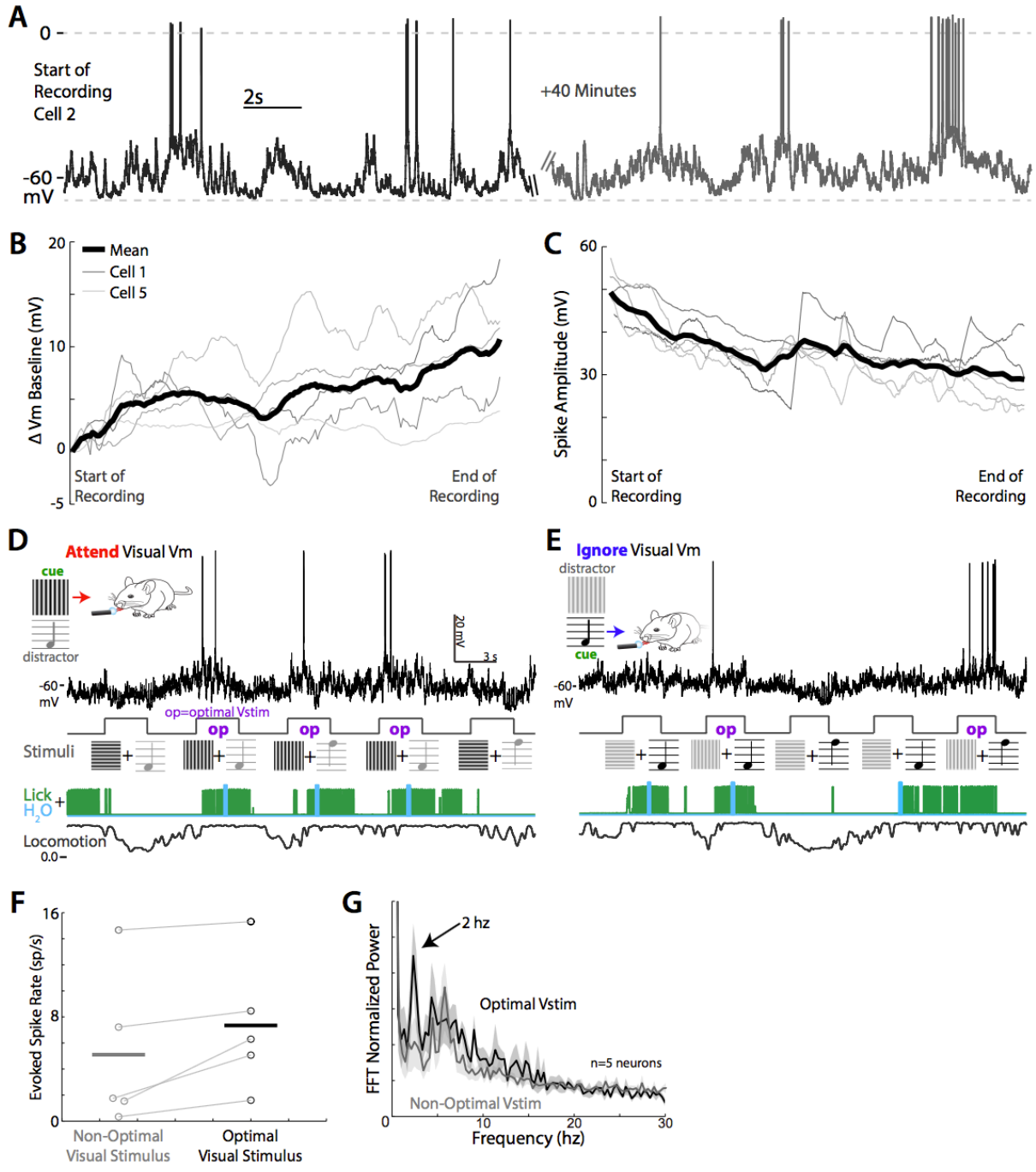

Figure 3-1. Whole-cell membrane potential characteristics as animals complete the multimodal attention task.

(A) Example Vm traces from a single neuron at the start of the recording and 40 minutes into the recording. The change in (B) Vm baseline and (C) spike amplitude over the course of

recordings from 5 neurons. The mean is shown as the thickest black line. Example traces from one neuron as the animal performs the (A) attend visual and (B) ignore visual tasks. The optimal visual stimulus, which evokes the greatest response from the neuron, is marked by the purple “op”. (F) The evoked spike rates during the non-optimal (grey) and optimal (black) visual stimuli for 5 neurons (WSRT, $p = 0.013$). (G) The frequency spectrum of the response to the optimal and non-optimal stimuli for 5 neurons.

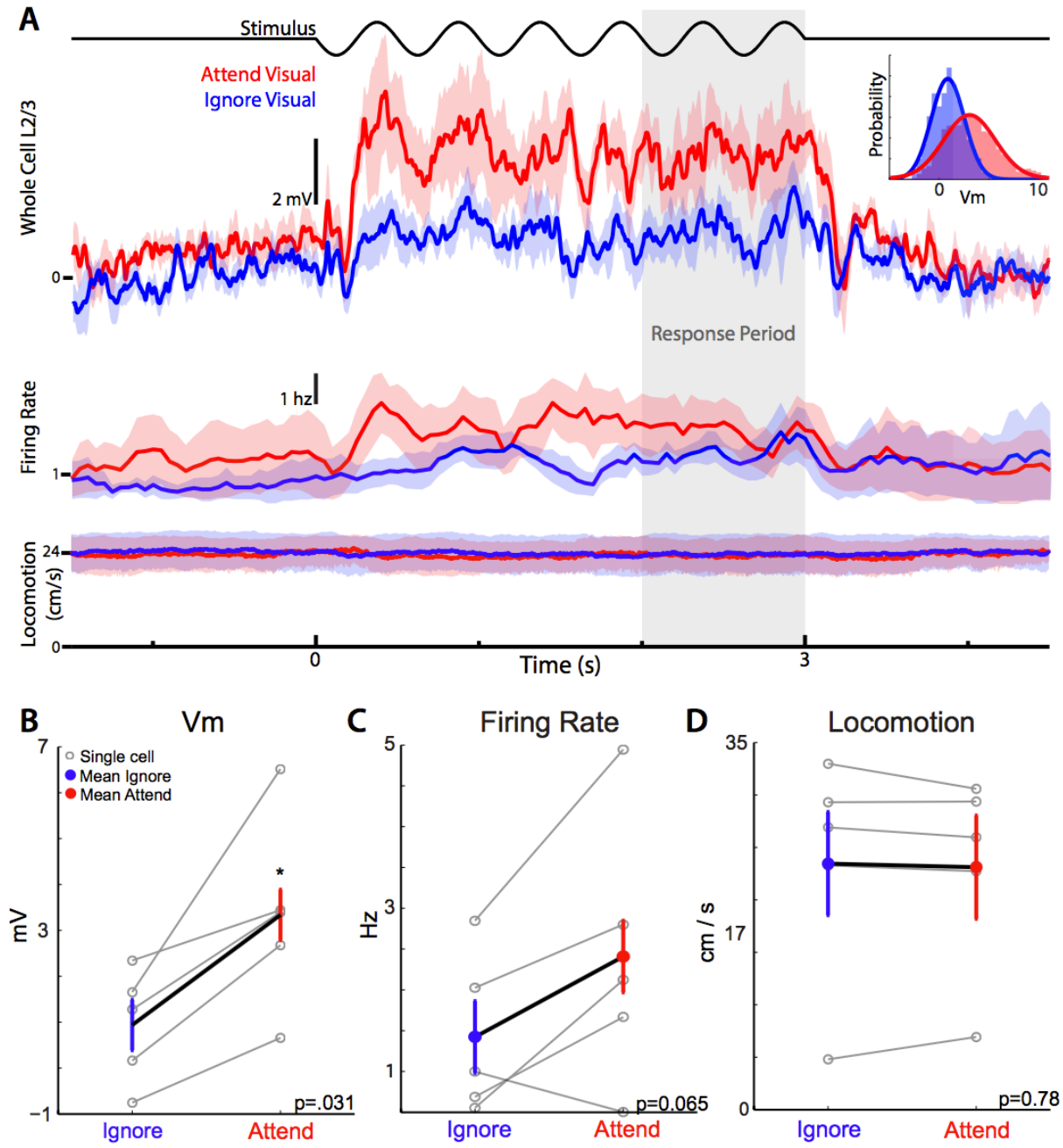

Figure 3-2. Neurons depolarize when animals attend the optimal visual stimulus.

(A) The mean Vm, histogram of the mean Vm, firing rate, and locomotion during whole-cell recordings of 5 neurons during viewing of the optimal visual stimulus in the attend (red) and ignore (blue) visual tasks. The response period is highlighted in grey. The mean (B) Vm

(WSRT, p = 0.031), (C) firing rate (WSRT, p = 0.065), and (D) locomotion (WSRT, p = 0.78) during stimulation in the attend (red) and (blue) ignore visual tasks.

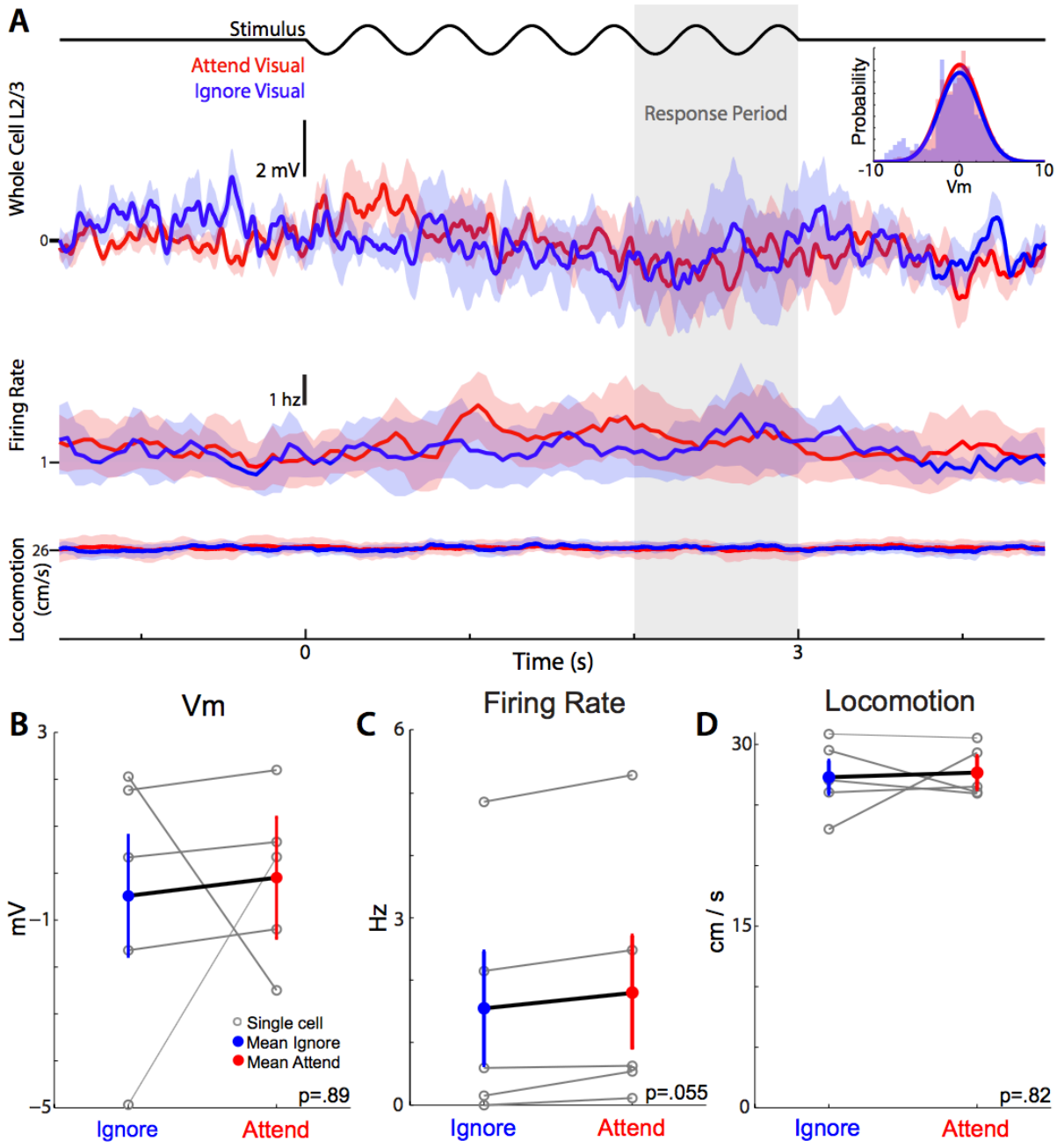

Figure 3-3. Neurons do not depolarize when animals attend the non-optimal visual stimulus.

(A) The mean Vm, histogram of the mean Vm, firing rate, and locomotion during whole-cell recordings of 5 neurons during viewing of the non-optimal visual stimulus in the attend (red) and ignore (blue) visual tasks. The response period is highlighted in grey. The mean (B) Vm (WSRT, $p = 0.89$), (C) firing rate (WSRT, $p = 0.055$), and (D) locomotion (WSRT, $p = 0.82$) during stimulation in the attend (red) and (blue) ignore visual tasks.

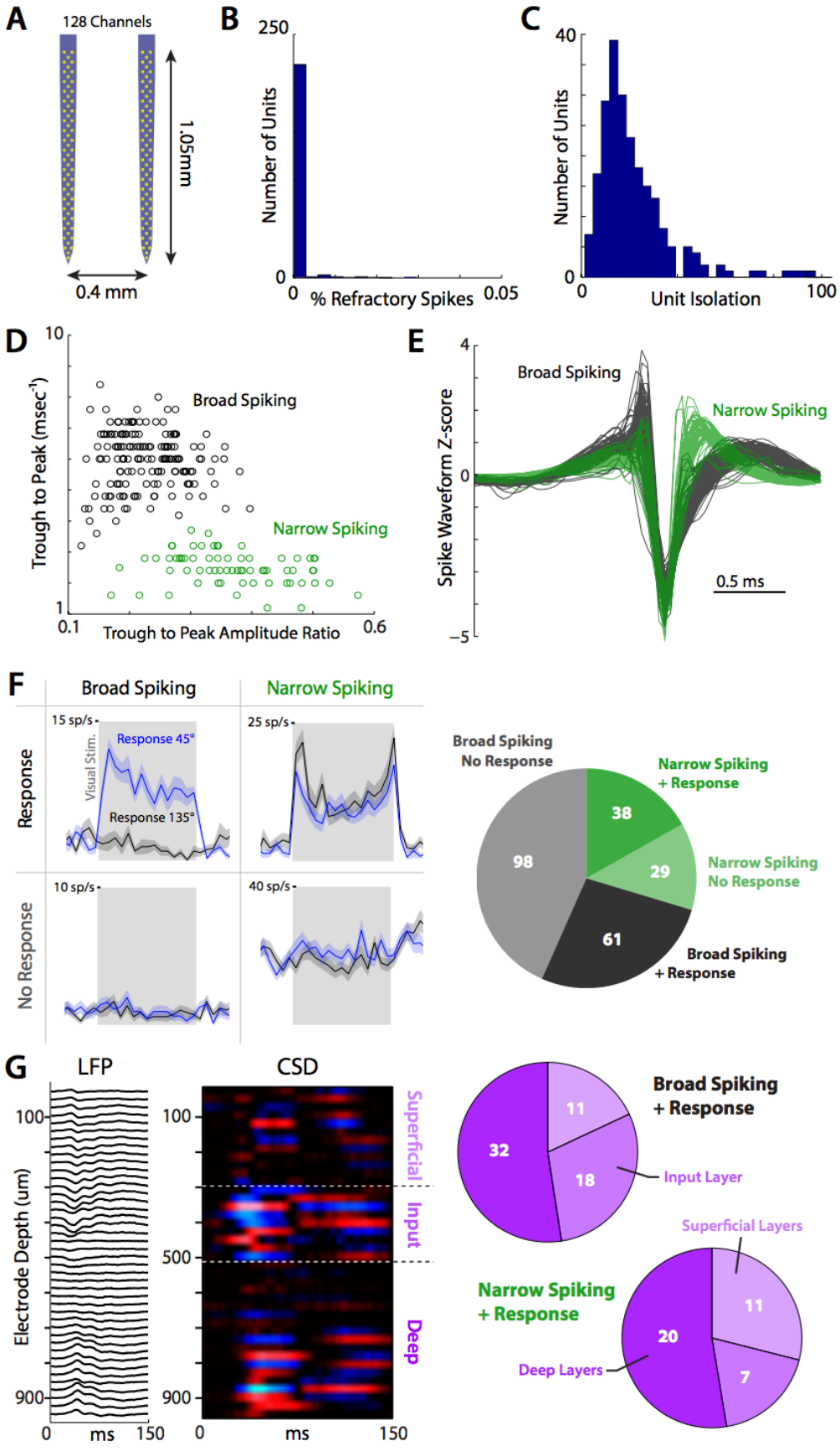
A
128 Channels
1.05mm
0.4 mm
B
250
Number of Units
0
0
% Refractory Spikes
0.05
C
40
Number of Units
0
0
Unit Isolation
100
D
10
Trough to Peak (msec-1)
Broad Spiking
Narrow Spiking
1
0.1
Trough to Peak Amplitude Ratio
0.6
E
4
Spike Waveform Z-score
Broad Spiking
Narrow Spiking
0
−5
0.5 ms
F
Broad Spiking
Narrow Spiking
Response
No Response
15 sp/s
Visual Stim.
Response 45°
Response 135°
25 sp/s
10 sp/s
40 sp/s
Broad Spiking
No Response
Narrow Spiking
+ Response
38
98
29
Narrow Spiking
No Response
61
Broad Spiking
+ Response
G
LFP
CSD
Electrode Depth (um)
100
500
900
0
ms
150
Superficial
Input
Deep
Broad Spiking
+ Response
11
32
18
Input Layer
Superficial Layers
Narrow Spiking
+ Response
11
20
7
Deep Layers

Figure 3-4. 128 channel silicon nanoprobes were used to record extracellularly from 226 units.

(A) Schematic of the 128 channel silicon nanoprobe. (B) The percent refractory spikes for each unit. The vast majority of units had 0 refractory spikes. (C) The unit isolation distance for each neuron (mean = 22.65 ± 1.93). (D) Broad and narrow spiking neurons were identified by their trough to peak time and tough to peak amplitude. (E) The mean spike waveform from each unit. Broad narrow spiking wave forms are shown in grey and green, respectively. (F) Broad and narrow spiking units were further classified by whether they exhibited a response to one of the two visual cues employed in the multimodal task. The distribution is units is shown in the pie charts. (G) The CSD was computed from the raw LFP traces to determine the depth of the units collected. The units that displayed a response were classified as superficial, input, or deep layer units. The distribution of the broad and narrow spiking responder units is shown in the pie charts.

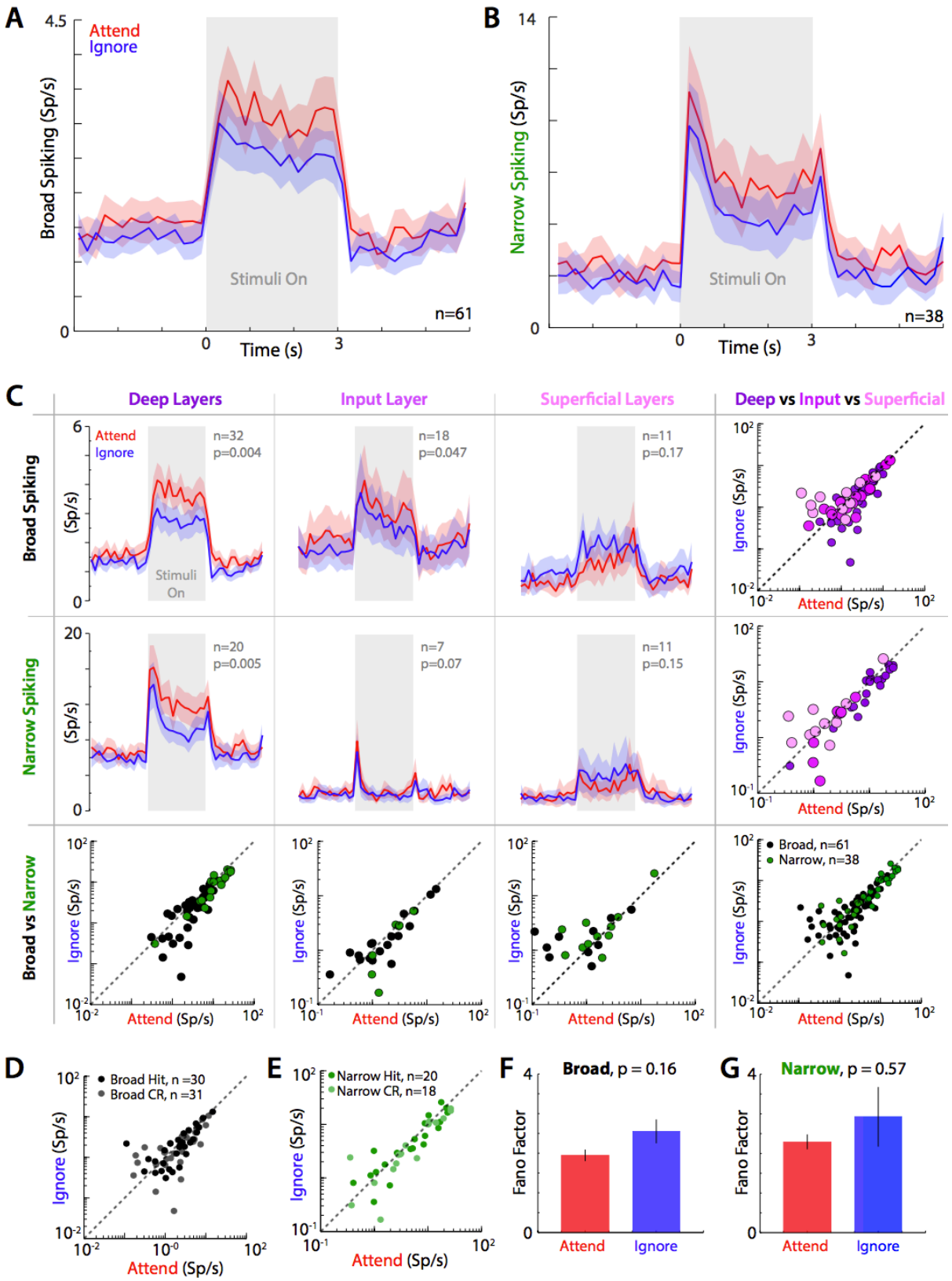
A
Attend
Ignore
Broad Spiking (Sp/s)
Stimuli On
n=61
Time (s)
B
Narrow Spiking (Sp/s)
Stimuli On
n=38
Time (s)
C
Deep Layers
Input Layer
Superficial Layers
Deep vs Input vs Superficial
Broad Spiking
Narrow Spiking
Broad vs Narrow
n=32 p=0.004
n=18 p=0.047
n=11 p=0.17
n=20 p=0.005
n=7 p=0.07
n=11 p=0.15
Ignore (Sp/s)
Attend (Sp/s)
Broad, n=61
Narrow, n=38
D
Broad Hit, n =30
Broad CR, n =31
E
Narrow Hit, n=20
Narrow CR, n=18
F
Broad, p = 0.16
Fano Factor
G
Narrow, p = 0.57

Figure 3-5. Broad and narrow spiking units in deep layers fire more when animals attend visual cues.

The mean firing rate of (A) broad (n = 61, WSRT, p = 0.0134) and (B) narrow (n = 38, WSRT, p = 0.03) spiking units when animals attend (red) and (ignore) identical visual cues. (C) The mean firing rates and mean distributions of broad (black), narrow (green) spiking units across cortical depths. Number of units and WSRT p values are shown on each figure. The mean firing rates of broad (D) and narrow (E) spiking units separated by whether the optimal stimulus aligned with the hit (darker) or CR (lighter) visual stimulus. (F) The trial-by-trial Fano factor for (F) broad and (G) narrow spiking units. WSRT p values are indicated on each figure.

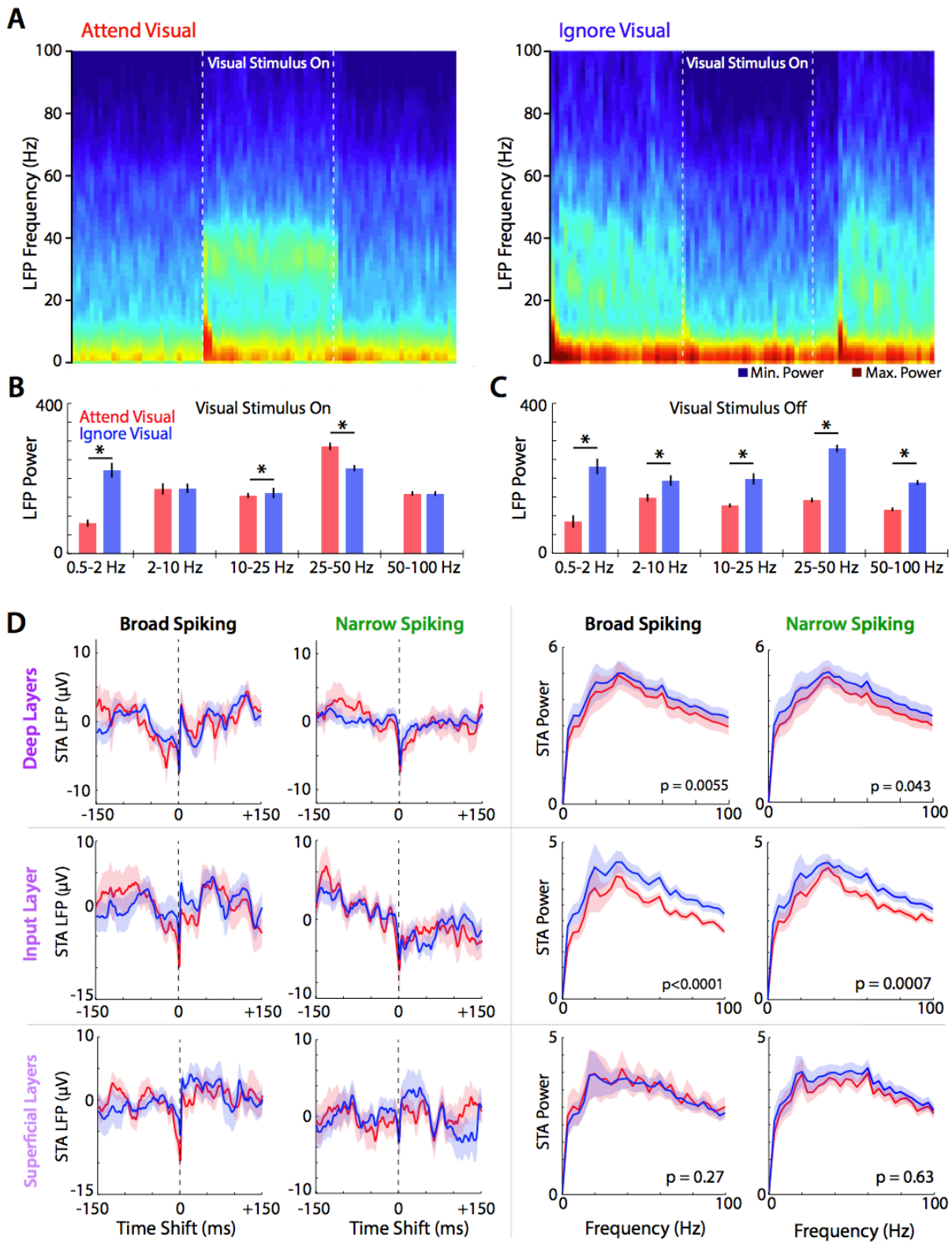

Figure 3-6. V1 desynchronizes during visual stimulation when animals attend visual cues.

(A) Mean spectrograms of V1 activity during attend and ignore visual tasks (n = 1 mouse). The mean LFP band power across 5 different frequency bands when the visual stimulus was (B) on or (C) off. During the visual stimulus, select low frequency bands (0.5-2 Hz, WSRT, $p<0.0001$; 10-25 Hz, WSRT, $p = 0.0084$) experienced a reduction in power and low gamma frequencies (25-50 Hz, WSRT, $p < 0.0001$) were more pronounced during attend visual trials than ignore visual trials. When the visual stimulus was off, power was reduced in all frequency bands (0.5-2 Hz, WSRT, $p < 0.0001$; 2-10 Hz, WSRT, $p < 0.0001$; 10-25 Hz, WSRT $p < 0.0001$; 25-50 Hz, WSRT, $p < 0.0001$; 50-100 Hz, WSRT, $p < 0.0001$) during attend visual trials as compared to ignore visual trials. (D) Mean STA and STA power for broad and narrow spiking units across cortical layers during visual stimulation. STAs were calculated by averaging ±150 ms of LFP recorded from the channel that recorded the unit waveform best for each spike during visual stimulation. WSRT p values are indicated on each STA power figure.

Afterword

Here, I have shown two mechanisms that adjust the responsiveness of neurons in V1 of mice. These findings illustrate the importance of studying the integrative properties of neurons because both mechanisms manifest only in the subthreshold Vm recordings. In the first example from chapter 1, I showed Vm oscillations that reduced the responsiveness of V1 neurons to visual input. In chapters 2 and 3, I demonstrated that attention to visual cues correlated with a small depolarization, enhancing responsiveness to visual stimulation. In both cases, Vm recordings made the findings possible and will enable each study to significantly impact their respective fields.

Despite the importance of measuring subthreshold activity in behaving animals, it is exceedingly difficult to perform such recordings. This is evidenced by the presence of only 5 neurons collected when I was studying the effects of attention in V1 in chapter 3. The failure rate of these recordings was approximately 90%, and attempts could only be made sparingly because it takes approximately a month to train animals prior to recording. Mostly, the high failure rate was due to the technically difficult nature of making whole-cell recordings in awake animals, especially ones that must also perform a very difficult behavior during recording in a short amount of time.

For these reasons, little is known about how neurons compute information in awake behaving animals. Without this information, researchers are forced to make compromises and mainly study neuronal output. While, theoretically, it is possible to understand how neural networks function by observing every neurons' output to each other and reconstructing how each neuron integrated each input, it is also technically impossible. Not knowing how neurons compute information makes it extremely difficult to create robust and flexible models that can be applicable to a wide variety of input schemes.

Yet, the day when new technology arrives that will enable the monitoring of subthreshold potentials from many neurons simultaneously is not far off. In the past decade, leaps and bounds have been made in imaging technology, especially when paired with

genetically-encoded indicators (Chen et al., 2013). Genetically encoded voltage indicators (GEVIs) are just beginning to be developed and fewer yet have been tested *in vivo* (Storace et al., 2017). So far, producing indicators that have decent signal-to-noise ratios with acceptable temporal resolution has proved difficult. But, progress seems inevitable, as small changes to these constructs can often make large and unpredictable improvements to these sensors. With enough tinkering, it seems optical measurements of membrane potential from genetically identified neural populations will soon be a reality.

In the meantime, extracellular recordings and optogentic manipulations paired with the novel multimodal attention task for mice will enable researchers to unravel the relative contributions of different sources of modulation to the increased responsiveness of V1 neurons. It will be especially important to understand how much influence arrives via thalamus versus direct cortical modulation. One could make recordings from visual thalamus and V1 and then manipulate prefrontal areas that project immediately to visual cortex versus those that are selective to determine the role of frontal areas. If this manipulation does not fully account for the attention effects found in V1, simultaneous extracellular recording from neuromodulatory areas or calcium imaging of terminals from neuromodulatory releasing neurons in V1 could be used to examine the role of neuromodulators. While progress has been made in understanding the frontal areas potentially involved, a more in depth profile of candidate frontal cortex areas could be in order prior to these experiments (Zhang et al., 2016; 2014).

All this work is done in the hopes that unraveling the mechanisms of cognition will enable new treatments for mental health deficits. Given the promise of new tools, animal models, and talent, the major constraint to progress will be money and time as the demand for knowledge of how the brain functions is ever increasing (Akil et al., 2016). A core part of this work will be understanding how the brain prioritizes information. While the research contained here will further progress in information prioritization in sensory areas, future research will extend to more complex functions as new reliable input-output relationships are detailed (e.g.

place cells). Hopefully, these findings will come to fruition in our lifetimes, creating a next generation of targeted neurotherapeutics for treating mental illness.

References

Adamou, M., Arif, M., Asherson, P., Aw, T.-C., Bolea, B., Coghill, D., Guðjónsson, G., Halmøy, A., Hodgkins, P., Müller, U., Pitts, M., Trakoli, A., Williams, N., Young, S., 2013. Occupational issues of adults with ADHD. BMC Psychiatry 13, 59. doi:10.1186/1471-244X-13-59

Akil, H., Balice-Gordon, R., Cardozo, D.L., Koroshetz, W., Posey Norris, S.M., Sherer, T., Sherman, S.M., Thiels, E., 2016. Neuroscience Training for the 21st Century. Neuron 90, 917–926. doi:10.1016/j.neuron.2016.05.030

Alho, K., Woods, D.L., Algazi, A., Näätänen, R., n.d. Intermodal selective attention. II. Effects of attentional load on processing of auditory and visual stimuli in central space. Electroencephalography and Clinical Neurophysiology 82, 356–368.

Amzica, F., Steriade, M., 1995. Short- and long-range neuronal synchronization of the slow (1 Hz) cortical oscillation. Journal of Neurophysiology 73, 20–38.

Anderson, E.B., Mitchell, J.F., Reynolds, J.H., 2013. Attention-dependent reductions in burstiness and action-potential height in macaque area V4. Nature Neuroscience 16, 1125–1131. doi:10.1038/nn.3463

Aston-Jones, G., Rajkowski, J., Cohen, J., 1999. Role of locus coeruleus in attention and behavioral flexibility. Biological Psychiatry 46, 1309–1320. doi:10.1016/S0006-3223(99)00140-7

Baker, M., 2013. Through the Eyes of a Mouse 1–3.

Bennett, C., Arroyo, S., Hestrin, S., 2013. Subthreshold Mechanisms Underlying State-Dependent Modulation of Visual Responses. Neuron 80, 350–357. doi:10.1016/j.neuron.2013.08.007

Bisley, J.W., 2011. The neural basis of visual attention. The Journal of Physiology 589, 49–57. doi:10.1113/jphysiol.2010.192666

Bisley, J.W., Goldberg, M.E., 2010. Attention, Intention, and Priority in the Parietal Lobe. Annual Review of Neuroscience 33, 1–21. doi:10.1146/annurev-neuro-060909-152823

Bollimunta, A., Mo, J., Schroeder, C.E., Ding, M., 2011. Neuronal Mechanisms and Attentional Modulation of Corticothalamic Alpha Oscillations. The Journal of Neuroscience: The Official Journal of the Society for Neuroscience 31, 4935–4943. doi:10.1523/JNEUROSCI.5580-10.2011

Bosman, C.A., Schoffelen, J.-M., Brunet, N., Oostenveld, R., Bastos, A.M., Womelsdorf, T., Rubehn, B., Stieglitz, T., De Weerd, P., Fries, P., 2012. Attentional Stimulus Selection through Selective Synchronization between Monkey Visual Areas. Neuron 75, 875–888. doi:10.1016/j.neuron.2012.06.037

Boyden, E.S., Zhang, F., Bamberg, E., Nagel, G., Deisseroth, K., 2005. Millisecond-timescale, genetically targeted optical control of neural activity. Nature Neuroscience 8, 1263–1268. doi:10.1038/nn1525

Briggs, F., Mangun, G.R., Usrey, W.M., 2013. Attention enhances synaptic efficacy and the signal-to-noise ratio in neural circuits. Nature 499, 476–480. doi:10.1038/nature12276

Buschman, T.J., Miller, E.K., 2007. Top-Down Versus Bottom-Up Control of Attention in the Prefrontal and Posterior Parietal Cortices. Science 315, 1860–1862. doi:10.1126/science.1138071

Buzsáki, G., Draguhn, A., 2004. Neuronal oscillations in cortical networks. Science (New York, N.Y.) 304, 1926–1929. doi:10.1126/science.1099745

Cai, D.J., Aharoni, D., Shuman, T., Shobe, J., Biane, J., Song, W., Wei, B., Veshkini, M., La-Vu, M., Lou, J., Flores, S.E., Kim, I., Sano, Y., Zhou, M., Baumgaertel, K., Lavi, A., Kamata, M., Tuszynski, M., Mayford, M., Golshani, P., Silva, A.J., 2016. A shared neural ensemble links distinct contextual memories encoded close in time. Nature 534, 115–118. doi:10.1038/nature17955

Carandini, M., Ferster, D., 1997. A Tonic Hyperpolarization Underlying Contrast Adaptation in Cat Visual Cortex. Science 276, 949–952. doi:10.1126/science.276.5314.949

Cardin, J.A., Palmer, L.A., Contreras, D., 2008. Cellular mechanisms underlying stimulus-

dependent gain modulation in primary visual cortex neurons in vivo. Neuron 59, 150–160. doi:10.1016/j.neuron.2008.05.002

Chalk, M., Herrero, J.L., Gieselmann, M.A., Delicato, L.S., Gotthardt, S., Thiele, A., 2010. Attention Reduces Stimulus-Driven Gamma Frequency Oscillations and Spike Field Coherence in V1. Neuron 66, 114–125. doi:10.1016/j.neuron.2010.03.013

Chen, T.-W., Wardill, T.J., Sun, Y., Pulver, S.R., Renninger, S.L., Baohan, A., Schreiter, E.R., Kerr, R.A., Orger, M.B., Jayaraman, V., Looger, L.L., Svoboda, K., Kim, D.S., 2013. Ultrasensitive fluorescent proteins for imaging neuronal activity. Nature 499, 295–300. doi:10.1038/nature12354

Chubykin, A.A., Roach, E.B., Bear, M.F., Shuler, M.G.H., 2013. A cholinergic mechanism for reward timing within primary visual cortex. Neuron 77, 723–735. doi:10.1016/j.neuron.2012.12.039

Cohen, M.R., Maunsell, J.H.R., 2009. Attention improves performance primarily by reducing interneuronal correlations. Nature Neuroscience 12, 1594–1600. doi:10.1038/nn.2439

Contreras, D., 2006. The role of T-channels in the generation of thalamocortical rhythms. CNS \& neurological disorders drug targets 5, 571–585.

Contreras, D., Steriade, M., 1995. Cellular basis of EEG slow rhythms: a study of dynamic corticothalamic relationships. The Journal of Neuroscience: The Official Journal of the Society for Neuroscience 15, 604–622.

Crochet, S., Petersen, C.C.H., 2006. Correlating whisker behavior with membrane potential in barrel cortex of awake mice. Nature Neuroscience 9, 608–610. doi:10.1038/nn1690

Deisseroth, K., Feng, G., Majewska, A.K., Miesenbock, G., Ting, A., Schnitzer, M.J., 2006. Next-Generation Optical Technologies for Illuminating Genetically Targeted Brain Circuits. The Journal of Neuroscience: The Official Journal of the Society for Neuroscience 26, 10380–10386. doi:10.1523/JNEUROSCI.3863-06.2006

Destexhe, A., Rudolph, M., Paré, D., 2003. The high-conductance state of neocortical

neurons in vivo. Nature Reviews Neuroscience 4, 739–751. doi:10.1038/nrn1198

DESTEXHE, A., Sejnowski, T.J., 2003. Interactions Between Membrane Conductances Underlying Thalamocortical Slow-Wave Oscillations. Physiological reviews 83, 1401–1453. doi:10.1152/physrev.00012.2003

Disney, A.A., Aoki, C., Hawken, M.J., 2007a. Gain Modulation by Nicotine in Macaque V1. Neuron 56, 701–713. doi:10.1016/j.neuron.2007.09.034

Disney, A.A., Aoki, C., Hawken, M.J., 2007b. Gain Modulation by Nicotine in Macaque V1. Neuron 56, 701–713. doi:10.1016/j.neuron.2007.09.034

Doniger, G.M., Silipo, G., Rabinowicz, E.F., Snodgrass, J.G., Javitt, D.C., 2001. Impaired Sensory Processing as a Basis for Object-Recognition Deficits in Schizophrenia. AJP 158, 1818–1826. doi:10.1176/appi.ajp.158.11.1818

Du, J., Blanche, T.J., Harrison, R.R., Lester, H.A., Masmanidis, S.C., 2011. Multiplexed, High Density Electrophysiology with Nanofabricated Neural Probes. PLOS ONE 6, e26204. doi:10.1371/journal.pone.0026204

Engel, A.K., Fries, P., Singer, W., 2001. Dynamic predictions: Oscillations and synchrony in top–down processing. Nature Reviews Neuroscience 2, 704–716. doi:10.1038/35094565

Fries, P., Neuenschwander, S., Engel, A.K., Goebel, R., Singer, W., 2001a. Rapid feature selective neuronal synchronization through correlated latency shifting. Nature Neuroscience 4, 194–200. doi:10.1038/84032

Fries, P., Reynolds, J.H., Rorie, A.E., Desimone, R., 2001b. Modulation of Oscillatory Neuronal Synchronization by Selective Visual Attention. Science 291, 1560–1563. doi:10.1126/science.1055465

Fries, P., Womelsdorf, T., Oostenveld, R., Desimone, R., 2008. The Effects of Visual Stimulation and Selective Visual Attention on Rhythmic Neuronal Synchronization in Macaque Area V4. Journal of Neuroscience 28, 4823–4835. doi:10.1523/JNEUROSCI.4499-07.2008

Gadow, K.D., DeVincent, C.J., Pomeroy, J., 2006. ADHD Symptom Subtypes in Children with Pervasive Developmental Disorder. J Autism Dev Disord 36, 271–283. doi:10.1007/s10803-005-0060-3

Ghosh, K.K., Burns, L.D., Cocker, E.D., Nimmerjahn, A., Ziv, Y., Gamal, A.E., Schnitzer, M.J., 2011. Miniaturized integration of a fluorescence microscope. Nat Meth 8, 871–878. doi:10.1038/nmeth.1694

Gilzenrat, M.S., Nieuwenhuis, S., Jepma, M., Cohen, J.D., 2010. Pupil diameter tracks changes in control state predicted by the adaptive gain theory of locus coeruleus function. Cognitive, Affective, \& Behavioral Neuroscience 10, 252–269. doi:10.3758/CABN.10.2.252

Goldstein, S., Schwebach, A.J., 2004. The Comorbidity of Pervasive Developmental Disorder and Attention Deficit Hyperactivity Disorder: Results of a Retrospective Chart Review. J Autism Dev Disord 34, 329–339. doi:10.1023/B:JADD.0000029554.46570.68

Gregoriou, G.G., Gotts, S.J., Zhou, H., Desimone, R., 2009a. High-Frequency, Long-Range Coupling Between Prefrontal and Visual Cortex During Attention. Science 324, 1207–1210. doi:10.1126/science.1171402

Gregoriou, G.G., Gotts, S.J., Zhou, H., Desimone, R., 2009b. High-frequency, long-range coupling between prefrontal and visual cortex during attention. Science (New York, N.Y.) 324, 1207–1210. doi:10.1126/science.1171402

Gregoriou, G.G., Rossi, A.F., Ungerleider, L.G., Desimone, R., 2014. Lesions of prefrontal cortex reduce attentional modulation of neuronal responses and synchrony in V4. Nature Neuroscience 17, 1003–1011. doi:10.1038/nn.3742

Hackley, S.A., Woldorff, M., Hillyard, S.A., 1990. Cross-Modal Selective Attention Effects on Retinal, Myogenic, Brainstem, and Cerebral Evoked Potentials. Psychophysiology 27, 195–208. doi:10.1111/j.1469-8986.1990.tb00370.x

Haider, B., Häusser, M., Carandini, M., 2012. Inhibition dominates sensory responses in the

awake cortex. Nature 493, 97–100. doi:10.1038/nature11665

Halassa, M.M., 2011. Thalamocortical dynamics of sleep: roles of purinergic neuromodulation. Seminars in cell \& developmental biology 22, 245–251. doi:10.1016/j.semcdb.2011.02.008

Harris, K.D., Thiele, A., 2011. Cortical state and attention. Nature Reviews Neuroscience 12, 509–523. doi:10.1038/nrn3084

Heinrichs, R.W., Zakzanis, K.K., 1998. Neurocognitive deficit in schizophrenia: A quantitative review of the evidence. Neuropsychology 12, 426–445. doi:10.1037/0894-4105.12.3.426

Herrero, J.L., Gieselmann, M.A., Sanayei, M., Thiele, A., 2013. Attention-Induced Variance and Noise Correlation Reduction in Macaque V1 Is Mediated by NMDA Receptors. Neuron 78, 729–739.

Herrero, J.L., Roberts, M.J., Delicato, L.S., Gieselmann, M.A., Dayan, P., Thiele, A., 2008. Acetylcholine contributes through muscarinic receptors to attentional modulation in V1. Nature 454, 1110–1114. doi:10.1038/nature07141

Holst, Y., Thorell, L.B., 2017. Neuropsychological Functioning in Adults With ADHD and Adults With Other Psychiatric Disorders. Journal of Attention Disorders 21, 137–148. doi:10.1177/1087054713506264

Holwerda, A., van der Klink, J.J.L., de Boer, M.R., Groothoff, J.W., Brouwer, S., n.d. Predictors of work participation of young adults with mild intellectual disabilities. Research in Developmental Disabilities 34, 1982–1990.

Hume, K., Odom, S., 2006. Effects of an Individual Work System on the Independent Functioning of Students with Autism. J Autism Dev Disord 37, 1166–1180. doi:10.1007/s10803-006-0260-5

Inoue, K.-I., Takada, M., Matsumoto, M., 2015. Neuronal and behavioural modulations by pathway-selective optogenetic stimulation of the primate oculomotor system. Nature Communications 6, 1–7. doi:10.1038/ncomms9378

Jahnsen, H., Llinás, R., 1984. Electrophysiological properties of guinea-pig thalamic neurones: an in vitro study. The Journal of Physiology 349, 205–226.

Javitt, D.C., 2009. Sensory Processing in Schizophrenia: Neither Simple nor Intact. Schizophrenia Bulletin 35, 1059–1064. doi:10.1093/schbul/sbp110

Kim, H., Ährlund-Richter, S., Wang, X., Deisseroth, K., Carlén, M., 2016. Prefrontal Parvalbumin Neurons in Control of Attention. Cell 164, 208–218. doi:10.1016/j.cell.2015.11.038

Klimesch, W., 2012. Alpha-band oscillations, attention, and controlled access to stored information. Trends in Cognitive Sciences 16, 606–617. doi:10.1016/j.tics.2012.10.007

Komiyama, T., Sato, T.R., O'Connor, D.H., Zhang, Y.-X., Huber, D., Hooks, B.M., Gabitto, M., Svoboda, K., 2010. Learning-related fine-scale specificity imaged in motor cortex circuits of behaving mice. Nature 464, 1182–1186. doi:10.1038/nature08897

Krauzlis, R.J., Lovejoy, L.P., Zénon, A., 2013. Superior Colliculus and Visual Spatial Attention. Annual Review of Neuroscience 36, 165–182. doi:10.1146/annurev-neuro-062012-170249

Lakatos, P., Karmos, G., Mehta, A.D., Ulbert, I., Schroeder, C.E., 2008. Entrainment of neuronal oscillations as a mechanism of attentional selection. Science (New York, N.Y.) 320, 110–113. doi:10.1126/science.1154735

Lampl, I., Reichova, I., Ferster, D., 1999. Synchronous Membrane Potential Fluctuations in Neurons of the Cat Visual Cortex. Neuron 22, 361–374. doi:10.1016/S0896-6273(00)81096-X

Laramee, M.-E., Boire, D., 2015. Visual cortical areas of the mouse: comparison of parcellation and network structure with primates. Frontiers in Neural Circuits 8, 62. doi:10.3389/fncir.2014.00149

Lee, H., Simpson, G.V., Logothetis, N.K., Rainer, G., 2005. Phase Locking of Single Neuron Activity to Theta Oscillations during Working Memory in Monkey Extrastriate Visual

Cortex. Neuron 45, 147–156. doi:10.1016/j.neuron.2004.12.025

Liebe, S., Hoerzer, G.M., Logothetis, N.K., Rainer, G., 2012. Theta coupling between V4 and prefrontal cortex predicts visual short-term memory performance. Nature Neuroscience 15, 456–462. doi:10.1038/nn.3038

Liu, D., Gu, X., Zhu, J., Zhang, X., Han, Z., Yan, W., Cheng, Q., Hao, J., Fan, H., Hou, R., Chen, Z., Chen, Y., Li, C.T., 2014. Medial prefrontal activity during delay period contributes to learning of a working memory task. Science 346, 458–463. doi:10.1126/science.1256573

Luck, S.J., Chelazzi, L., Hillyard, S.A., Desimone, R., 1997. Neural Mechanisms of Spatial Selective Attention in Areas V1, V2, and V4 of Macaque Visual Cortex. J Neurophysiol 77, 24–19. doi:10.1038/363345a0

Makino, H., Komiyama, T., 2015. Learning enhances the relative impact of top-down processing in the visual cortex. Nature Neuroscience 18, 1116–1122. doi:10.1038/nn.4061

McAdams, C.J., 2005. Attention Modulates the Responses of Simple Cells in Monkey Primary Visual Cortex. The Journal of Neuroscience: The Official Journal of the Society for Neuroscience 25, 11023–11033. doi:10.1523/JNEUROSCI.2904-05.2005

McAdams, C.J., Maunsell, J.H.R., 1999. Effects of Attention on the Reliability of Individual Neurons in Monkey Visual Cortex. Neuron 23, 765–773. doi:10.1016/S0896-6273(01)80034-9

McAlonan, K., Cavanaugh, J., Wurtz, R.H., 2008. Guarding the gateway to cortex with attention in visual thalamus. Nature 456, 391–394. doi:10.1038/nature07382

McCormick, D.A., 1989. Cholinergic and noradrenergic modulation of thalamocortical processing. Trends in Neurosciences 12, 215–221.

McCormick, D.A., Wang, Z., Huguenard, J., 1993. Neurotransmitter control of neocortical neuronal activity and excitability. Cerebral Cortex (New York, N.Y.: 1991) 3, 387–398.

McGinley, M.J., David, S.V., McCormick, D.A., 2015. Cortical Membrane Potential Signature of Optimal States for Sensory Signal Detection. Neuron 87, 179–192. doi:10.1016/j.neuron.2015.05.038

Mehta, A.D., 2000a. Intermodal Selective Attention in Monkeys. I: Distribution and Timing of Effects across Visual Areas. Cerebral Cortex 10, 343–358. doi:10.1093/cercor/10.4.343

Mehta, A.D., 2000b. Intermodal Selective Attention in Monkeys. II: Physiological Mechanisms of Modulation. Cerebral Cortex 10, 359–370. doi:10.1093/cercor/10.4.359

Mitchell, J.F., Sundberg, K.A., Reynolds, J.H., 2009. Spatial attention decorrelates intrinsic activity fluctuations in macaque area V4. Neuron 63, 879–888. doi:10.1016/j.neuron.2009.09.013

Mitchell, J.F., Sundberg, K.A., Reynolds, J.H., 2007. Differential Attention-Dependent Response Modulation across Cell Classes in Macaque Visual Area V4. Neuron 55, 131–141. doi:10.1016/j.neuron.2007.06.018

Mitzdorf, U., 1985. Current source-density method and application in cat cerebral cortex: investigation of evoked potentials and EEG phenomena. Physiol Rev 65, 37.

Moore, T., 2003. Microstimulation of the Frontal Eye Field and Its Effects on Covert Spatial Attention. Journal of Neurophysiology 91, 152–162. doi:10.1152/jn.00741.2002

Moore, T., Armstrong, K.M., 2003. Selective gating of visual signals by microstimulation of frontal cortex. Nature 421, 370–373. doi:10.1038/nature01341

Moosmann, M., Ritter, P., Krastel, I., Brink, A., Thees, S., Blankenburg, F., Taskin, B., Obrig, H., Villringer, A., 2003. Correlates of alpha rhythm in functional magnetic resonance imaging and near infrared spectroscopy. NeuroImage 20, 145–158. doi:10.1016/S1053-8119(03)00344-6

Moran, J., Desimone, R., 1985. Selective attention gates visual processing in the extrastriate cortex. Science (New York, N.Y.) 229, 782–784.

Motter, B.C., 1993. Focal attention produces spatially selective processing in visual cortical

areas V1, V2, and V4 in the presence of competing stimuli. Journal of Neurophysiology 70, 909–919.

Mottron, L., Dawson, M., Soulières, I., Hubert, B., Burack, J., 2006. Enhanced Perceptual Functioning in Autism: An Update, and Eight Principles of Autistic Perception. J Autism Dev Disord 36, 27–43. doi:10.1007/s10803-005-0040-7

Nandy, A.S., Nassi, J.J., Reynolds, J.H., 2017. Laminar Organization of Attentional Modulation in Macaque Visual Area V4. Neuron 93, 235–246. doi:10.1016/j.neuron.2016.11.029

Niell, C.M., Stryker, M.P., 2010. Modulation of Visual Responses by Behavioral State in Mouse Visual Cortex. Neuron 65, 472–479. doi:10.1016/j.neuron.2010.01.033

Niell, C.M., Stryker, M.P., 2008. Highly Selective Receptive Fields in Mouse Visual Cortex. The Journal of Neuroscience: The Official Journal of the Society for Neuroscience 28, 7520–7536. doi:10.1523/JNEUROSCI.0623-08.2008

Noudoost, B., Moore, T., 2011. Control of visual cortical signals by prefrontal dopamine. Nature 474, 372–375. doi:10.1038/nature09995

Nowak, L.G., Sanchez-Vives, M.V., McCormick, D.A., 2005. Role of Synaptic and Intrinsic Membrane Properties in Short-Term Receptive Field Dynamics in Cat Area 17. Journal of Neuroscience 25, 1866–1880. doi:10.1523/JNEUROSCI.3897-04.2005

Palmer, B.W., Dawes, S.E., Heaton, R.K., 2009. What Do We Know About Neuropsychological Aspects Of Schizophrenia? Neuropsychology Review 19, 365–384.

Perry, R.J., 1999. Attention and executive deficits in Alzheimer's disease: A critical review. Brain 122, 383–404. doi:10.1093/brain/122.3.383

Petersen, C.C.H., Hahn, T.T.G., Mehta, M., Grinvald, A., Sakmann, B., 2003. Interaction of sensory responses with spontaneous depolarization in layer 2/3 barrel cortex. Proceedings of the National Academy of Sciences 100, 13638–13643. doi:10.1073/pnas.2235811100

Pfurtscheller, G., Stancák, A., Jr, Neuper, C., 1996. Event-related synchronization (ERS) in the alpha band — an electrophysiological correlate of cortical idling: A review. International Journal of Psychophysiology 24, 39–46. doi:10.1016/S0167-8760(96)00066-9

Pinto, L., Goard, M.J., Estandian, D., Xu, M., Kwan, A.C., Lee, S.-H., Harrison, T.C., Feng, G., Dan, Y., 2013. Fast modulation of visual perception by basal forebrain cholinergic neurons. Nature Neuroscience 16, 1857–1863. doi:10.1038/nn.3552

Polack, P.-O., Friedman, J., Golshani, P., 2013. Cellular mechanisms of brain state-dependent gain modulation in visual cortex. Nature Neuroscience 16, 1331–1339. doi:10.1038/nn.3464

Pologruto, T.A., Sabatini, B.L., Svoboda, K., 2003. ScanImage: Flexible software for operating laser scanning microscopes. BioMedical Engineering OnLine 2, 13. doi:10.1186/1475-925X-2-13

Posner, M.I., 1980. Orienting of attention. The Quarterly Journal of Experimental Psychology 32, 3–25.

Poulet, J.F.A., Petersen, C.C.H., 2008. Internal brain state regulates membrane potential synchrony in barrel cortex of behaving mice. Nature 454, 881–885. doi:10.1038/nature07150

Purushothaman, G., Marion, R., Li, K., Casagrande, V.A., 2012a. Gating and control of primary visual cortex by pulvinar. Nature Neuroscience 15, 905–912. doi:10.1038/nn.3106

Purushothaman, G., Marion, R., Li, K., Casagrande, V.A., 2012b. Gating and control of primary visual cortex by pulvinar. Nature Neuroscience 15, 905–912. doi:10.1038/nn.3106

Reimer, J., Froudarakis, E., Cadwell, C.R., Yatsenko, D., Denfield, G.H., Tolias, A.S., 2014. Pupil Fluctuations Track Fast Switching of Cortical States during Quiet Wakefulness.

Neuron 84, 355–362. doi:10.1016/j.neuron.2014.09.033

Reynolds, J.H., Chelazzi, L., Desimone, R., 1999. Competitive Mechanisms Subserve Attention in Macaque Areas V2 and V4. J. Neurosci. 19, 1736–1753. doi:10.1146/annurev.ne.18.030195.001205

Reynolds, J.H., Pasternak, T., Desimone, R., 2000a. Attention Increases Sensitivity of V4 Neurons. Neuron 26, 703–714. doi:10.1016/S0896-6273(00)81206-4

Reynolds, J.H., Pasternak, T., Desimone, R., 2000b. Attention Increases Sensitivity of V4 Neurons. Neuron 26, 703–714. doi:10.1016/S0896-6273(00)81206-4

Riga, D., Matos, M.R., Glas, A., Smit, A.B., Spijker, S., Van den Oever, M.C., 2014. Optogenetic dissection of medial prefrontal cortex circuitry. Front. Syst. Neurosci. 8, 1025. doi:10.3389/fnsys.2014.00230

Roelfsema, P.R., Lamme, V.A., Spekreijse, H., 1998. Object-based attention in the primary visual cortex of the macaque monkey. Nature 395, 376–381. doi:10.1038/26475

Saalmann, Y.B., Pinsk, M.A., Wang, L., Li, X., Kastner, S., 2012. The Pulvinar Regulates Information Transmission Between Cortical Areas Based on Attention Demands. Science 337, 753–756. doi:10.1126/science.1223082

Saper, C.B., Scammell, T.E., Lu, J., 2005. Hypothalamic regulation of sleep and circadian rhythms. Nature 437, 1257–1263. doi:10.1038/nature04284

Sarter, M., Hasselmo, M.E., Bruno, J.P., Givens, B., 2005. Unraveling the attentional functions of cortical cholinergic inputs: interactions between signal-driven and cognitive modulation of signal detection. Brain Research Reviews 48, 98–111. doi:10.1016/j.brainresrev.2004.08.006

Schmitzer-Torbert, N., Jackson, J., Henze, D., Harris, K., Redish, A.D., 2005. Quantitative measures of cluster quality for use in extracellular recordings. Neuroscience 131, 1–11.

Schneider, D.M., Nelson, A., Mooney, R., 2014. A synaptic and circuit basis for corollary discharge in the auditory cortex. Nature 513, 189–194. doi:10.1038/nature13724

Schroeder, C.E., Lakatos, P., 2009. Low-frequency neuronal oscillations as instruments of sensory selection. Trends in Neurosciences 32, 9–18. doi:10.1016/j.tins.2008.09.012

Shobe, J.L., Claar, L.D., Parhami, S., Bakhurin, K.I., Masmanidis, S.C., 2015. Brain activity mapping at multiple scales with silicon microprobes containing 1,024 electrodes. Journal of Neurophysiology 114, 2043–2052.

Squire, R.F., Noudoost, B., Schafer, R.J., Moore, T., 2013. Prefrontal Contributions to Visual Selective Attention. Annual Review of Neuroscience 36, 451–466. doi:10.1146/annurev-neuro-062111-150439

Steriade, M., McCormick, D.A., Sejnowski, T.J., 1993. Thalamocortical oscillations in the sleeping and aroused brain. Science (New York, N.Y.) 262, 679–685.

Steriade, M., Timofeev, I., Grenier, F., 2001. Natural waking and sleep states: a view from inside neocortical neurons. Journal of Neurophysiology 85, 1969–1985.

Storace, D., Sepehri Rad, M., Kang, B., Cohen, L.B., Hughes, T., Baker, B.J., 2017. Toward Better Genetically Encoded Sensors of Membrane Potential. Trends in Neurosciences 39, 277–289. doi:10.1016/j.tins.2016.02.005

Sundberg, K.A., Mitchell, J.F., Gawne, T.J., Reynolds, J.H., 2012. Attention Influences Single Unit and Local Field Potential Response Latencies in Visual Cortical Area V4. The Journal of Neuroscience: The Official Journal of the Society for Neuroscience 32, 16040–16050. doi:10.1523/JNEUROSCI.0489-12.2012

Tan, A.Y.Y., Chen, Y., Scholl, B., Seidemann, E., Priebe, N.J., 2014. Sensory stimulation shifts visual cortex from synchronous to asynchronous states. Nature 509, 226–229. doi:10.1038/nature13159

Taniguchi, H., 2014. Genetic dissection of GABAergic neural circuits in mouse neocortex. Frontiers in Cellular Neuroscience 8, 8. doi:10.3389/fncel.2014.00008

Treue, S., Maunsell, J.H., 1996a. Attentional modulation of visual motion processing in cortical areas MT and MST. Nature 382, 539–541. doi:10.1038/382539a0

Treue, S., Maunsell, J.H.R., 1996b. Attentional modulation of visual motion processing in cortical areas MT and MST. Nature 382, 539–541. doi:10.1038/382539a0

Vaughan, B., Kratochvil, C.J., 2012. Pharmacotherapy of Pediatric Attention-Deficit/Hyperactivity Disorder. Psychopharmacology 21, 941–955.

Vinck, M., Batista-Brito, R., Knoblich, U., Cardin, J.A., 2015. Arousal and locomotion make distinct contributions to cortical activity patterns and visual encoding. Neuron 86, 740–754. doi:10.1016/j.neuron.2015.03.028

Vyazovskiy, V.V., Olcese, U., Hanlon, E.C., Nir, Y., Cirelli, C., Tononi, G., 2011. Local sleep in awake rats. Nature 472, 443–447. doi:10.1038/nature10009

Wang, Q., Burkhalter, A., 2007. Area map of mouse visual cortex. J. Comp. Neurol. 502, 339–357. doi:10.1002/cne.21286

Wang, Z., McCormick, D.A., 1993. Control of firing mode of corticotectal and corticopontine layer V burst-generating neurons by norepinephrine, acetylcholine, and 1S,3R- ACPD. J. Neurosci. 13, 2199.

Wiest, M.C., Nicolelis, M.A.L., 2003. Behavioral detection of tactile stimuli during 7–12 Hz cortical oscillations in awake rats. Nature Neuroscience 6, 913–914. doi:10.1038/nn1107

Wimmer, R.D., Schmitt, L.I., Davidson, T.J., Nakajima, M., Deisseroth, K., Halassa, M.M., 2015. Thalamic control of sensory selection in divided attention. Nature 526, 705–709. doi:10.1038/nature15398

Woods, D.L., Alho, K., Algazi, A., n.d. Intermodal selective attention. I. Effects on event-related potentials to lateralized auditory and visual stimuli. Electroencephalography and Clinical Neurophysiology 82, 341–355.

Woody, C.D., Gruen, E., 1978. Characterization of electrophysiological properties of intracellularly recorded neurons in the neocortex of awake cats: a comparison of the response to injected current in spike overshoot and undershoot neurons. Brain Research 158, 343–357.

Yizhar, O., 2012. Optogenetic Insights into Social Behavior Function. Biological Psychiatry 71, 1075–1080.

Yizhar, O., Fenno, L.E., Prigge, M., Schneider, F., Davidson, T.J., O'Shea, D.J., Sohal, V.S., Goshen, I., Finkelstein, J., Paz, J.T., Stehfest, K., Fudim, R., Ramakrishnan, C., Huguenard, J.R., Hegemann, P., Deisseroth, K., 2011. Neocortical excitation/inhibition balance in information processing and social dysfunction. Nature 477, 171–178. doi:10.1038/nature10360

Zagha, E., Ge, X., McCormick, D.A., 2015. Competing Neural Ensembles in Motor Cortex Gate Goal-Directed Motor Output. Neuron 88, 565–577. doi:10.1016/j.neuron.2015.09.044

Zhang, S., Xu, M., Chang, W.-C., Ma, C., Hoang Do, J.P., Jeong, D., Lei, T., Fan, J.L., Dan, Y., 2016. Organization of long-range inputs and outputs of frontal cortex for top-down control. Nature Neuroscience 19, 1733–1742. doi:10.1038/nn.4417

Zhang, S., Xu, M., Kamigaki, T., Hoang Do, J.P., Chang, W.-C., Jenvay, S., Miyamichi, K., Luo, L., Dan, Y., 2014. Selective attention. Long-range and local circuits for top-down modulation of visual cortex processing. Science (New York, N.Y.) 345, 660–665. doi:10.1126/science.1254126

Zhou, M., Liang, F., Xiong, X.R., Li, L., Li, H., Xiao, Z., Tao, H.W., Zhang, L.I., 2014. Scaling down of balanced excitation and inhibition by active behavioral states in auditory cortex. Nature Neuroscience 17, 841–850. doi:10.1038/nn.3701